ADDIS ABABA UNIVERSITY

ADDIS ABABA INSTITUTE OF TECHNOLOGY

SCHOOL OF CIVIL AND ENVIRONMENTAL ENGINEERING

The Role of Bond in Shear Transfer of Shear Critical Reinforced Concrete Slender Beams

A Thesis in structural engineering

By Weyneshet Getachew

20/01/2022

Addis Ababa

A Thesis

Submitted in Partial Fulfillment of the Requirements for the Degree of Master of Science

The undersigned have examined the thesis entitled '**The Role of Bond in Transfer of Shear Critical Reinforced Concrete Slender Beams**' presented by **Weyneshet Getachew**, a candidate for the degree of **Master of Science** and hereby certify that it is worthy of acceptance.

Dr. Esayas G/youhannes		13/06/2022
Advisor	Signature	Date
Dr.Adil Zekaria		13/06/2022
Internal Examiner	Signature	Date
Prof.Girma Zerayohannes		Feb. 04/2022
External Examiner	Signature	Date
Dr.Ing.Mebruk Mohammed	Mebruk Mohammed (Dr.-Ing.) Dean,Sch... of Civil & Environmental Engineering	
Chair person	Signature	Date

UNDERTAKING

I certify that research work titled “The Role of Bond in Shear Transfer of Shear Critical Reinforced Concrete Slender Beams” is my own work. The work has not been presented elsewhere for assessment. Where material has been used from other sources it has been properly acknowledged / referred.

Weyneshet Getachew

ABSTRACT

Due to its complex nature, the effect of bond loss between concrete and longitudinal bar on the shear transfer mechanism lacks a complete framework. So far, all ranges of bond losses are considered as a total bond loss, leaving no gap to address intermediate ranges. Advancement in this area will aid in the assessment of the service life time of various structures and provide insight for rehabilitative engineers in their efforts. An experimental program was undertaken to investigate two ranges of bond losses, complete bond loss and bond losses induced by transversal cracks in relation to the effect of the location of the bond deterioration.

In first set Pullout test was used to determine the best approach for bond cutting without compromising the cracking pattern. This set experimented on the location of the artificial bond cut. It included the control beam and two beams with artificial bond cutting material covering 75% of their shear span, with a sole difference being the location of the artificial bond cut. The second set experimented on bond losses induced by transversal cracks. The transversal cracks were induced by introducing slits and a water proof tape was wounded around the slits to simulate the bond deterioration zone. This set included four beams with 75% and 50% of their shear span designed to imitate transversal cracks.

During testing, the shear strain at specified points of the 8 beams were measured to compare the two sets. A number of mold strain gauges were also used in the second set of specimens to monitor the transfer of shear force to the web. The results of the beam specimens in the first set have attained 90% up to 100% of their flexural capacity, while the control has attained 53% of the flexural capacity. It was also observed that the critical diagonal crack initiation, propagation and location is severely affected by the experimental variables. Finally, it was observed that the location of the bond cut or bond deterioration resulted in a different effect on the two sets.

ACKNOWLEDGMENTS

My heartfelt thanks go to Dr. Esayas G/youhannes, my advisor. I've never met an individual as invested in my work and success. Working with him on this research paper has been both educational and enticing. His insight and patience were endless.

I'd also like to thank my colleague and friend Mohammed Sirage for his ongoing encouragement and advice. I'd like to thank Dr.-Ing. Adil Zekaria, professor Girma Zerayohannes and Dr. Abraham Gebre for their insightful comments and suggestions.

I'd like to take this opportunity to express my heartfelt gratitude to my friends Kalkidan Tefaye, Mahelt Wondowsen, and my family for providing all of the emotional support I required throughout the Experimental program. The experimental program would not have been a reality without their encouragement and support. I would also like to thank Binyam F., Demess, Fikru B. and Wubet A. in the construction materials testing laboratory.

TABLE OF CONTENTS

ABSTRACT ..... **V**

ACKNOWLEDGMENTS ..... **VI**

TABLE OF CONTENTS ..... **VII**

LIST OF TABLES ..... **X**

LIST OF FIGURES ..... **XI**

CHAPTER 1 INTRODUCTION **1**

1.1 Problem statement 3

1.2 Objective 4

1.2.1 General objective 4

1.2.2 Specific objectives 4

1.3 Motivation 4

1.4 Scope of the research 5

1.5 Methodology 5

1.6 Organization of the Thesis 7

CHAPTER 2 LITERATURE REVIEW **8**

2.1 Theoretical Background 8

2.1.1 Bond stress in reinforced concrete 8

2.1.2 Environmental and other forces affecting bond in reinforced concrete 8

2.1.3 Bond loss and arch action(Feldman & Bartlett, 2008) 9

2.1.4 Bond and crack initiation(Kim & White, 1991) 11

2.2 General literature review 13

CHAPTER 3 EXPERIMENTAL PROGRAM **25**

3.1 Specimen 25

3.1.1 The trial beam 26

3.1.2 The first series (BB series) 27

3.1.3 The second series (DCB series) 33

3.2 Material 40

3.2.1 Concrete 40

3.2.2 Steel 43
3.3 Specimen fabrication 44
3.3.1 Trial beam fabrication 44
3.3.2 The fabrication of first series (BB series) 46
3.3.3 The fabrication of the second series (DCB series) 47
3.4 Test set up 52
3.5 Instrumentation 53
CHAPTER 4 FEM ANALYSIS USING VECTOR 2D 57
4.1 About the software 57
4.2 Specimens 58
4.3 Material 58
4.4 Modeling 58
4.5 Loading and Support conditions 59
4.6 Results of the FEM models 59
CHAPTER 5 RESULT AND DISCUSSION 62
5.1 Result of the experimental program 62
5.1.1 The result of Trial beam 62
5.1.2 The result of Control beam 63
5.1.3 The result of the beam 75BB1 65
5.1.4 The result of the beam 75BB2 67
5.1.5 The result of beam 50DCB1 69
5.1.6 The result of beam 50DCB2 71
5.1.7 The result of beam 75DCB1 73
5.1.8 The result of beam 75DCB2 74
5.2 Discussion 76
5.2.1 The effect of location of bond cut or bond deterioration 83
5.2.2 The effect of percentage of length affected by bond cut or bond deterioration 90
5.2.3 The effect of bond cutting and bond damage by cracking 93

5.2.4 Comparison of FEM analysis results with experimental results 96

5.2.5 Comparison with available design codes.....97

CHAPTER 6 CONCLUSIONS AND RECCOMENDATIONS.....102

6.1 Conclusion 102

6.2 Recommendation 103

REFERENCES 104

APPENDIX A, PULL OUT SPECIMEN DESIGNING BOND STRENGTH EQUATIONS FROM CODES AND RESEARCHER'S 106

APPENDEX B, DCB SERIES SLIT AND BOND DETERIORATION PLACEMENT DETAILS 108

APPENDEX C, DETAILED GRAPHS OF RESULTS FROM THE EXPERIMENTAL PROGRAM.....110

APPENDIX D, PICTORIAL REPRESENTATION OF DEFORMATION AT 50KN INTERVAL OF SPECIMEN.....116

LIST OF TABLES

Table 2-1 Test results Leonhard's tests with varying reinforcement configuration. Translated from (Leonhard and Walther, 1962)(Y.Yang et al., 2016) 13
Table 2-2 Test results: Part B of test program and details of specimen(Cairns & Zhao, 1994) 18
Table 2-3 Result of carnis specimen 21
Table 2-4 Test results for1999 woo Kim and Richard N. White(Kim & White, 1999) ... 23
Table 3-1 Details of the pullout specimen 29
Table 3-2 Number of slits calculation 33
Table 3-3 Detail calculation of crack spacing 36
Table 3-4 Details of experiment specimen 40
Table 3-5 The mix design and aggregate properties 41
Table 3-6 Mix design results 41
Table 3-7 Trial beam concrete compressive strength 42
Table 3-8 Concrete compressive strength of damaged concrete section in trial beam 42
Table 3-9 BB series concrete compressive strength 42
Table 3-10 BB series concrete tensile strength 42
Table 3-11 DCB series concrete compressive strength 42
Table 3-12 DCB series concrete tensile strength 43
Table 3-13 Concrete compressive strength of damaged concrete section in DCB series 43
Table 3-14 Mechanical property of reinforcement bars 43
Table 3-15 Roughness Euro Code standard(de Normalisation & NORMUNG, 2003) ... 49
Table 3-16 The result of the sand patch test 49
Table 4-1 Detail of modeled specimen 58
Table 5-1 The results of the experimental program 76
Table 5-2 Normalized ultimate failure of specimen 77
Table 5-3 change in ultimate capacity from the control beam 89
Table 5-4 Concrete shear capacity according to codes 99
Table 5-5 Different codes coefficient of variation in relation with experimental result 101
Table 5-6 Different codes coefficient of variation in relation with each series experimental result 101

LIST OF FIGURES

Figure 1-1 A flow chart of the methodology 6
Figure 2-1 Variation in bond strength with corrosion(Bilcik & Holly, 2013) 9
Figure 2-2 Left figure before loss of bond ,the right side after the loss of bond(Feldman & Bartlett, 2008) 10
Figure 2-3 Shear stress in reinforced concrete beam(Kim & White, 1991) 11
Figure 2-4 Measured steel force and bond stress :(a) steel force (b) bond stress(Kim & White, 1991) 12
Figure 2-5 Crack patterns for beams reinforced with plain and ribbed bars(Y.Yang et al., 2016) 13
Figure 2-6 Tests BP0 and BP2 cracking pattern and theoretical strut position(Muttoni & Ruiz, 2008) 14
Figure 2-7 Load-carrying mechanisms after development of critical shear crack: (a) elbow-shaped strut; (b) straight strut(enabled by aggregate interlock); and (c) combined response(Muttoni & Ruiz, 2008) 14
Figure 2-8 Kani's test for investigation of various bond qualities(Masukawa, 2012) 15
Figure 2-9 Moment and shear stress to shear span ratio relationships for Ikeda's test (Masukawa, 2012) 16
Figure 2-10 Schematic diagram for bond – maximum moment relationship(Masukawa, 2012) 16
Figure 2-11 Details of test specimen(Cairns & Zhao, 1994) 17
Figure 2-12 Alternative loading arrangements(Cairns & Zhao, 1994) 18
Figure 2-13 Contrast in crack formation between beam T4 with bonded reinforcement, and beam T8 with bars exposed(Cairns & Zhao, 1994) 19
Figure 2-14 Details of test specimen in A series 20
Figure 2-15 Details of test specimen in B series 20
Figure 2-16 Details of test specimen in C series 21
Figure 2-17 Development of cracking, series B specimen 22
Figure 2-18 Beams in UBB series(Kim & White, 1999) 22
Figure 2-19 Load vs deflection of the UBB series(Kim & White, 1999) 23
Figure 2-20 Crack patern of the control and the UBB series beams(Kim & White, 1991) 24
Figure 3-1 Guide for naming of the beams 26

Figure 3-2 Rough surface formation....26
Figure 3-3 The trial beam's damaged concrete section rough surface formation 26
Figure 3-4 Details of the trial beam....27
Figure 3-5 Vertical section of the pullout specimen....28
Figure 3-6 Materials used for bond cutting in pullout test 29
Figure 3-7 Bar preparation for the pull out specimen A, using the water proof tape B, using the gasket 29
Figure 3-8 The pull out specimen....30
Figure 3-9 Load cell used for pullout test....30
Figure 3-10 Test set up of the pullout test 30
Figure 3-11 Slip Vs bond stress result of pullout test....31
Figure 3-12 Comparison b/n the gasket and water proof tape pullout results 31
Figure 3-13 Cross section of all specimen....32
Figure 3-14 Details of the control beam 32
Figure 3-15 Details of beam 75BB1....32
Figure 3-16 Details of beam 75BB2....32
Figure 3-17 CEP-FIP Effective embedment zone 33
Figure 3-18 Euro Code effective embedment parameters 34
Figure 3-19 Euro Code effective embedment zone 34
Figure 3-20 The effective embedment zone implemented 35
Figure 3-21 Cracks formed after trial damaged concrete section loading....36
Figure 3-22 Visual of bond deterioration zone (K. Maekawa, A. Pimanmas and H. Okamura,2003) 37
Figure 3-23 Model for the bond deterioration zone (Salem and maekawa,1999) 37
Figure 3-24 Positioning of slits and bond deterioration zones in the damaged bond section 38
Figure 3-25 Cross section A-A....38
Figure 3-26 Details of beam 75DCB1....38
Figure 3-27 Details of beam 75DCB2....39
Figure 3-28 Details of beam 50DCB1....39
Figure 3-29 Details of beam 50DCB2....39
Figure 3-30 The silt test and concrete property testing 41
Figure 3-31 Steel mechanical property testing machine....43
Figure 3-32 Form work for trial beam damaged concrete section....44

Figure 3-33 Trial beam damaged concrete section with roughened surface 44
Figure 3-34 Trial beam damaged concrete section loading.....44
Figure 3-35 Trial beam damaged concrete section loading procedure.....45
Figure 3-36 Placing of the top bars to the damaged concrete section 45
Figure 3-37 Placing of the damaged concrete section inside the trial beam formwork ...45
Figure 3-38 75BB1 beam application of gasket 46
Figure 3-39 75BB2 beam application of gasket 46
Figure 3-40 Finshing of the first series (BBseries) casting 46
Figure 3-41 laminated paper used for slit formation 47
Figure 3-42 The bond deterioration imitation by winding water proof tape 47
Figure 3-43 Placement of the laminated paper slit 47
Figure 3-44 Casting of the damaged bond concert sections.....48
Figure 3-45 Principle of sand area method for the qualification of the roughness of an interface 48
Figure 3-46 the process followed during sand patch test 48
Figure 3-47 Patch selection of the sand patch test in damaged bond concrete sections..49
Figure 3-48 A typical manufactured strain mold gauge 50
Figure 3-49 Fashioning of the mold strain gage.....50
Figure 3-50 Placement and finished look of strain mold gage 51
Figure 3-51 Load Vs strain of mica strain mold gage 51
Figure 3-52 Placing of the mold strain gage.....52
Figure 3-53 Placement of the damaged bond section and casting of the second set of beams 52
Figure 3-54 Test set up of the tests.....53
Figure 3-55 Hydraulic jack and the load cell used for one point loading.....53
Figure 3-56 Surface measurement instrumentation set up of the trial beam 54
Figure 3-57 Close up of the trial beam surface measurement instrumentation 54
Figure 3-58 The front side surface measurement set up.....55
Figure 3-59 The back side surface measurement set up 55
Figure 3-60 A surface measurement set up on series BB and DCB.....55
Figure 3-61 The DATA COM transducers.....55
Figure 3-62 The data logger system 56
Figure 3-63 The DATA COM transducers monitoring system.....56
Figure 4-1 FEM control beam load vs deflection analysis 59

Figure 4-2 Cracking pattern of control beam according to VECTOR model.....60
Figure 4-3 FEM beam 75BB1 load vs deflection analysis.....60
Figure 4-4 Cracking pattern of beam 75BB1 according to VECTOR model.....60
Figure 4-5 Comparison of the FEM beams result.....61
Figure 5-1 The load deflection progression of trial beam.....62
Figure 5-2 Close up crack patterns.....63
Figure 5-3 Load vs deflection of control beam.....64
Figure 5-4 The control beam after failure.....64
Figure 5-5 Close up on the cracks of control beam.....65
Figure 5-6 Load vs deflection of beam 75BB1.....65
Figure 5-7 The beam 75BB1 after failure.....66
Figure 5-8 Close up on the cracks of beam 75BB1.....66
Figure 5-9 Cracks just before failure beam 75BB1.....67
Figure 5-10 Load vs deflection of beam 75BB1.....68
Figure 5-11 After failure beam 75BB2.....68
Figure 5-12 Close up on the cracks of beam 75BB2.....69
Figure 5-13 Load vs deflection of beam 50DCB1.....70
Figure 5-14 The beam 50DCB1 after failure.....70
Figure 5-15 Close up on the cracks of beam 50DCB1.....71
Figure 5-16 Load vs deflection of beam 50DCB2.....71
Figure 5-17 The beam 50DCB2 after failure.....72
Figure 5-18 Cracks just before failure beam 50DCB2.....72
Figure 5-19 Close up on the cracks of beam 50DCB2.....72
Figure 5-20 Load vs deflection of beam 75DCB1.....73
Figure 5-21 The beam 75DCB1 after failure.....73
Figure 5-22 Cracks just before failure beam 75DCB1.....74
Figure 5-23 Close up on the cracks and spalling of beam 75DCB1.....74
Figure 5-24 Load vs deflection of beam 75DCB2.....74
Figure 5-25 The beam 75DCB2 after failure.....75
Figure 5-26 Just before failure cracks beam 75DCB2.....75
Figure 5-27 Close up on the cracks and spalling of beam 75DCB2.....75
Figure 5-28 Normalized stress vs deflection of all specimens.....77
Figure 5-29 Normalized stress vs deflection of BB series specimens.....78
Figure 5-30 Normalized stress vs deflection of DCB series specimens.....78

Figure 5-31 Load vs front side shear strain of BB series 79
Figure 5-32 Load vs front side shear strain of DCB series.....79
Figure 5-33 Front side horizontal strain Vs load of BB series 80
Figure 5-34 Comparison of crack formation of BB series A, control B,75BB1 C,75BB2 81
Figure 5-35 Front side horizontal strain Vs load of DCB series 82
Figure 5-36 Strain mold gage results of the DCB series 82
Figure 5-37 Comparison of crack formation of DCB series A, 50DCB1 B, 50DCB2 C, 75DCB1 D,75DCB2 83
Figure 5-38 Load vs deflection of the BB series 84
Figure 5-39 The diagonal critical crack of beam 75BB1 85
Figure 5-40 The diagonal critical crack of beam 75BB2 85
Figure 5-41 Specimen for the dowel test(Krefeld & Thurston, 1966) 85
Figure 5-42 Control beam critical diagonal crack 87
Figure 5-43 Beam 75BB1 critical diagonal crack 87
Figure 5-44 Beam 75BB2 critical diagonal crack 87
Figure 5-45 The effect of location of bond deterioration zone in the DCB series 87
Figure 5-46 Load vs deflection of the DCB series 88
Figure 5-47 Beam 50DCB2 critical diagonal crack 89
Figure 5-48 Beam 75DCB1 critical diagonal crack 89
Figure 5-49 Beam 75DCB2 critical diagonal crack 89
Figure 5-50 Relation between shear capacity enhancement and % of bond cut from other researchers work 90
Figure 5-51 The load vs deflection of beams 50DCB1 and 75DCB1 92
Figure 5-52 The load vs deflection of beams 50DCB2 and 75DCB2 92
Figure 5-53 A, positive shear strain deformation B, negative shear deformation.....94
Figure 5-54 Angle θ for the BB series.....94
Figure 5-55 Angle θ for the DCB series.....95
Figure 5-56 Mohr's circle at point of failure for the BB series.....95
Figure 5-57 Mohr's circle at point of failure for the DCB series 96
Figure 5-58 Comparing the FEM and experimental result of control beam.....97
Figure 5-59 Comparing the FEM and experimental result of beam 75BB1.....97

CHAPTER 1 INTRODUCTION

There is no obsolescence for concrete. The fact that the elements required to manufacture cement are among the eight elements that make up 98 percent of the earth's crust demonstrates this. Concrete manufacturing also emits the least CO2 compared to clay, steel, and lumber manufacturing on weight or volume basis. Indicating that, while the world may see some revolutions in cement manufacturing and applications in the future, the need for concrete and reinforced concrete in building technologies is here to stay.

The importance of thoroughly comprehending reinforced concrete's non-uniformity cannot be overstated. The suitability of the two materials to act together in resisting the external load determines the development of a section's strength in tension. To avoid discontinuity or separation of the two materials under stress, the reinforcing element, such as a reinforcing bar, must be subjected to the same strain as the surrounding concrete. To increase the capacity of the reinforced concrete section, the reinforcement's modulus of elasticity, ductility and yield or rupture strength must all be significantly higher than those of the concrete. Most importantly, the parameter that maintains composite action between the two materials is the bond between them.

Since the aim of design is to achieve a structure or part structure that will result in a safe and economical solution, any marginal gain in optimization in safety and economy should be perused. That happens to be the case in estimating the life time and evaluating the seismic performance of structures. Most of the manuals and codes customarily suggest a factor for reducing the shear capacity of members. It is clear that a seismic force on a reinforced concrete member causes a degradation in stiffness and loss of bond. Though the loss of stiffness has obviously a negative effect on the member’s seismic performance, previous experiments that involved cyclical loading and bond cutting by artificial methods have shown an enhancement in the shear capacity of the member compared to their control specimen. The difference between the manuals and the experiments should be reconciled to reach a wholesome understanding of the mechanism at work.

The other area that should be addressed in the study area of bond is the consideration of the loss of bond by corrosion and cyclic load as a complete removal of bond. which is represented in laboratory experiments and in the calculation of capacity. All ranges of bond

losses are considered as a total bond loss (in various models), leaving no gap to address intermediate ranges. Insight on how the different bond loss scales affect the shear capacity is also lacking. Because of the contact between the aggregate and the ribs of the bars, there will be mobilization of a bond stress depending on the arrangement and position of the aggregate. The assumption of loss of a complete bond fails to address the reality of the situation.

Many researchers have explored the effect of bond loss on shear behavior and capacity. Many of them have utilized different methods of bond cutting and hypostasized different rationales for the enhancement of capacity they have witnessed. While most point out bond loss facilitating arch action, others suggest the delay of formation of bond concentration at the start of flexural cracking. A clear understanding of how shear is transferred from longitudinal bars to the web of the concrete section is surely paramount in understanding the mechanism behind the shear behavior. This includes how the various qualities of bond loss, cases of complete bond loss and bond damage, affect the shear capacity.

Leonhardt and Walther (1962) were the first researchers to mention their observation of the shear enhancement in their experiment. Later, Kani explained enhancement by using his Teeth Model, stating that *"For two beams, identical in every respect except bond resistance, the one with poor bond, and therefore large crack distance, will have a higher load carrying capacity than the beam with good bond."* The surprising result is: the better the bond, the lower the diagonal load-carrying capacity ". While Ikeda, S., and Uji, K (1980) suggested that this was due to the resistance of arch action that allowed the unbounded beams to reach their flexural capacity**,** Woo Kim and Richard N. White(Kim & White, 1999) theorized that the nature of local concentration immediately after flexural cracking is a major cause of the initiation of flexural shear cracking in reinforced concrete beams and that the loss of bond might interfere with the crack formation.

On the other hand, authors like Y. Yang (Y.Yang, Veen, Hordijk, & Boer, 2016) have reported that the comparison did not show a clear difference between specimens reinforced with plain bars and the reference group regarding the shear behavior. The researcher, Cairns, J(Cairns & Zhao, 1994) also reported little to no change from the control specimen, even though, rather than un-bonding the bars, exposing the bars to the external elements was applied. These authors also did not expand on why their results were significantly different from the previously mentioned.

The researchers above have investigated the effect of un-bonding of the reinforcement by numerous artificial methods and at different quotients of the shear span. However, the effect of the location of the un-bonding and the imitation of the bond loss on the real life situations of corrosion, cyclic and seismic forces is not addressed. Also, little is said about how this mechanism operates and comes into play. There is no solid framework to predict the shear enhancement or predict the sensitivity of variables that are suspected to have an influence on the results. Usually, design codes give different variable values in cases of poor bond condition, but there is no correlation involved with the level of bond loss, the length of un-bonding and with the location of un-bonding in calculating the shear capacity of a member, in this case, beams. The other misconception is that in all previous shear models, full bond is assumed. The majority of the models are based on a truss analogy, which results in large tensile forces in the longitudinal reinforcement, limiting the shear capacity. As a result, it's critical to gain better knowledge of how reduced bonding affects load carrying ability.

1.1 Problem statement

There is a gap between the seismic performance evaluation manuals and the service life estimation procedures' assumption of cyclic and seismic forces decreasing the shear capacity of the member, while in some cases experiments show otherwise. There is also a lack of explicit clarity on the definition of bond loss; partial loss or complete loss. The details behind the mechanism causing shear enhancement are not explored and tested, which explains why existing codes are not adequate enough to answer the following questions.

- How does the dominant shear transfer mechanism change when there is un-bonding or loss of bond due to damaged concrete in the vicinity of reinforcing bars?
- How does the length of the no-bond affect the failure process?
- How does the location of the no-bond affect the failure process and shear capacity?
- How does the length of damaged concrete section affect the failure process?
- How is the complete loss of bond different from that of concrete damage?
- How does the location of the no-bond affect the failure process and shear capacity?

- Do the codes available capture the experimental results correctly?

"All ranges of bond losses are considered as a total bond loss (in various models), leaving no gap to address intermediate ranges. Insight on how the different bond loss scales and bond loss locations affect the shear capacity is paramount. "

1.2 Objective

1.2.1 General objective

The main purpose of this paper is to have an understanding of how the mechanism of shear transfer works in times of un-bonding and concrete damage. The researcher aims to fulfill the following specific goals.

1.2.2 Specific objectives

- To study the role of bonds in the shear transfer mechanism (To study the behavior of the mechanism with variables of damaged concrete, length of no-bond and location of no-bond).
- To study the justifications for the enhancement of the shear capacity in un-bonding cases.
- To explore if the enhancement of the shear capacity applies to damaged concrete cases.
- To see the relationship between the damage concrete series and the forces that cause bond loss, i.e. cyclic and seismic forces.
- To model the experimental specimens for verification. using VECTOR (software)

1.3 Motivation

This study is helpful in understanding the workings behind the shear transfer mechanism in cases of un-bonding and damaged concrete. It could also explain the gap between service life estimation and experiments by providing valuable information for rehabilitation engineers assessing historical structures. It also could answer cases like corrosion effect on shear strength, because one of the dire effects of corrosion is the loss of bond. Finally, it could serve as an input in the extension of design rules to cover future changes in practice.

1.4 Scope of the research

This study does not investigate the role of the bond in the shear transfer mechanism for reinforced concrete beams with transversal reinforcement and will include only slender beams with internal force of flexure and shear. Deep beams, short beams, beam-columns, pre-stressed beams and beams made of high-strength concrete are not be covered in this study. The study only considers bond losses involving complete bond losses and bond loss caused by transversal cracking.

1.5 Methodology

The study is broken down into parts, with the first being an extensive literature review to identify the gaps. The reasons for the role and significance of bond in reinforced concrete beam shear transfer. The experimental specimens, method of un-bonding, and instruments were then chosen based on the gaps discovered in the literature review and the study's objective. Finally, an experimental program is carried out, with the findings organized and analyzed in conjunction with a finite element software. The results of chosen experimental specimens are compared to their corresponding finite element models. Finally, the results of the experiment are compared with selected code provisions.

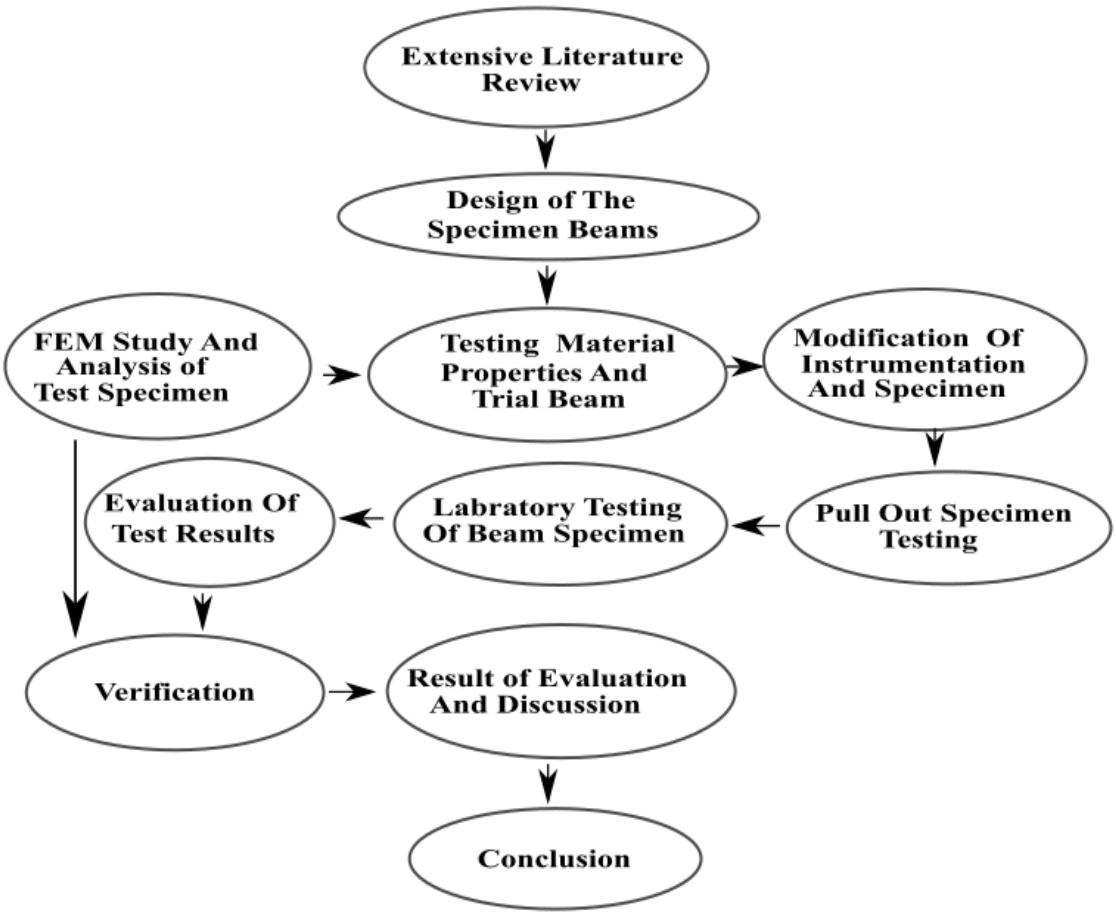

Figure 1-1 A flow chart of the methodology

1.6 Organization of the Thesis

Chapter 2 includes a breakdown of sub-topics influencing the relationship between shear and bond. Each subtopic is examined with an intensive literature review of papers that investigated the effect of the un-bonding of the longitudinal reinforcement on the shear capacity and also how different bond cutting methods impacted the shear capacity. Including what variables were found to be paramount and how each researcher explained the mechanism that caused the enhancement.

Chapter 3 explains the experimental program with the methodology used with a thorough explanation of the methods and procedures used. This part of the paper explains the instrumentation used and what analysis and tests went into study appropriate specimens. The material properties, the fabrication of the specimen and the test setup.

Chapter 4 includes the nonlinear finite element study using the vector 2 software with a description of the features chosen and justification for the selection.

Chapter 5 this chapter presents the results of the experiment and the finite element analysis. It discusses the results separately and then in tandem with the incorporation of relevant data from other researchers. Finally, investigate how the result fits with available design codes.

Chapter 6 concludes the study by presenting the facts and phenomena witnessed and recorded. Also goes into the recommendations for future studies and areas of study that were not explored because of limitations.

CHAPTER 2 LITERATURE REVIEW

2.1 Theoretical Background

2.1.1 Bond stress in reinforced concrete

The shear interlock between the reinforcing element and the enclosing concrete is the primary cause of bond stress. A local shearing stress per unit area of the bar surface is referred to as bond stress. This direct stress is transferred from the concrete to the bar contact, causing the tension of the reinforcing bar to fluctuate along its length. Bond strength is determined by the adhesion of the concrete and reinforcing components. The bond strength is affected by the shear interlock between the bar deformations and the surrounding concrete, as well as the gripping effect generated by the surrounding concrete's drying shrinkage. Frictional resistance to sliding and interlocking helps with the bond strength as the reinforcing element is subjected to tensile stress.

2.1.2 Environmental and other forces affecting bond in reinforced concrete

2.1.2.1 Corrosion

One of the most common causes of structural degradation in concrete structures is reinforcement corrosion, which can cause damage to the structure by initiating expansion, cracking, and eventually spalling of the concrete cover. A loss of bond between the reinforcement and the concrete, as well as a loss of reinforcement cross-sectional area, can cause structural damage and lead to structural failure.

In an experimental investigation, researchers examined the bond strength of reinforced concrete structures due to the impact of reinforcing bar corrosion. Their studies demonstrated that as the percent of corrosion increases, the bond strength increases at first until concrete fractures develop, and then continues to diminish as the percentage of corrosion increases. The effect of varying the degree of corrosion on the bond strength between reinforcing bar and concrete is shown in Figure 2-1.(Bilcik & Holly, 2013)(Ouglova et al., 2008)

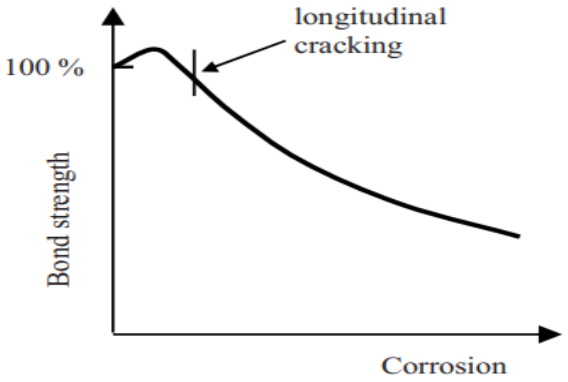

Figure 2-1 Variation in bond strength with corrosion(Bilcik & Holly, 2013)

2.1.2.2 Cyclic loading

In an experimental investigation, YE et al. (2016) evaluated the effect of fatigue stress on the bond behavior between reinforcing bar and concrete. The test was a pull-out test using the eccentric reinforcing bar. Fatigue loadings of various cycles and amplitudes were applied to test specimens. Splitting failure is a problem that affects all specimens. Increasing the number of fatigue load cycles enhances bond strength until it reaches a critical value. Nevertheless, increasing the number of fatigue load cycles diminishes bond strength because damage accumulation exceeds a critical value. The adhesion force between the bar and the concrete contact was likewise destroyed as the number of fatigue load cycles grew, and the bond strength reached a critical threshold at early loading if fewer cycles with a large range of amplitude were used.

2.1.3 Bond loss and arch action(Feldman & Bartlett, 2008)

The gradient of bending moment along the length of the member is known as one-way shear V. That is, the shear resulting from a gradient in steel tensile tension on a constant lever arm is carried by "beam action" as the first component of Eq. [2-1]. Bond forces between the concrete and the steel are required for beam action shear. Beam action is common in slender flexural members and is limited by yielding of the reinforcement or by bond failure.

$$v = \frac{dM}{dx} = \frac{d(Tjd)}{dx} = jd\frac{dT}{dx} + T\frac{d(jd)}{dx} \quad ----------(2.1)$$

"Internal "arching action," which is the second component of Eq. [2-1,] carries the shear that results from a constant steel tensile tension acting on a moving lever arm. All that is

needed is for the reinforcement to be anchored from afar. Shear transfer by arching action is predominant in deep beams and regions adjacent to discontinuities or disturbances in the member's loading or shape. Because bond slip and cracking cannot produce the whole bond force required for beam action, the two mechanisms will provide combined resistance in most beams.

$$u_{ave} = \frac{V}{jd \sum p} \quad ----------(2.2)$$

In regions where only beam action occurs, the average bond stress u_{ave} is proportional to the applied shear V. The shear carried by beam action (V in Eq. (2-2)) can be limited by the bond capacity u_{ave}, requiring more shear to be carried by arch action (Eq. (2-1)).

Flexural cracking decreases the strain compatibility of plain longitudinal reinforcement and surrounding concrete, increasing relative slip and perhaps lowering the average bond stress in the cracked beam zone. Local strain incompatibility is exacerbated by reinforcing yielding in high-moment zones, which increases relative slip and lowers average bond resistance minimizing the shear carried by beam action.

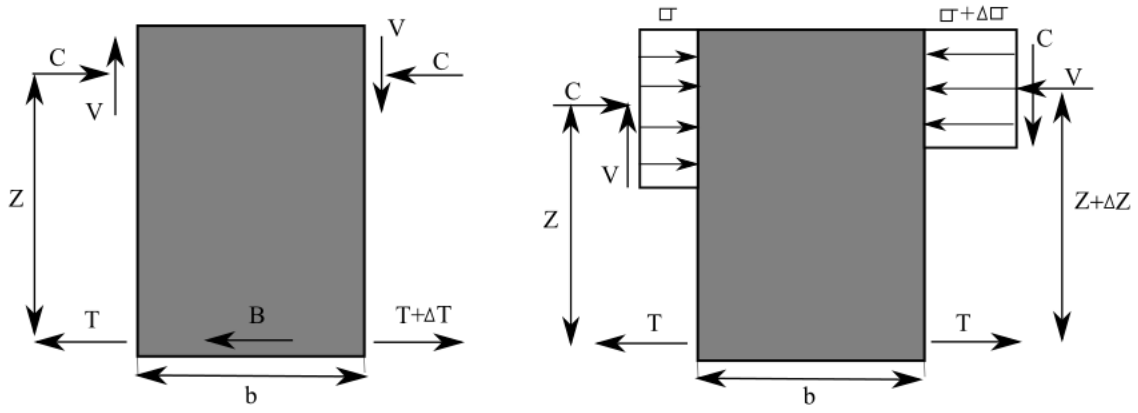

Figure 2-2 Left figure before loss of bond ,the right side after the loss of bond(Feldman & Bartlett, 2008)

After bond failure, the Figure 2-2 depicts the change in the equilibrium conditions of a beam element between two successive cracked sections, assuming that arch action is insignificant prior to bond failure. The loss of the bond force causes an expansion of the right-hand side flexural crack, which causes an increase z of the lever arm z, resulting in CΔ z=Va. The extension of the flexural cracks, on the other hand, decreases the depth of the neutral axis and thus increases the intensity of the compressive stress block on the element's right side.

2.1.4 **Bond and crack initiation**(Kim & White, 1991)

Woo Kim and Richard N. White explained how bond concertation at a flexural crack causes the formation of flexural shear cracks in their paper "Initiation of Shear Cracking in Reinforced Concrete Beams with No Web Reinforcement."

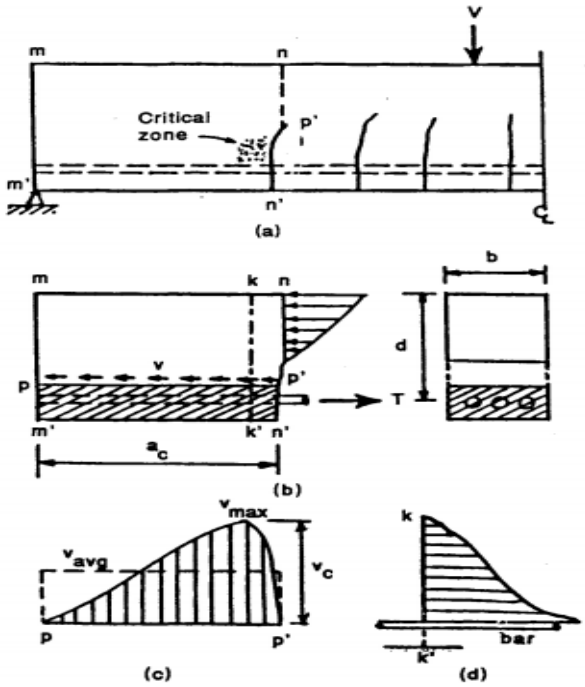

Figure 2-3 Shear stress in reinforced concrete beam(Kim & White, 1991)

The shear Surface pp_1 in figure 2-3 is close to the level of the longitudinal reinforcement, and the shear stresses on surface pp1 fluctuate along the length as well as across the width, and the reinforcing force T is transferred to the concrete through bond. To calculate the shear stress quantitatively, it is assumed that the shear stress distribution is uniform across the beam's width, therefore only the distribution along the length needs to be taken into account. Because shear stresses are caused by bond stresses, the distribution of shear stresses on the surface will approximate that of the bond stress along the bar when the shear surface pp_1 is sufficiently close to the level of reinforcement. Bond stresses experimentally measured along the longitudinal reinforcement by Mains are shown in Figure 2-3(b). The figure shows that the local maximum bond stress in the middle of the shear span is a factor of two or more higher than the calculated average value. Indicating that the highest bond stress is near the outer flexural crack, with a variation along its length as shown in Figure. 2-3(c) and along its depth as shown in Figure. 2-3(d). The variation of T and the accompanying bond stress over the length of the element are both relatively consistent prior to flexural cracking. The flexural crack n_1p_1 causes a significant shift,

resulting in shear stress concentration and incipient inclined-shear cracking near the flexural crack.

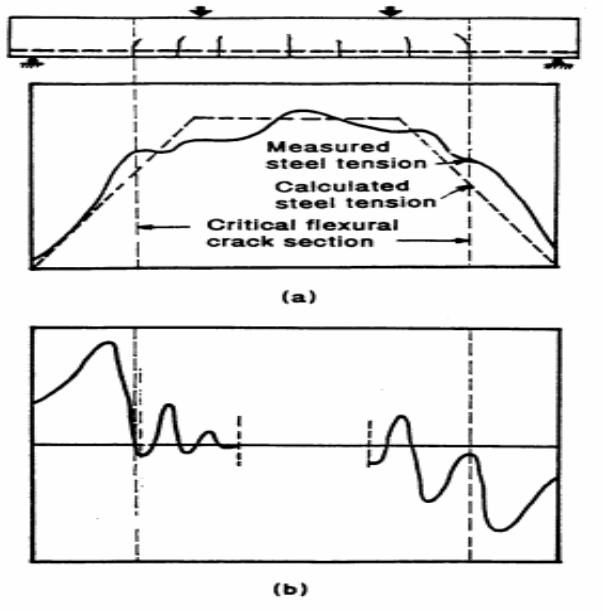

Figure 2-4 Measured steel force and bond stress :(a) steel force (b) bond stress(Kim & White, 1991)

2.2 General literature review

The shear enhancement caused by bond loss was first identified by Leonhard and Walther (1962) while investigating the influence of bar diameter on load carrying capacity. In their experiment, two of the beams were reinforced with plain bars (EB1 & EB2) and the remaining two with ribbed bars (EA1 & EA2). In their analysis, they realized that the shear capacity of the beams reinforced with plain bars was much greater than the corresponding beams reinforced with ribbed bars. Not only was the crack pattern of the plain-bar beams less extensive than that of the ribbed beams, but the circle in Figure 2-5 indicates cracks in the compression region above the supports, which is typically documented in deep beams.(Y.Yang et al., 2016)(Committee & Tension, 1964)

Table 2-1 Test results Leonhard's tests with varying reinforcement configuration. Translated from (Leonhard and Walther, 1962)(Y.Yang et al., 2016)

Specimen	Configuration	D_{eq} [mm]	ρ	a/d [-]	d [mm]	$f_{cm,cube}$ [MPa]	P_u [kN]	V_u [kN]
EA 1	2ø24+1ø6	22.1	1.89	2.78	270	24.6	116.6	58.3
EA 2	2ø14+3ø16	15.1	1.88	2.78	270	24.6	149	74.5
EB 1	2ø25	25	1.91	2.78	270	24.6	226.4	113.2
EB 2	5ø14+1ø16	14.4	1.88	2.78	270	24.6	198	100

Were D_{eq} is the equivalent diameter of the reinforcement configuration, $D_{eq=\sum D^2/D}$ D is the diameter of each bar, ρ longitudinal reinforcement ratio

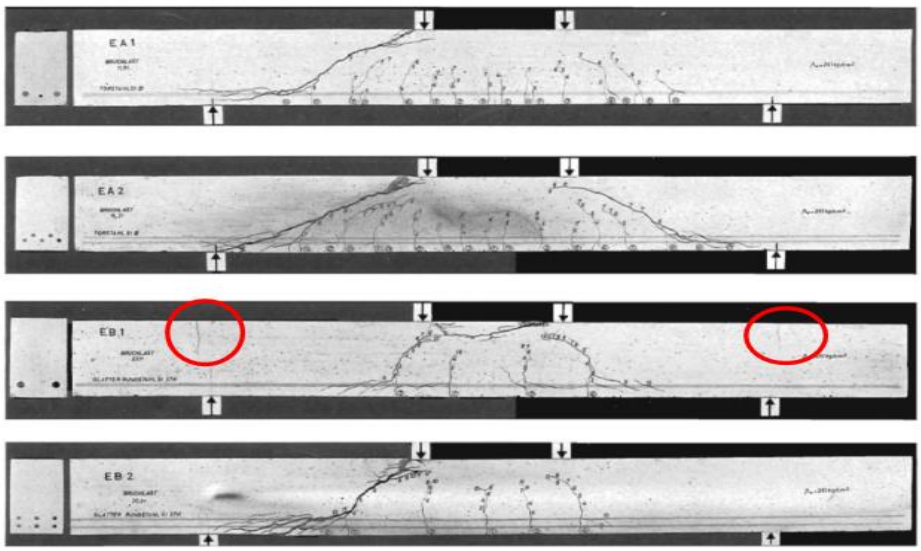

Figure 2-5 Crack patterns for beams reinforced with plain and ribbed bars(Y.Yang et al., 2016)

The same behavior of cracking in the compression region above the supports was observed in experiments on beams BP0 and BP2 (Figure 2-5) by Muttoni and Thürlimann in 1986. Two beams with matching shear spans were tested to failure (a/d equal to 2.44). Beam BP0 had only flexural reinforcement, whereas Beam BP2 contained reinforcement for crack control (spiral 6 mm at 60 mm) in the region of the theoretical strut. This reinforcement was very effective in controlling the width of the critical shear crack. Based on the theory of plasticity, the first beam (BP0) reached 50% of its strength. Beam BP2, however, attained its full flexural strength thanks to the spiral reinforcement, and the strength of the strut was not decreased. The formation of the cracks in the compression is explained in the paper by the load-carrying mechanisms after the development of the critical shear crack as shown in Figure 2-7.(Muttoni & Ruiz, 2008)

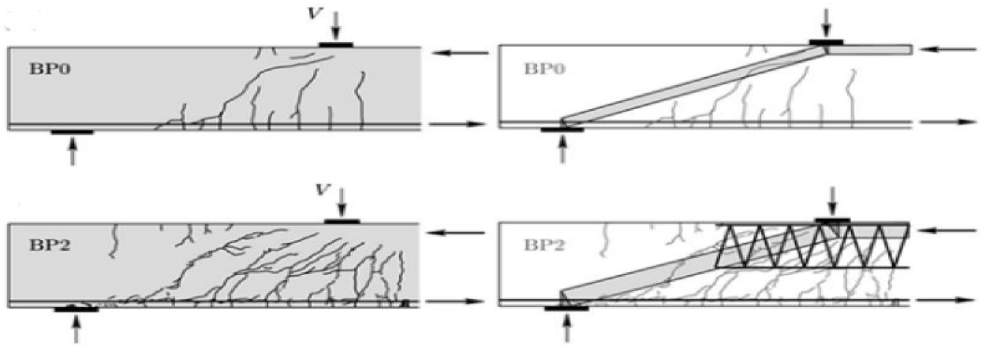

Figure 2-6 Tests BP0 and BP2 cracking pattern and theoretical strut position(Muttoni & Ruiz, 2008)

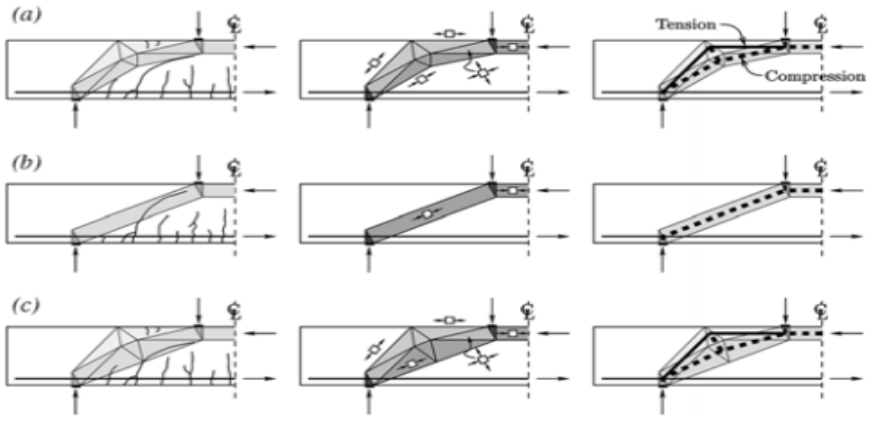

Figure 2-7 Load-carrying mechanisms after development of critical shear crack: (a) elbow-shaped strut; (b) straight strut(enabled by aggregate interlock); and (c) combined response(Muttoni & Ruiz, 2008)

A series of beams to further investigate the significance of changing bond quality were tested after analyzing the work of Leonhardt and Walther (1962) by Kani [Kani et al. 1979]. A layer of a vermiculite-cement mix (Vermiculite concrete is a low density non-structural construction product. It is normally made simply by mixing exfoliated vermiculite as the aggregate, with cement and water, plus additives) between the reinforcement and the concrete was used to vary bond and four layers of friction tape were wound about the reinforcing bar for the zero bond specimen. Figure 2-8 shows the test results of the relationships between maximum moment to ultimate flexural moment ratio and bond strength of pull out tests. The results clearly show beams with low bond quality have a better maximum moment to ultimate flexural moment ratio.(Masukawa, 2012)

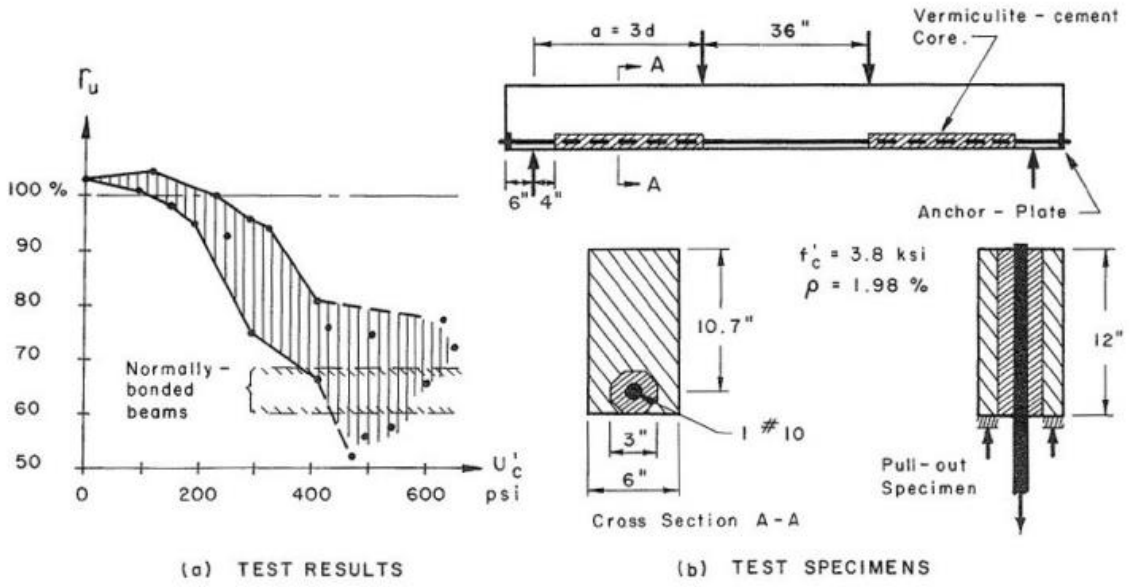

Figure 2-8 Kani's test for investigation of various bond qualities(Masukawa, 2012)

The next evolution came in 1980, when Ikeda experimented on 16 simply-supported beams (10cm x 20cm) with or without stirrups, changing the shear-span-to-depth ratio (a/d) from 1.5 to 5.0. The researcher eliminated bond for half of the specimen along the whole span between supports by covering the valleys between reinforcement ribs with wax, winding vinyl tape on them and coating the surface with grease before casting the concrete. Three D13 (1.267 cm^2) bars were used for longitudinal reinforcement ($\rho = 2.1\%$) and plain 6 mm (0.3167 cm^2) bars for web reinforcement.(Masukawa, 2012)

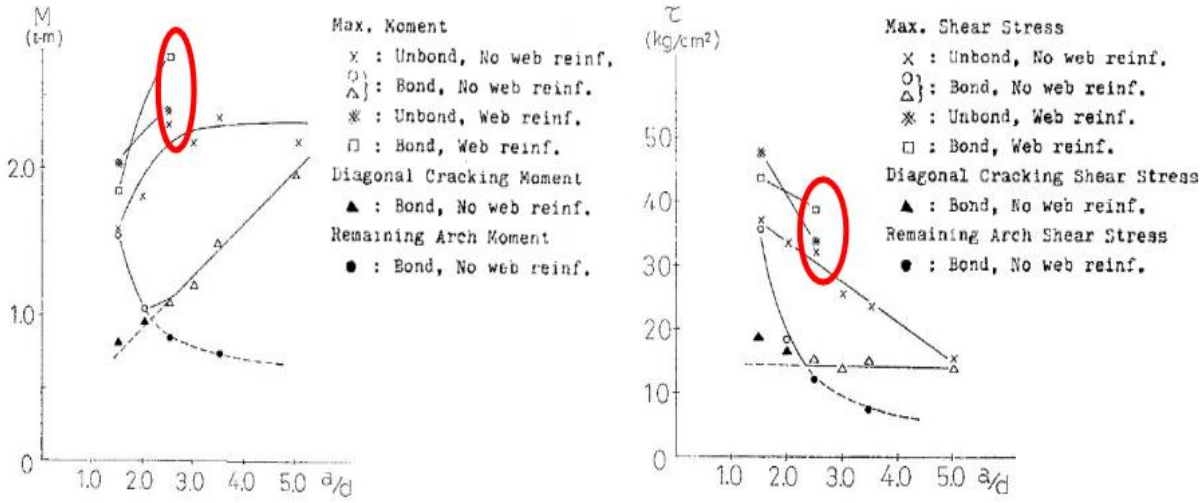

Figure 2-9 Moment and shear stress to shear span ratio relationships for Ikeda's test (Masukawa, 2012)

Figure 2-9 clearly shows that un-bonded beams with web or no web reinforcement showed better performance than their corresponding bonded beams, except for only two beams containing web reinforcement, shown by the circle. It was suggested the resistance of arch action that allowed the unbounded beams to reach their flexural capacity was the reason for the enhancement. Because there are fewer flexural cracks in the un-bonded beam, a strut-and-tie force resisting mechanism can form and carry the shear all the way up to the flexural capacity.

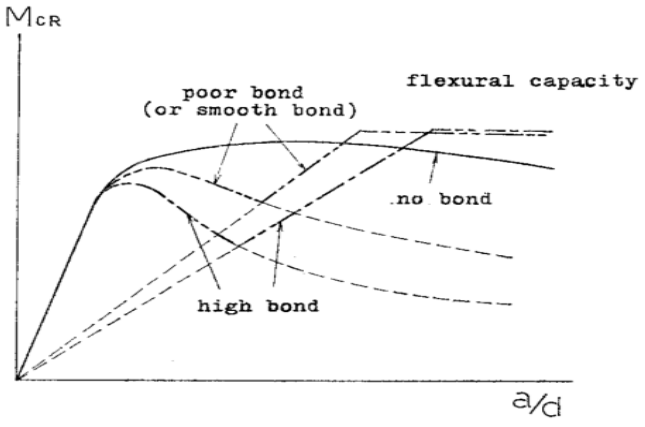

Figure 2-10 Schematic diagram for bond – maximum moment relationship(Masukawa, 2012)

The researchers also stated that the force in reinforcement can be transferred smoothly to surrounding concrete without inducing severe bond cracks if large-diameter longitudinal

bars are replaced by smaller-diameter bars with the same total area due to less bond stress for each bar. They have categorized this as a "smooth bond."

J. Cairns investigated longitudinal reinforcement corrosion in beams with exposed longitudinal reinforcement in 1993. Because most repair work at the time involved replacing the section with concrete or mortar after the concrete around the affected reinforcement had broken out, exposing the reinforcement was suitable for the experiment. A total of nineteen reinforced concrete beams were put through their paces. Two series of experiments were carried out. Part A has two specimens that are entirely connected with all reinforcement. In part B a further 17 beams were tested to evaluate ultimate strength of beams with exposed reinforcement under three forms of loading as the distance over which tension reinforcement was exposed was successively increased.(Cairns & Zhao, 1994)

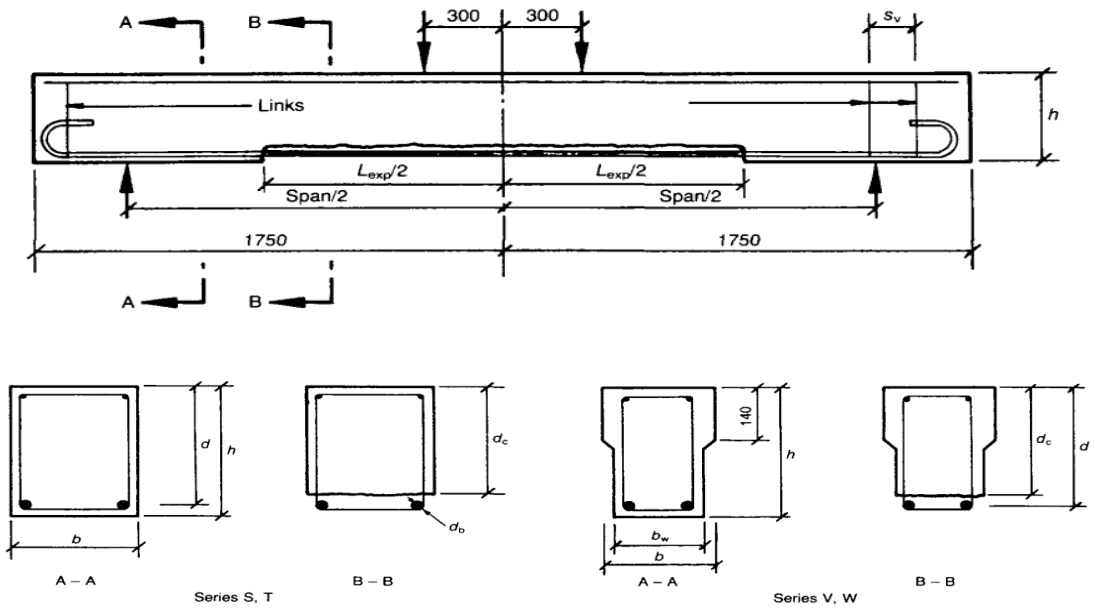

Figure 2-11 Details of test specimen(Cairns & Zhao, 1994)

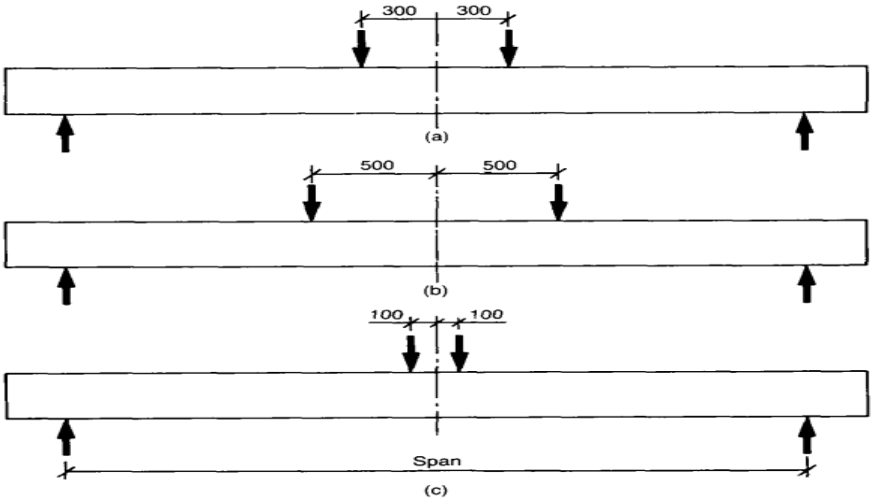

Figure 2-12 Alternative loading arrangements(Cairns & Zhao, 1994)

Table 2-2 Test results: Part B of test program and details of specimen(Cairns & Zhao, 1994)

Specimen	Span	B/B_w	Concrete Depth	Cube Strength	Exposed Concrete Depth	Failure load	Failure Mode	Failure Mode Bonded	M_{test}/M_{bond}
PART A									
T1	3000	233	303	27.7	230				
V1	2700	205/160	300	23.2	225				
PART B									
S1	2700	225	405	29.9		107	4	99.5	1.08
T4	3000	230	300	24.6		99.4	1	98.6	1.01
V4	2700	200/160	300	24.8		80.4	4	86	0.93
S2	2700	225	405	25	350	96.5	1	111.1	0.87
S3	2700	225	400	31.2	340	113	1	115.7	0.98
S4	2700	230	290	38.2	225	61.4	1	74.8	0.82
S4B	2700	221	270	24.9	205	46.1	1	63.6	0.72
S5	2700	230	230	35.4	155	28.9	1	55.1	0.52
S5R	2700	230	230	26.5	140	24	2	46.4	0.52
S7	2700	228	410	30.3	340	135.5	1	153.8	0.88
S8	2700	150	405	29.6	320	92.1	1	133	0.69
S9	2700	230	400	32.4	340	69.2	1	70.1	0.99
S10	2700	230	230	29.9	180	27.4	1	31.8	0.86
S11	2700	230	230	34.9	180	30	1	32	0.94
T8	3000	230	310	26.1	230	63.8	2 & 3	95.8	0.67
W1	2700	210/160	300	25.5	225	58.3	1 & 2	87.7	0.66
W2	2700	210/160	300	25.4	225	67.2	1	90.4	0.74

1 Concrete crushing within constant moment zone. **2** Concrete crushing at end of exposed length. **3** Anchorage failure.**4** Shear failure

Crack patterns in beams in Part B and A of the test program differed significantly from each other. For comparison, the pattern of cracking in beams T4 and T8 with the only difference being the exposure of reinforcement in the T8 beam is shown in Figure 2-13. The prominent variances seen on the exposed beam were the wider spacing and the greater height of cracks within the constant moment zone. These cracks also bifurcated at the tip and formed horizontal cracks. Outside the constant moment zone, there were no cracks on the tension face, and finally, there were cracks at the end of the exposure zone on the compression zones, which is typical in deep beams.

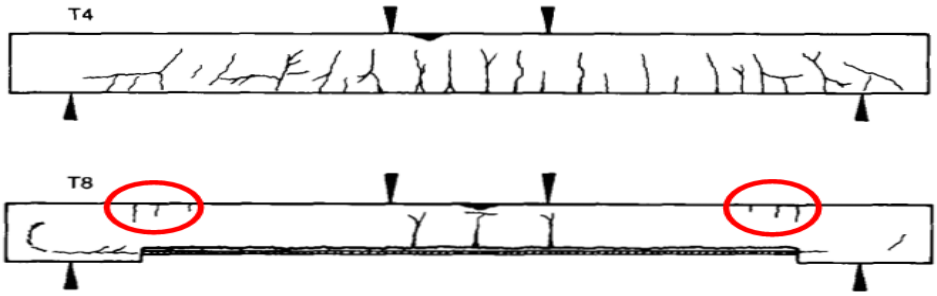

Figure 2-13 Contrast in crack formation between beam T4 with bonded reinforcement, and beam T8 with bars exposed(Cairns & Zhao, 1994)

The paper concluded that for beams with exposed bars, the maximum compressive strain in concrete increases in the constant moment zone. While shear failure did not occur in these beams, the chance of anchorage was amplified with the length of exposure extending close to the support. The author finalized the conclusion by mentioning key factors found to influence the change in behaviors as

- Length of exposed bar
- Exposed length position
- The percentage of reinforcement area in the beam section
- Concrete strength, reinforcement, and bond between the two form of loading
- A cross-sectional shape made of concrete

Again in 1995 carnis experimented on reinforced concrete beams with longitudinal reinforcement is disbanded over a part of the span. the paper intended to develop a procedure to assess ultimate shear strength of this beams. The experiment contained 3

series with one reference specimen in each series. The following figures show the details of the ten specimens.

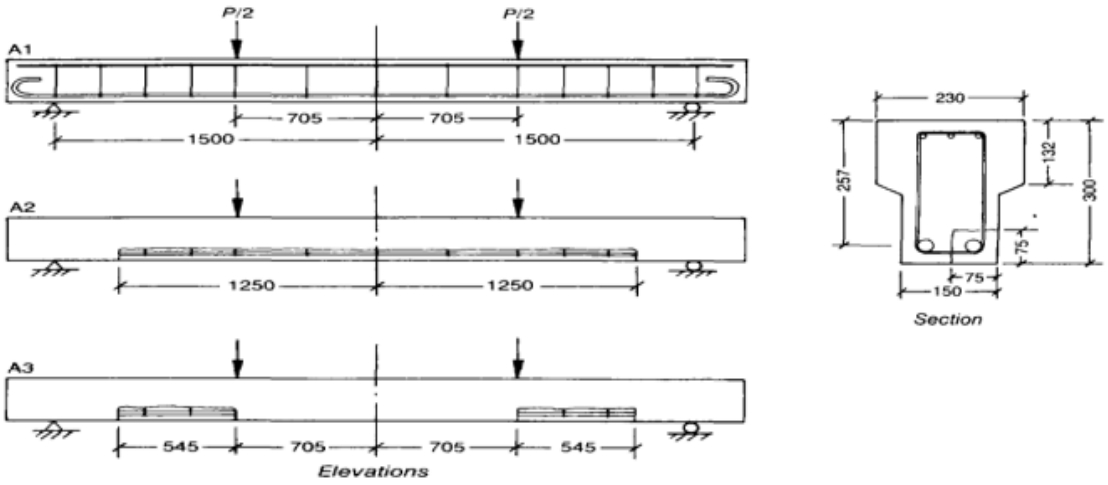

Figure 2-14 Details of test specimen in A series

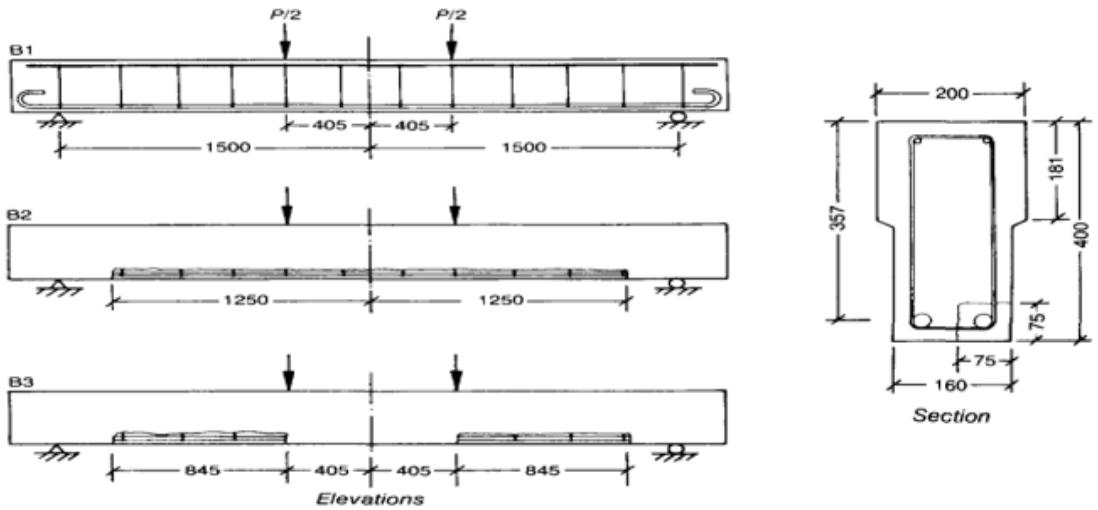

Figure 2-15 Details of test specimen in B series

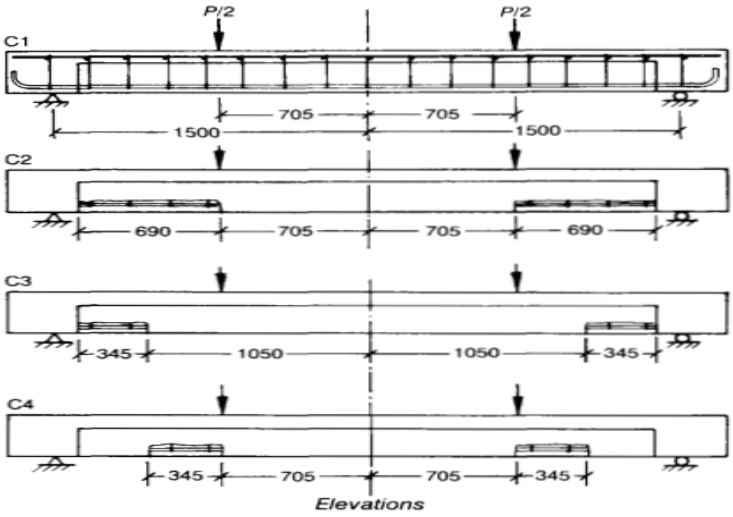

Figure 2-16 Details of test specimen in C series

Table 2-3 Result of carnis specimen

Specimen	Exposed Length (mm)	Cubic Strength (MPa)	Measured Failure Load	Failure Mode	Calculated Failure Load	
					Shear (kN)	Bending(kNm)
A1		32.1	138	V	161	264
A2	1250	43.1	240+	+	171	281
A3	545	35.7	220	A	165	264
B1		36	184	V	180	278
B2	1250	31.5	212	A	176	270
B3	845	31.5	200	V	176	270
C1		29.5	205	V	210	316
C2	690	25.7	229	V	206	311
C3	345	32.2	264	V	214	319
C4	345	30.1	324	V	211	318

V Shear failure
A End anchorage failure
+beam did not fail

The paper reported that exposure of the tension bars resulted in an increase in beam strength. Failure load for beams with exposed bars averaged 67%, 13%, and 33%higher than companion 'fully bonded' specimens in series A, B, and C respectively. The average increases in strength are 43%, 14%, and 30%for series A, B, and C, respectively. The greatest increase in strength for an individual specimen is then 58% for beam C_4. This specimen attained its full flexural capacity, as determined by BS 810.

The author concluded that though the surface strain measurement didn't record the dominance of the arching action, the possibility of a limited amount of arching cannot be discounted. Diagonal cracking in all tests was associated with failure, although the exact

form of the cracking was modified to some degree by the exposure of the reinforcement as shown in specimen B in Figure 2-17. Even specimen C4 exhibited the characteristics of a shear. Exposure of bars was found to increase the strength of beams designed to fail in shear.

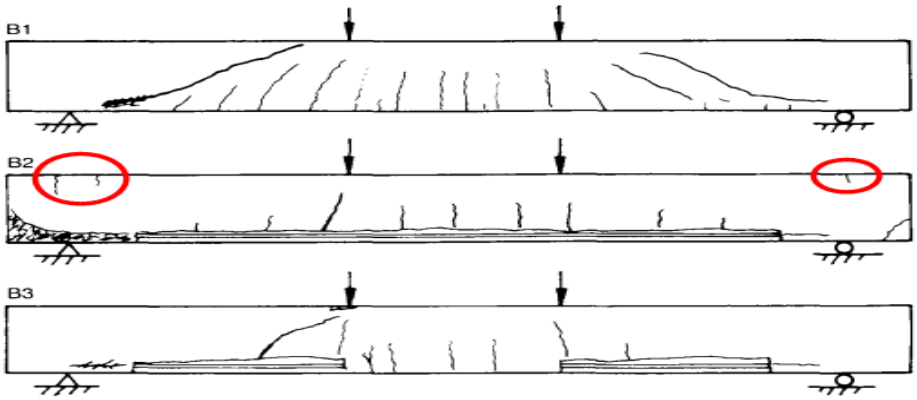

Figure 2-17 Development of cracking, series B specimen

Later in 1999, Woo Kim and Richard N. White conducted a series of experiments focused on inclined shear cracking (the mechanism of inclined shear crack initiation and the manner of inclined shear crack propagation). In one of the series (the UBB series), four beams were used to investigate the effect of unbounded tension reinforcement. The bond between the tension bars and the concrete was artificially eliminated using lengths of PVC pipe covers over selected lengths of the reinforcement along the shear span. The variable in this series was the length and location of the unbounded zone along the tension bar.(Kim & White, 1999)

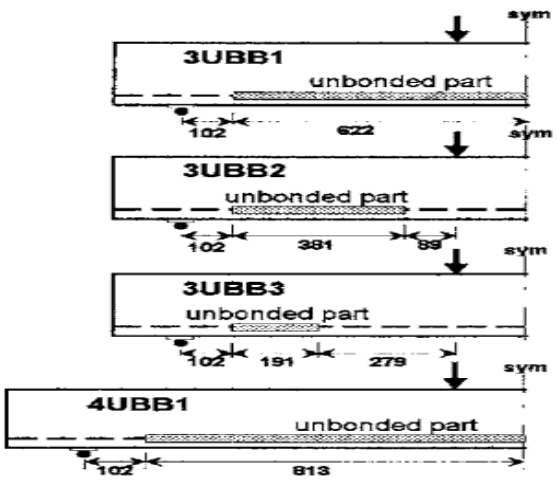

Figure 2-18 Beams in UBB series(Kim & White, 1999)

Beams 3UBB1 and 4UBB1 had ultimate loads that were 94 and 98 percent of their flexural strength, respectively. critical crack in 3UBB3 formed at a lower load stage, developed much more extensively, and opened far more widely because the bars were unbounded. However, the failure load was 24% higher than the control beam. The failure of 3UBB2 occurred as a result of crushing in the compression zone at a load of 104 percent of the calculated flexural capacity.(Kim & White, 1999)

Table 2-4 Test results for1999 woo Kim and Richard N. White(Kim & White, 1999)

Specimen	Concert strength (MPa)	Ultimate load (kN)	Flexural strength Mu/M_n
3CNB	30.1	58.7	0.54
4CNB	30.1	60.5	0.75
3UBB1	27.1	96.5	0.94
3UBB2	33.6	110.3	1.04
3UBB3	30.1	64.9	0.62
4UBB1	28.4	76.1	0.98

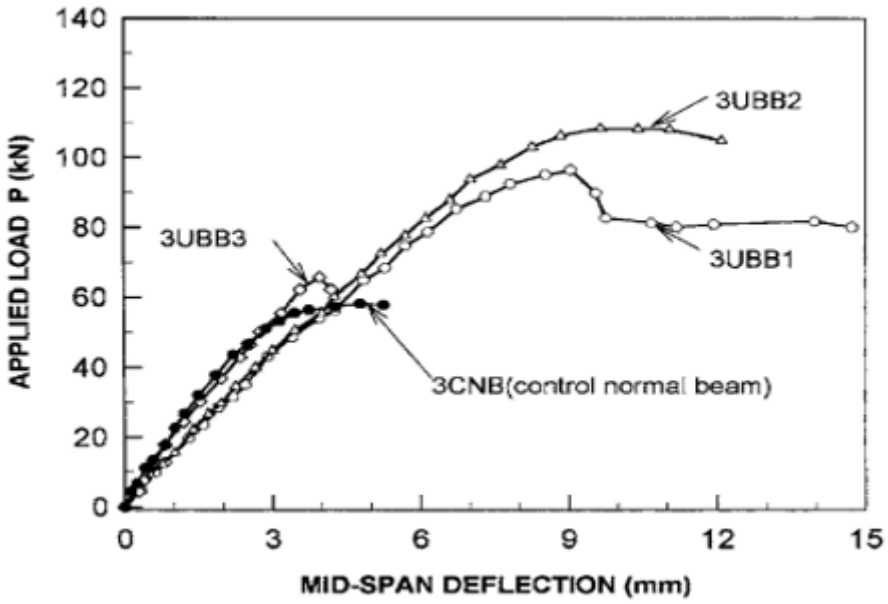

Figure 2-19 Load vs deflection of the UBB series(Kim & White, 1999)

The researchers claimed that the bond forces existing between the two different materials (concrete and steel) would appear to be the primary cause for the initiation of the shear crack and its propagation into the compression zone. They also state that this zone of the local shear stress concentration coincides well with the experimentally observed zone of shear crack initiation. The paper concluded that with no bond between the concrete and

the reinforcement in the shear span zone of the beams in the UBB series, the bond induced shear stress was absent, and a shear crack did not form, resulting in the avoidance of a shear failure in one of the specimens.

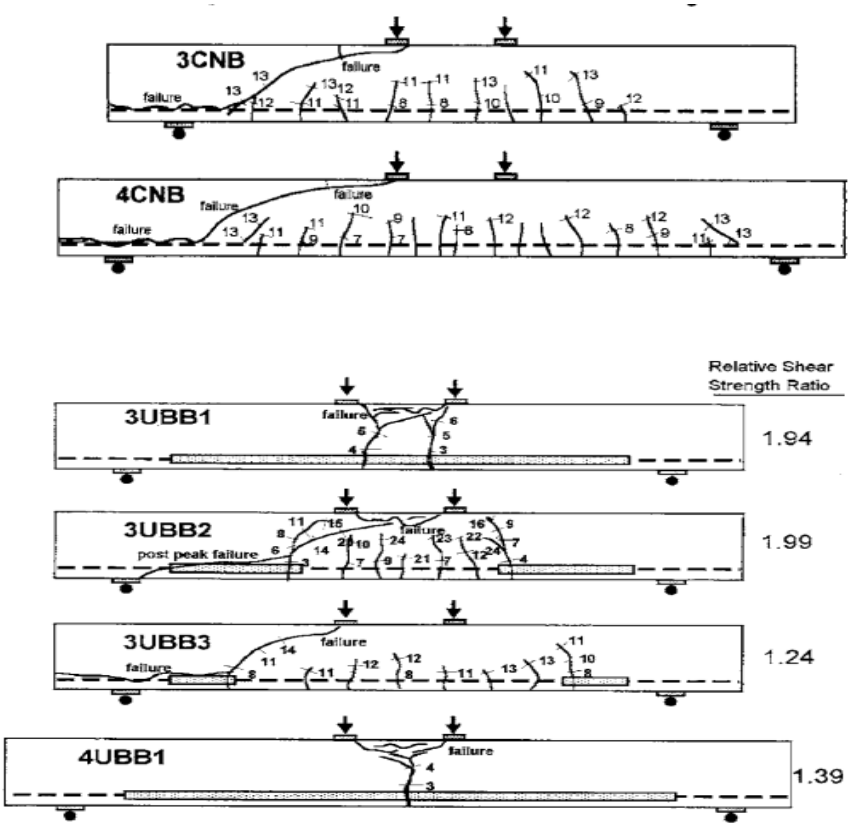

Figure 2-20 Crack patern of the control and the UBB series beams(Kim & White, 1991)

This study is designed to investigate the effect location of un-bonding, the percentage of shear span affected by the un-bonding and also method used for deterioration of bond quality. The paper investigates the gap that how intermediate bond qualities other than complete bond loss affect the shear capacity in beams.

CHAPTER 3 EXPERIMENTAL PROGRAM

This chapter will focus on experiments conducted in the materials laboratory of the Addis Ababa Institute of Technology (AAIT). The experiment's purpose was to further investigate the role of bond in the shear transfer mechanism (arch and beam action) of slender beams. In the subsections below, the narrative and justification for specimen selection, material properties, specimen manufacturing, test setup and instrumentation are explained.

Seven beams and a trial beam were casted in three groups for the experimental program. The experimental variables being the position of the un-bond or deterioration, the percentage of bond cut and the methods of degrading the bond. All of the beams have a uniform cross section and no web reinforcement was used over the shear span. shear failure was achieved by using an over strength factor of 2.3 based on ACI capacity calculations.

A 2.3 over-strength factor was chosen to compensate for the reduction in flexural capacity. The literature review revealed that un-bonding the longitudinal bars increases the capacity of the beams to the point where some specimens reach their flexural capacity. Because this study focuses on shear capacity, a greater margin between flexural and shear capacity was ideal. Prior to the experiment, shear failure was determined by comparing flexural and shear capacity using manual calculations in accordance with EC, ACI, and CSA codes, as well as modeling the control beam with VECTOR 2D and RESPONSE 2000.

3.1 Specimen

The 7 RC beams had a length of 1.9m (the trial beam had 2m length) with a rectangular cross section with a constant width and depth of 250 and 300 mm, respectively. The sole distinction between the beams are the experimental variables. A trial beam was first casted before the two series to verify the fabrication and instrumentation. Three RC beams are in the first group, while four RC beams are in the second group. The control beam and two beams with un-bonding of 75% of the shear span are in the first group, with the position of un-bonding varied. The second group has un-bonding of 50% and 75% of the shear span and also experiments with the location of un-bonding. The significant difference between the two sets is the method of bond degradation.

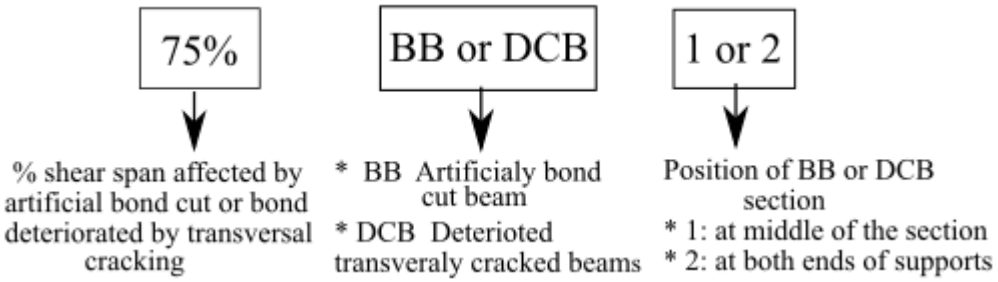

Figure 3-1 Guide for naming of the beams

3.1.1 The trial beam

In the trial phase of the experiment a trial beam was casted. This beam was casted to verify if the fabrication of the DCB series was possible, mainly the formation of the rough surface to avoid the formation of joints. The formation of the rough surface was first tried on a cylindrical section, but the application on larger sections like that of 75DCB1 was questioned.

Figure 3-2 Rough surface formation

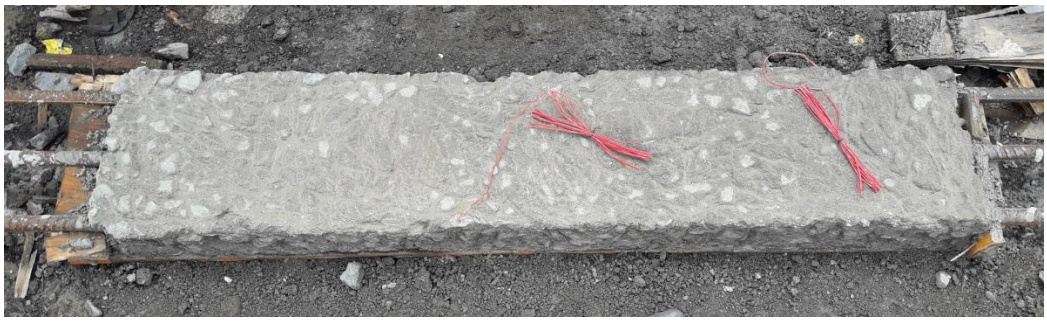

Figure 3-3 The trial beam's damaged concrete section rough surface formation

The second reason for testing a trial beam was to verify that the chosen instrumentations were applicable. On the trial beam the cracks on the damaged concrete were created by loading the section on both sides to create flexural cracks.

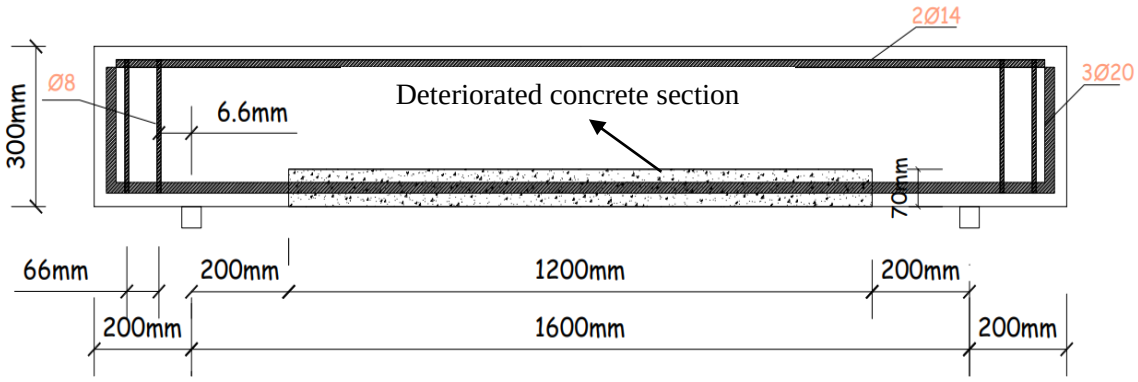

Figure 3-4 Details of the trial beam

3.1.2 The first series (BB series)

The aim of this series was to experiment with almost complete bond loss without altering the shear failure process or the cracking pattern. The variable in this series was the location of unbounding. The BB series includes the control beam, 75BB1 and 75BB2. Despite the fact that PVC pipes are commonly used for bond cutting, the available PVC pipes would leave a considerable gap between the longitudinal bars and the PVC pipe.

In their research, Yang (2014) pointed out that crack spacing is primarily a concern at the reinforcing level in their investigation of crack spacing and width. The surface reinforcement and an effective concrete region $A_{c,\,eff}$ surrounding it can be thought of as a tensile member for flexural members and represent minimum crack spacing (l_t)as

$$l_{t=\frac{f_{ctm\Phi}}{4\times\tau_{bm}\times\rho_{eff}}} \qquad ----------(3.1)$$

where:

τ_{bm}	is the average friction between re-bars and concrete
ρ_{eff}	is the effective reinforcement ratio, $\rho_{eff} = A_s/A_{c,eff}$;
$A_{c,eff}$	effective concrete area
Φ	is the diameter of the rebar
f_{ctm}	is the mean tensile strength of the concrete.

As seen in the equation above, the loss of effective concrete area due to the space between the bar and the PVC could potentially vary the crack spacing, hence influencing the failure process. So other better-fitting choices besides PVC were investigated.

3.1.2.1 The pull out test

The artificially bond loss was finally accomplished with the aid of a gasket, which is commonly used to seal leaks. Because of its workability and snug fit to the longitudinal reinforcement, the material was found to be a better un-bonding material. The effectiveness of its un-bonding was measured using a concentric pullout test that compared the effectiveness of waterproof tape (the other option) and a normal pull out specimen with no un-bonding. The details of pullout experiments are described in detail below.

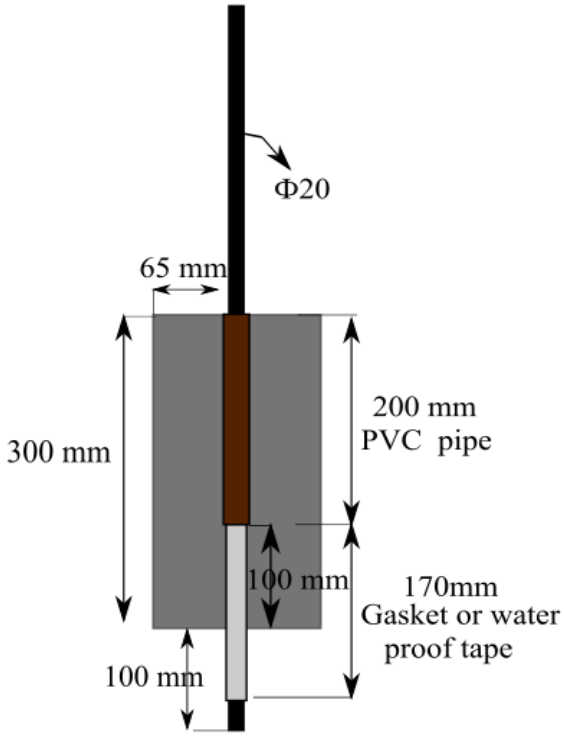

Figure 3-5 Vertical section of the pullout specimen

The first 200mm of the bars in the cylinder are covered by a PVC pipe, followed by 100mm (embedment length) of the bond cutting material (gasket or water proof tape). To facilitate slippage, 70 mm of the bar with bond cutting material was left at the bottom of the cylindrical specimen.

Table 3-1 Details of the pullout specimen

Specimen	Cylindrical specimen		Embedment length	Un-bonding material
	H(mm)	D(mm)		
PP1	300	150	100	waterproof tape
PP2	300	150	100	waterproof tape
PG1	300	150	100	gasket
PG2	300	150	100	gasket
PG3	300	150	100	gasket
PN15	300	150	150	No unbounding

Figure 3-6 Materials used for bond cutting in pullout test

A **B**

Figure 3-7 Bar preparation for the pull out specimen A, using the water proof tape B, using the gasket

Figure 3-8 The pull out specimen

Figure 3-9 Load cell used for pullout test

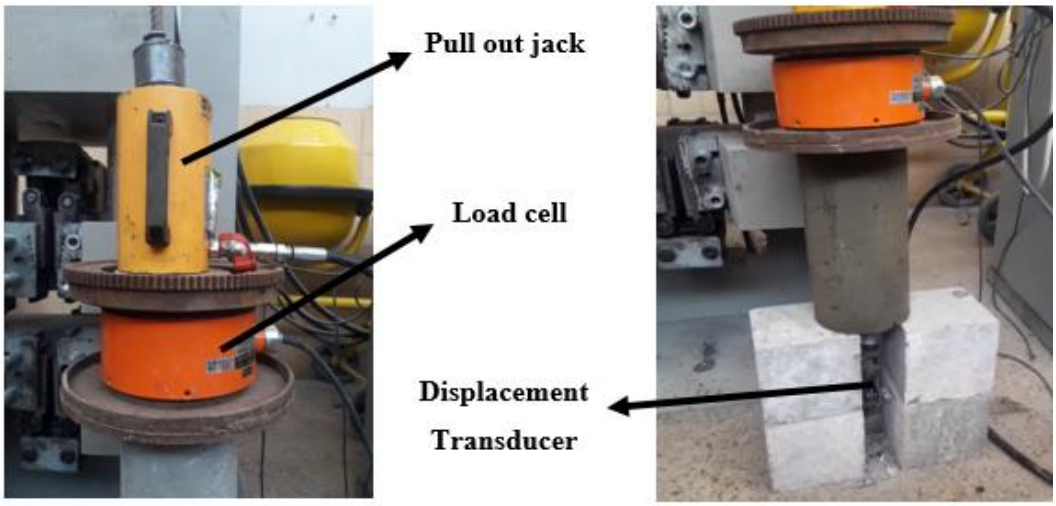

Figure 3-10 Test set up of the pullout test

Different equations and codes proposed by researchers shown on appendix A were considered to avoid splitting failures. The standard embedment length of 5Φ (Φ=20mm l_d=100mm) and a side cover of 3.5Φ (side cover=70mm) were recommended. Because the 70mm side cover mold was unavailable, a 65mm side cover was adapted. Implementing these values was found to be sound because the possibility of split failure while using this

standard was very low due to the unbounding done using gasket and water proof tape in the pullout specimen. To measure the slip of the test, the bar was extended 100mm below the cylinder. In the experiment, a load cell and a transducer were used to monitor the load and the slip at the bottom of the cylinder, respectively. The result showed that the gasket has a better bond cutting property than that of the waterproof plaster.

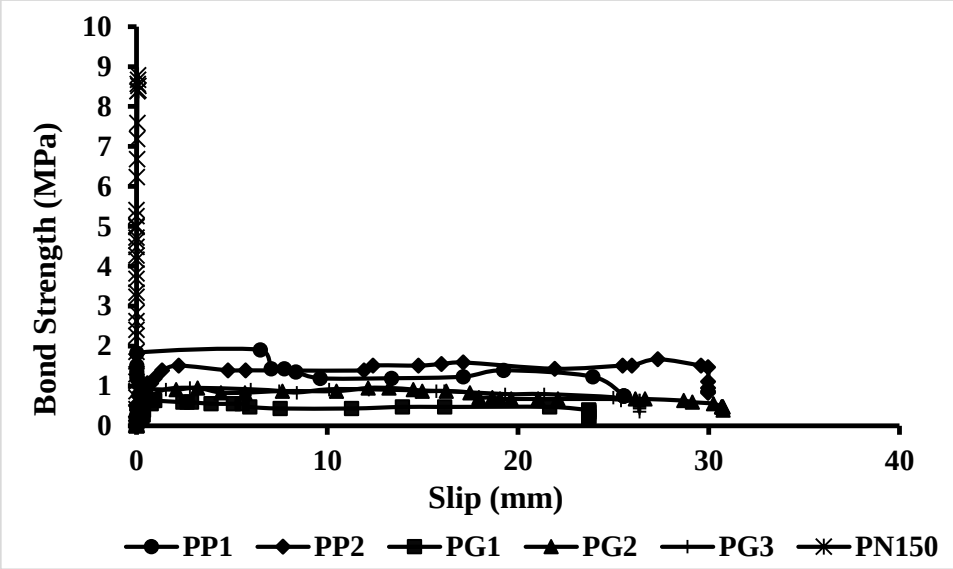

Figure 3-11 Slip Vs bond stress result of pullout test

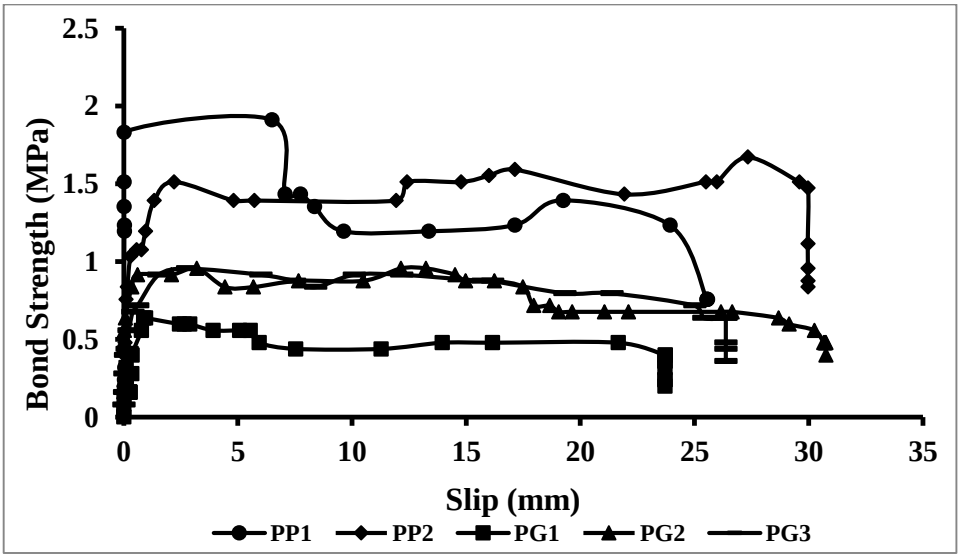

Figure 3-12 Comparison b/n the gasket and water proof tape pullout results

Based on the pullout test results the BB series is constructed with unbounding of the bottom longitudinal bars using gasket. The details of this series are as shown below. The black rectangular block represents the areas that is covered by the gasket.

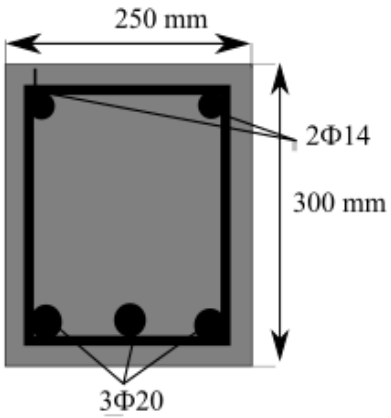

Figure 3-13 Cross section of all specimen

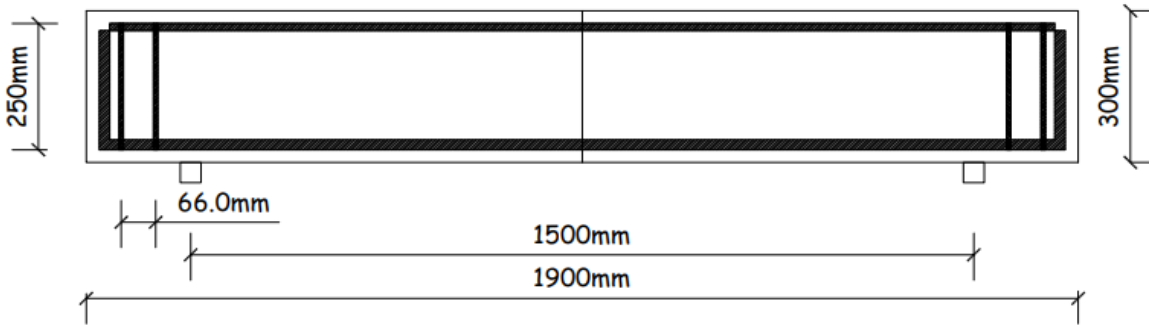

Figure 3-14 Details of the control beam

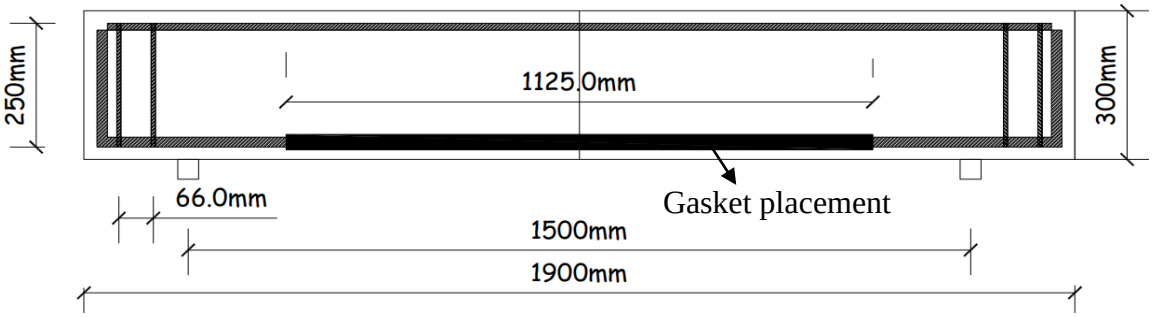

Figure 3-15 Details of beam 75BB1

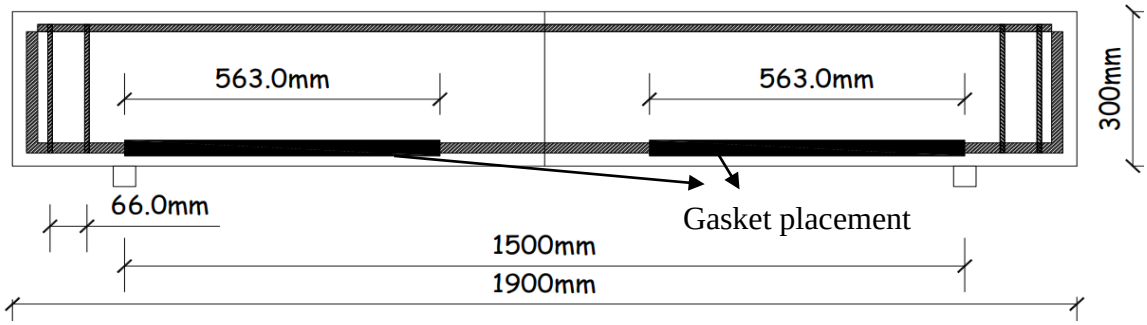

Figure 3-16 Details of beam 75BB2

3.1.3 The second series (DCB series)

This series was created to investigate how a bond loss caused by transversal cracking affects shear capacity, taking into account variables like the percentage of the shear span length affected and the location of the concrete damage. This series includes beams with concrete damage along the longitudinal reinforcement. The concrete damage was created by forming rectangular sections (damaged concrete sections) and inserting this sections in selected positions during casting of the beams. The concept of average strain (ΔL/L) was used to inflict the same level of damage on all of the specimens. This was accomplished by facilitating the formation of cracks by inserting slits in the effective area of concrete surrounding the reinforcement that is influenced by the bond (effective embedment zone). These slits were only placed in the effective embedment zone. The calculations for the number of slits and position are shown in Table 3-2.

Table 3-2 Number of slits calculation

Specimen	Total length(mm)	$S_{r,max}$ (mm)	Number of slits	$\frac{\Delta L}{L}$	Number of slits used
75DCB1	1125	140	8.036	0.00714	8
75DCB2	1125	140	8.036	0.00714	8
50DCB1	750	140	5.357	0.00714	5
50DCB2	750	140	5.357	0.00714	5

Recommendations of both CEP-FIP and Euro Code were considered as shown from figures below. The CEP-FIP recommends to consider the area around the bar that is inside 7.5Φ from the surface of the bar as the effective embedment zone.

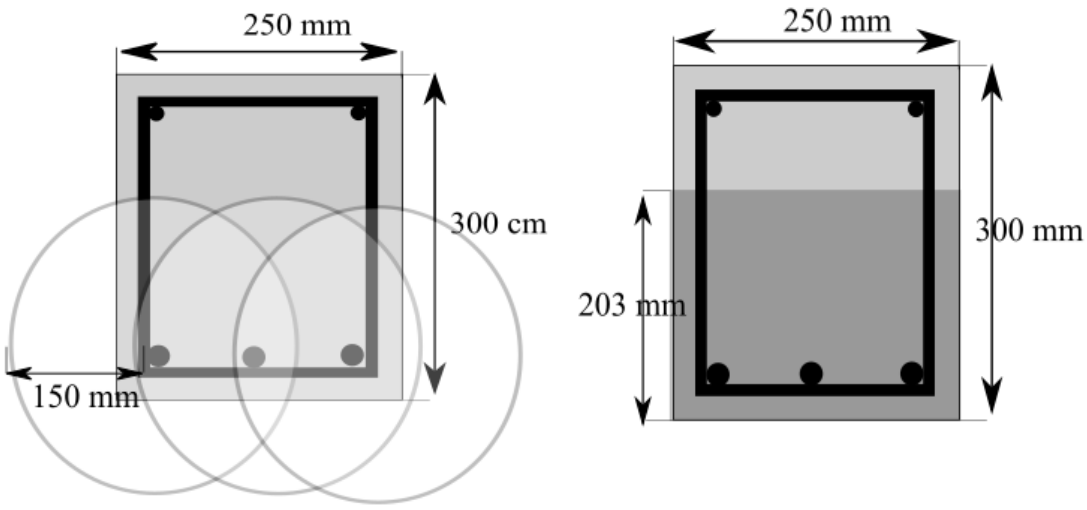

Figure 3-17 CEP-FIP Effective embedment zone

The Euro Code puts forward the following figure and formula to determine the effective embedment zone.

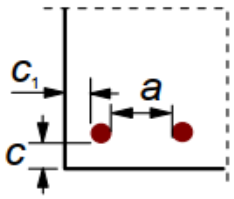

Figure 3-18 Euro Code effective embedment parameters

$$a = \frac{b - (2 \times c_1 + s \times \Phi)}{n} \quad \text{(3.2)}$$

$c_1 = 25m$, $c = 25mm$, n= $number\ of\ space\ between\ bars$ and s= $no\ of\ bars$

$$a = \frac{250 - (2 \times 25 + 3 \times 20)}{2}$$

$$a = 35, cd = 25mm$$

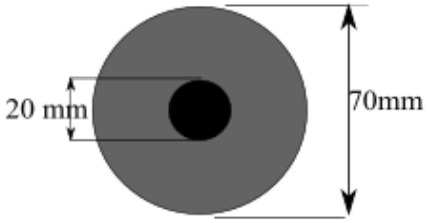

Figure 3-19 Euro Code effective embedment zone

The Euro Code recommendations are employed in this study. So, the total diameter of the section that is influenced by the bond is 70mm. Since the fabrication of a cylindrical section with a reinforced bar in the middle was found to be difficult, a rectangular section was utilized as shown in the figure below.

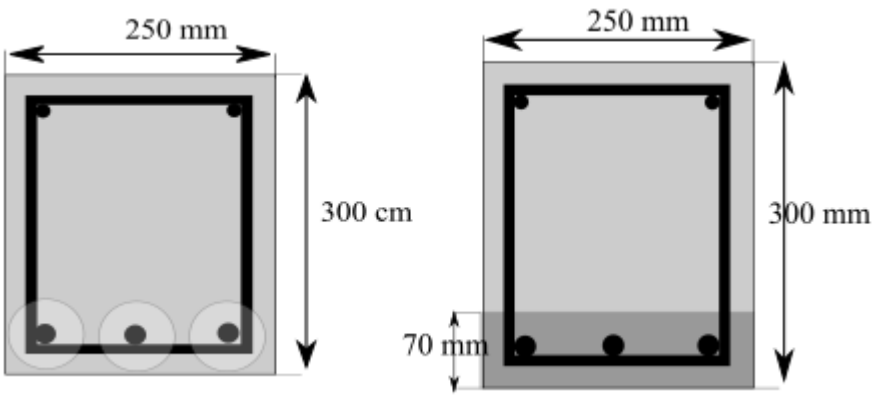

Figure 3-20 The effective embedment zone implemented

In the case of the slits that are used to facilitate cracking, an appropriate crack spacing was chosen using the euro code recommendations for maximum crack spacing ($s_{r,max}$) to decide their placement.

$$s_{r,max} = 3.4c + \frac{0.425 k_1 k_2 \Phi}{\rho_{p,eff}} \quad (3.3)$$

Φ is the bar diameter. Where a mixture of bar diameters is used in a section, an equivalent diameter, Φ_{eq}, should be used. For a section with n_1 bars of diameter Φ_1 and Φ_2 bars of diameter $\Phi 2$, the following expression should be used.

$$\Phi_{eq} = \frac{n_1 \Phi_1^2 + n_2 \Phi_2^2}{n_1 \Phi_1 + n_2 \Phi_2} \quad (3.4)$$

C is the cover to the reinforcement

K_1 is a coefficient which takes account of the bond properties of the bonded reinforcement:

= 0,8 for high bond bars

= 1,6 for bars with an effectively plain surface (e.g. pre-stressing tendons)

k_2 is a coefficient which takes account of the distribution of strain

= 0,5 for bending

= 1,0 for pure tension

Table 3-3 Detail calculation of crack spacing

Parameter	Value	Unit
c	25	mm
φ	20	mm
d	265	mm
x	123	mm
b	250	mm
h	300	mm
As	942	mm^2
k_1	0.8	
k_2	0.5	
$h_{c,ef}$	59	mm
$A_{c,eff}$	14750	mm^2
$\rho_{p,eff}$	0.063864407	
$S_{r,max}$	138.24	mm

The crack spacing for the beam with dimensions 25cm x 30cm and with the specifics of the specimens were found to be 138mm. The formation of crack at the position of the slits was made sure by loading trial damaged concrete sections. As it could be seen from figure 3-21 the cracks formed at locations the slits were placed after loading of the damaged concrete section.

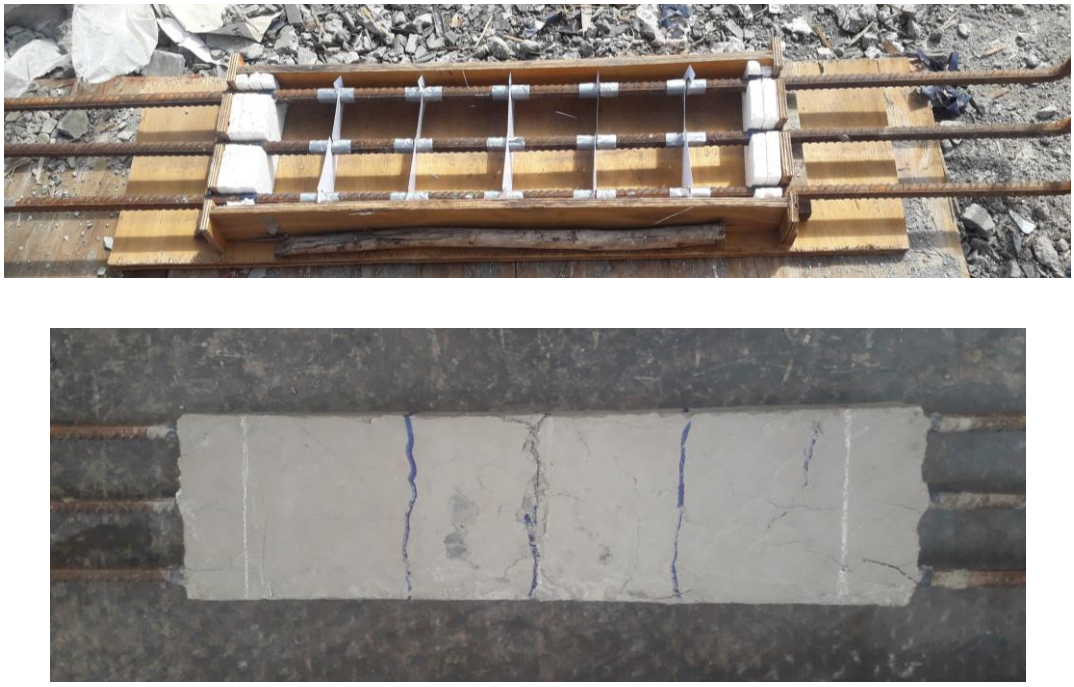

Figure 3-21 Cracks formed after trial damaged concrete section loading

The final issue to address is the likeliness of the cracks formed by the slits to actual cracks. Normally, when a visible crack is formed, there is an area around the crack that is also experiencing smaller and less prominent cracks that cause a bond deterioration. This can be seen in K. Maekawa, A. Pimanmas and H. Okamura,2003.

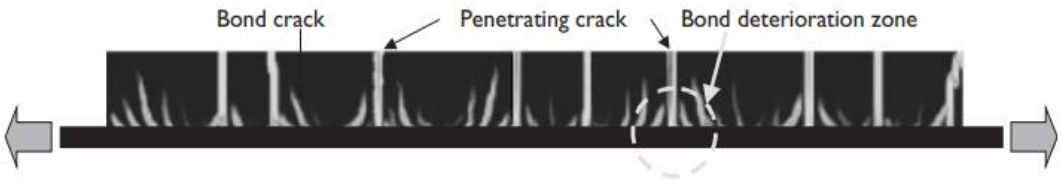

Figure 3-22 Visual of bond deterioration zone (K. Maekawa, A. Pimanmas and H. Okamura,2003)

(Qureshi & Maekawa, 1996) and (Soltani, An, & Maekawa, 2003) assumed that bond stress declines linearly to zero at a distance of 5d from the crack surface and drops abruptly at a distance of 5d from the crack surface. In their bond deterioration model, Salem & Maekawa (1999) gave a bond deterioration zone value that depends on the value of crack spacing. Because the conical splitting fractures cannot physically connect when the crack spacing drops below 10d, the length of the bond deterioration cannot logically equal 5d. Concrete spalling is also impossible when the crack spacing is less than 5d. As a result, when the crack spacing is less than 5d, the bond degradation length is assumed to be zero, and it changes linearly from zero to 5d when the crack spacing changes from 5d to 10d.

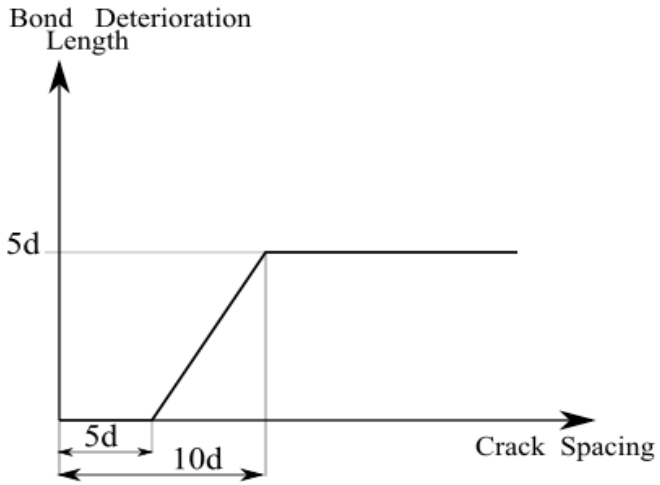

Figure 3-23 Model for the bond deterioration zone (Salem and maekawa,1999)

In this study, the bond deterioration zone was created by winding a waterproof tape on the bar adjacent to the placement of the slits with a length calculated according to the crack space previously. This value 30mm was determined according to the graph shown above. And was applied on both sides of the slit. The details of each specimen deteriorated concrete section is shown in Appendix B.

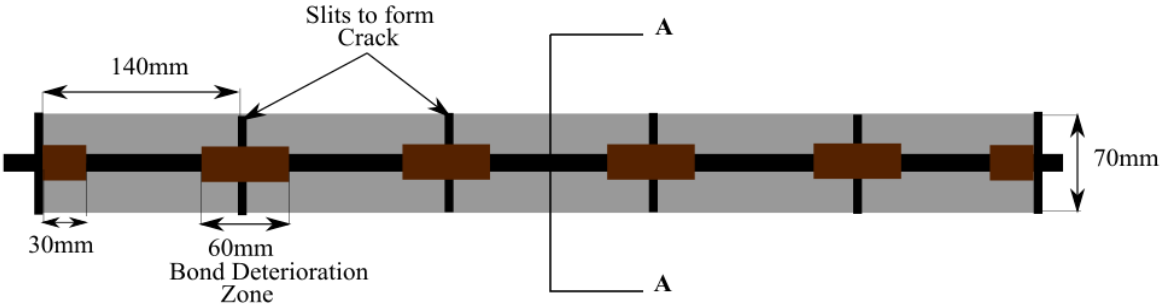

Figure 3-24 Positioning of slits and bond deterioration zones in the damaged bond section

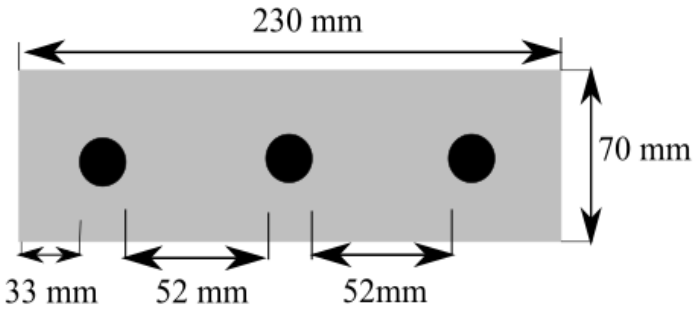

Figure 3-25 Cross section A-A

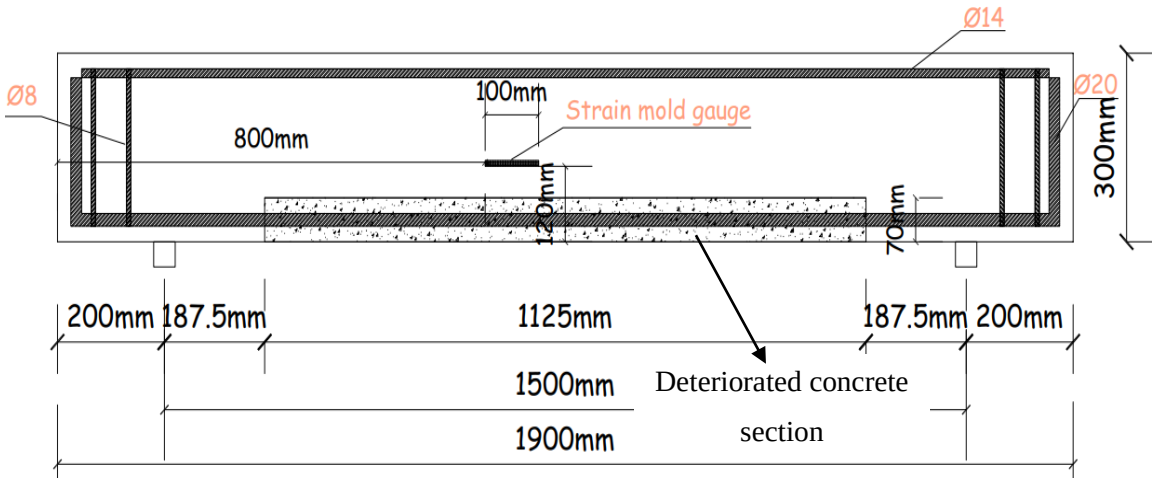

Figure 3-26 Details of beam 75DCB1

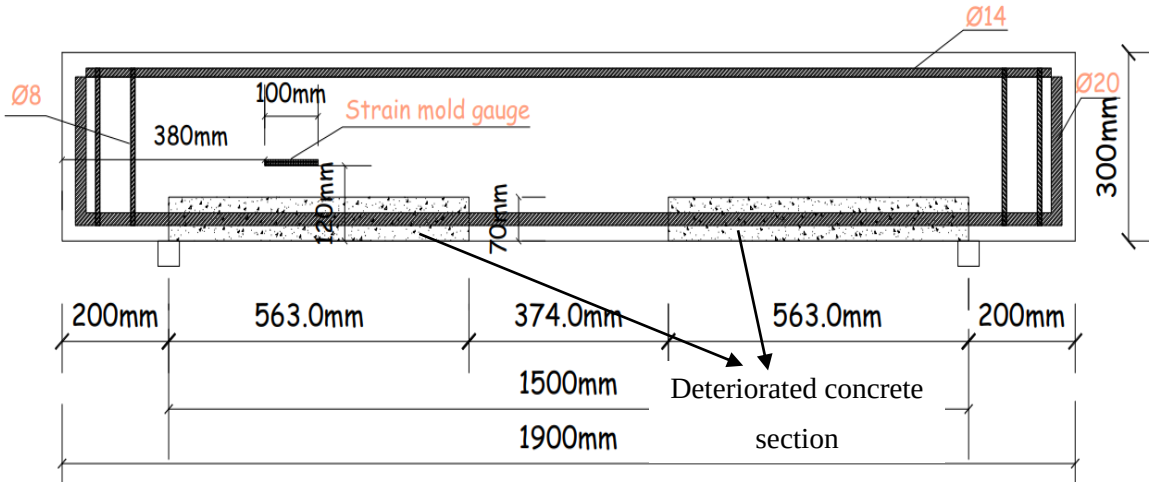

Figure 3-27 Details of beam 75DCB2

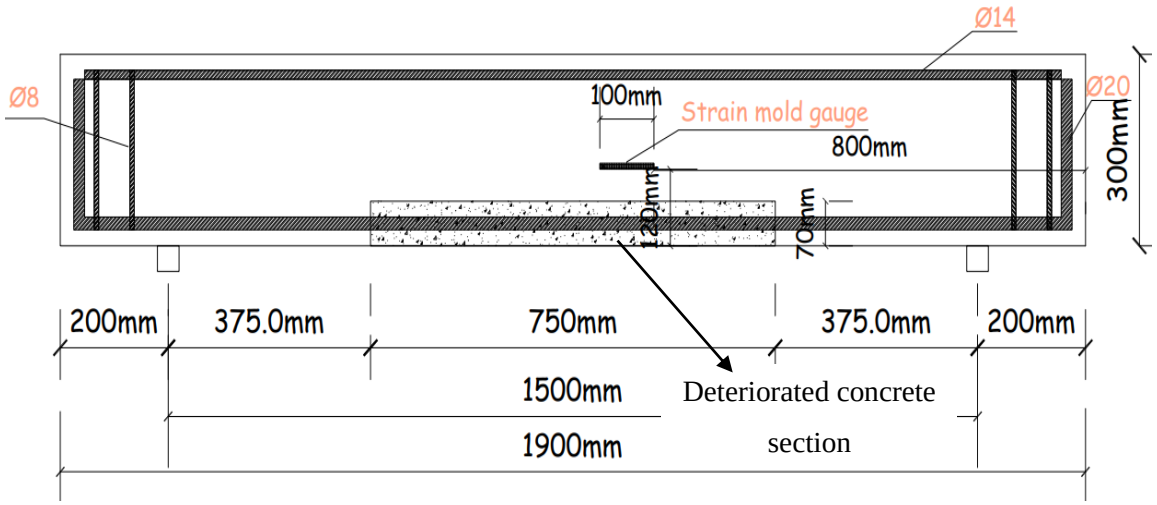

Figure 3-28 Details of beam 50DCB1

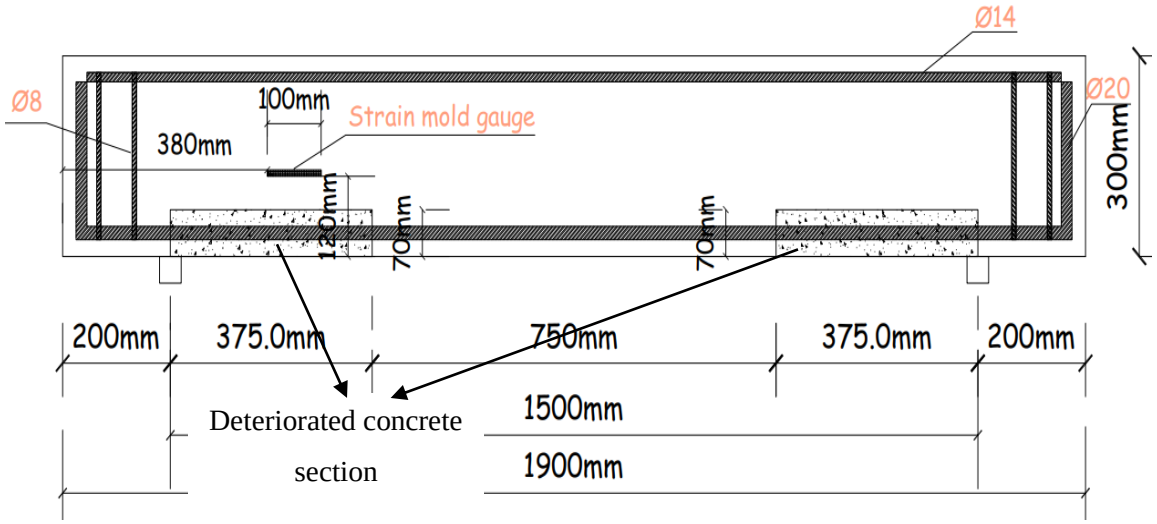

Figure 3-29 Details of beam 50DCB2

The strain mold gages were placed in the middle of the section not on surface, this could be observed in the instrumentation section of this chapter.

Table 3-4 Details of experiment specimen

Specimen	Set	Dimension L/W/H	Reinforcement		% of shear span affected by bond cut or concrete damage	Position of bond cut
			Top bars	bottom bars		
Trial beam		2 m /25cm/30cm	2Φ14	3Φ20	75%	at middle
CB	BB series	1.9m/25cm/30cm	2Φ14	3Φ20	0%	-
75BB1		1.9m/25cm/30cm	2Φ14	3Φ20	75%	at middle
75BB2		1.9m/25cm/30cm	2Φ14	3Φ20	75%	near supports
75DCB1	DCB series	1.9m/25cm/30cm	2Φ14	3Φ20	75%	at middle
75DCB2		1.9m/25cm/30cm	2Φ14	3Φ20	75%	near supports
50DCB1		1.9m/25cm/30cm	2Φ14	3Φ20	50%	at middle
50DCB2		1.9m/25cm/30cm	2Φ14	3Φ20	50%	near supports

3.2 Material

The concrete compressive and tensile strengths for each series were collected directly from the three castings in the experiment. The mechanical behavior of longitudinal and transverse reinforcements was also obtained from AAIT's material testing laboratory experiments.

3.2.1 Concrete

The concrete mix was designed according to the ACI mix design recommendations using Ordinary Portland cement, after implementing the necessary tests to determine the coarse and fine aggregate properties. Before the necessary tests were carried out, a silt test on the fine aggregate was carried out, and the coarse aggregate was sieved, so the maximum aggregate size was 25mm. A trial mix was run to confirm target strength. Cubic and cylindrical concrete specimens were casted with every casting to determine the compressive and tensile strength of the concrete beams. Cylinders and cubes specimens were tested using a compression testing machine.

Table 3-5 The mix design and aggregate properties

Properties	Value	Unit
Coarse Aggregate		
Dry rodded mass	1570.03	kg/m^3
Water content	2	%
Absorption	1.54	%
Fines modulus	2.6	
Nominal Aggregate size	25	mm
Sand		
Water content	8	
Absorption	0.8	
Mix design details		
Slump	75-100	mm
Mixing water	193	kg/m^3
Amount of entrapped air	1	%
W/c ration	0.54	
Cement	357.4074	
Aggregate, volume	0.69	
Aggregate, mass	1083.321	kg
Assumed mass of wet concrete	2380	kg
Fine aggregate, mass	746.2719	kg

Table 3-6 Mix design results

Material	Amount(kg)
Cement	357.407
Sand	838.374
Aggregate	1104.987
Water	132.125

[

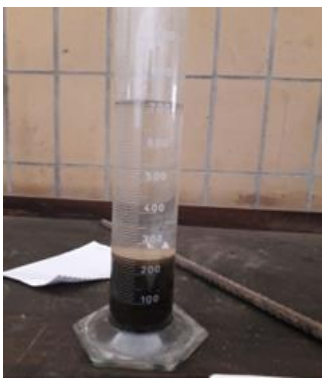

Figure 3-30 The silt test and concrete property testing

Table 3-7 Trial beam concrete compressive strength

Sample	Days	Failure Load(kN.)	Compressive Stress (MPa)	Average cubic stress(MPa)	Fc,Cylinderical (MPa)
1	91	805.3	35.79	34.2	27.36
2	91	795.8	35.37		
3	91	797.5	31.44		

Table 3-8 Concrete compressive strength of damaged concrete section in trial beam

Sample	Failure Load (kN.)	Compressive Stress (MPa)	Average cubic stress(MPa)	Fc,Cylinderical(MPa)
1	819.3	36.41	35.09	28.07
2	754.3	33.53		
3	795.1	35.34		

Table 3-9 BB series concrete compressive strength

Sample	Days	Failure Load(kN.)	Compressive Stress (MPa)	Average cubic stress (MPa)	Fc,Cylinderical(MPa)
1	120	905	40.21	42.1425	33.714
2	120	961.9	42.75		
3	121	970.4	43.13		
4	121	955.9	42.48		

Table 3-10 BB series concrete tensile strength

Sample	Days	Failure Load (kN.)	Tensile Stress (MPa)	Average (MPa)
1	121	155.2	3.45	3.23
2	121	123.7	2.75	
3	121	144.6	3.21	
4	121	165	3.5	

Table 3-11 DCB series concrete compressive strength

Sample	Days	Failure Load (kN.)	Compressive Stress (MPa)	Average cubic stress (MPa)	Fc,Cylinderical(MPa)
1	95	395.1	22.36	18.91	18.91
2	95	301.6	17.06		
3	95	305.8	17.31		

Table 3-12 DCB series concrete tensile strength

Sample	Failure Load (kN.)	Tensile Stress (MPa)	Average(MPa)
1	117.7	2.54	2.66
2	115.7	2.51	
3	137.6	2.94	

Table 3-13 Concrete compressive strength of damaged concrete section in DCB series

Sample	Failure Load(kN.)	Compressive Stress (MPa)	Average cubic stress (MPa)	Fc,Cylinderical(MPa)
1	643	28.57	30.12	24.1
2	699.6	31.09		
3	690.7	30.7		

3.2.2 Steel

In the research, all of the rebar was ribbed. And to determine the stress-strain relationship, a tensile test was conducted. The mechanical properties of the bars are shown in the table below.

Table 3-14 Mechanical property of reinforcement bars

Bar diameter	Position	Yield stress (MPa)	Failure stress(MPa)
Φ8	transversal	589.37	749.82
Φ14	longitudinal	511.69	776.78
Φ20	longitudinal	633.02	729.10

Figure 3-31 Steel mechanical property testing machine

3.3 Specimen fabrication

In the fabrication of the beam specimen a wood formwork was used to achieve a smooth finishing.

3.3.1 Trial beam fabrication

The trial beam was fabricated with a damaged concrete section with the specifications of the beam 75DCB1, with the only exception being the formation of the damage. The damaged concrete section shown in the figure was cast and a rough finish was achieved by removing the aggregates within hours of casting. This section is then loaded on both sides to form flexural cracks after a week. Then, top bars are added to the section to form the bar detail of the trial beam. Finally, the damaged concrete section is inserted into the formwork and the trial beam is cast.

Figure 3-32 Form work for trial beam damaged concrete section

Figure 3-33 Trial beam damaged concrete section with roughened surface

Figure 3-34 Trial beam damaged concrete section loading

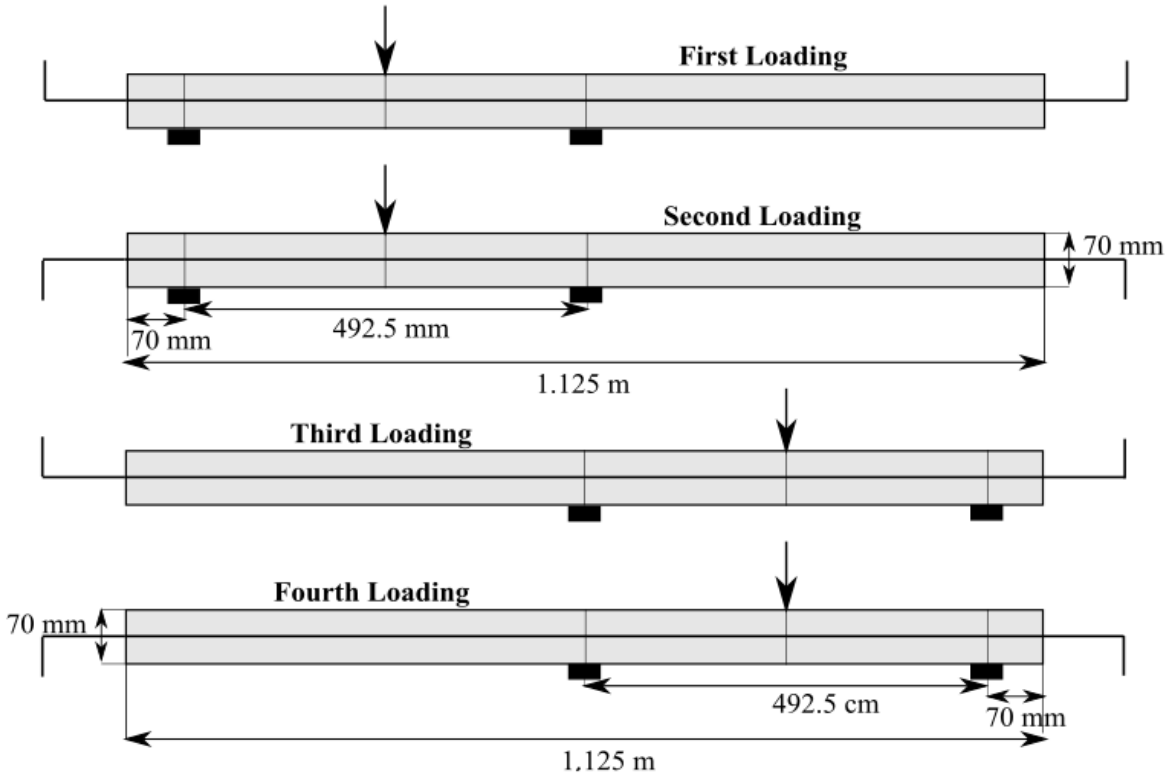

Figure 3-35 Trial beam damaged concrete section loading procedure

Figure 3-36 Placing of the top bars to the damaged concrete section

Figure 3-37 Placing of the damaged concrete section inside the trial beam formwork

3.3.2 The fabrication of first series (BB series)

In the first set of castings, the reinforcements were prepared by using the un-bonding material (gasket). The material was applied in the appropriate locations shown in figure 3-13, 3-14 & 3-15 and placed in the formwork after drying. The application of the gasket was assisted by oil for workability and a smooth finish.

Figure 3-38 75BB1 beam application of gasket

Figure 3-39 75BB2 beam application of gasket

Figure 3-40 Finshing of the first series (BBseries) casting

3.3.3 The fabrication of the second series (DCB series)

In the second set, the rectangular damaged concrete section was cased and allowed to dry. The slits that are used for the facilitation of cracks were fabricated by laminating paper and cutting openings for the bottom longitudinal reinforcements. These slits were placed at the calculated crack positions, and the bond deterioration zone was addressed by winding of the water-proof tape at the calculated length. This could be seen on figure 3-41

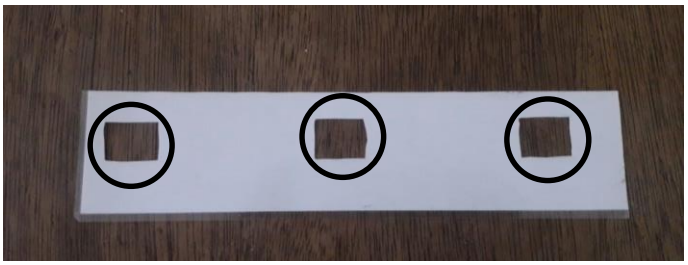

Holes in the laminated paper for the reinforcements to pass through

Figure 3-41 laminated paper used for slit formation

Figure 3-42 The bond deterioration imitation by winding water proof tape

Figure 3-43 Placement of the laminated paper slit

Figure 3-44 Casting of the damaged bond concert sections

Since the next step was to insert the damaged concrete sections in to the beam formworks and cast the whole beam avoidance of joint between the two castings is paramount. To avoid the formation of a joint, the surface of the damaged concrete section was roughened to facilitate bonding between the two castings by removing the aggregate. The roughness of the section was measured using a sand patch test (This test method is used to determine the average depth of voids beneath the surface's high points of a road surface). On each damaged bond specimen, two circles with a diameter of 50mm were marked, and one was chosen at random to be subjected to the sand patch test. The Euro Code recommends the following formula and standard to determine the roughness parameter.

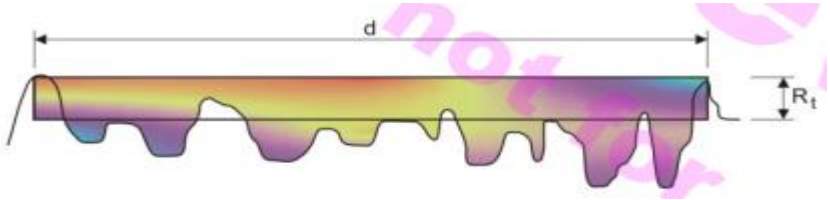

Figure 3-45 Principle of sand area method for the qualification of the roughness of an interface

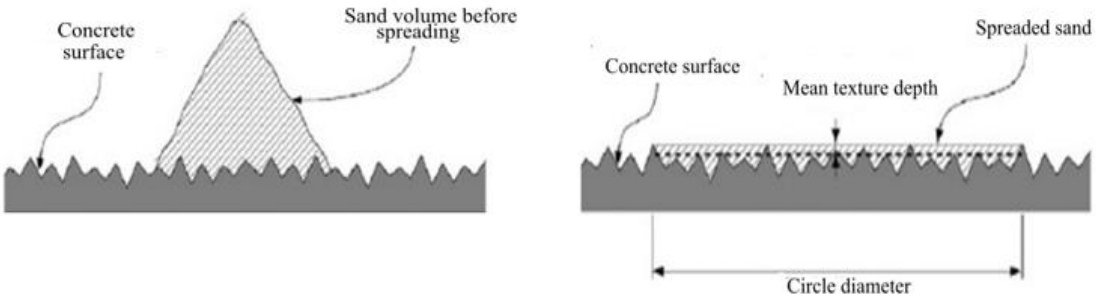

Figure 3-46 the process followed during sand patch test

$$R(mm) = \frac{40 \times V(mm^3)}{\Pi \times d^2} \quad ------------(3.5)$$

Table 3-15 Roughness Euro Code standard(de Normalisation & NORMUNG, 2003)

Surface Condition	Roughness Parameter (r)
Not Measurable(Very Smooth)	-
Smooth	<1.5mm
Rough	≥1.5mm
Very Rough	>3mm

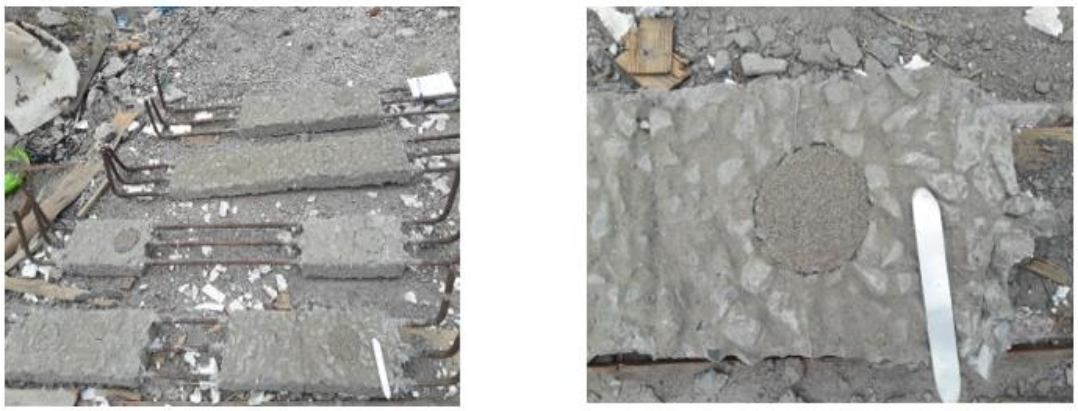

Figure 3-47 Patch selection of the sand patch test in damaged bond concrete sections

The roughness of the deteriorated bond concrete sections in the DCB series are quantified in the table shown below.

Table 3-16 The result of the sand patch test

Specimen	patch 1	patch 2	Volume(mm^3)	d(mm)	R(mm)	remark
75DCB1	×		24000	50	12.22	Rough
75DCB2	×		25000	50	12.73	Rough
50DCB1		×	20000	50	10.18	Rough
50DCB2		×	22000	50	11.20	Rough

In the second set of specimens, to monitor the amount of shear transferred to the web of the cross section, a strain mold gage was positioned above the damaged bond concrete section. Normally, strain mold gauges are small gauges implanted in concrete or mortar for use in loading tests as well as other purposes. They can also be incorporated into smaller test subjects. The gauges' backing material is made of super engineering polymers, which is water resistant.

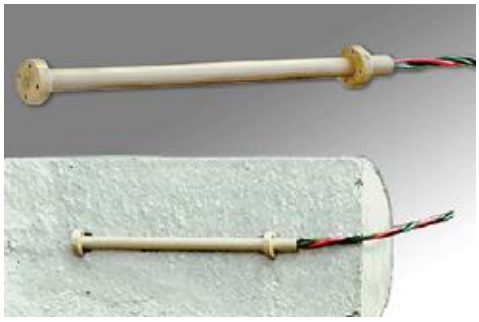

Figure 3-48 A typical manufactured strain mold gauge

In this study, a similar device was created by attaching a concrete surface strain gage on a piece of mica and winding this prototype with water-proof tape to prevent damage and add water resistance. Another option was to use aluminum instead of mica, but this was ruled out due to noise in the measurement. To test the accuracy of the fabricated strain mold gage, it was placed vertically in a cylindrical mold with diameter 10cm & height 20cm along the height at the center of the section. The cylinder specimen was casted, and after 3 days, the compressive strength of the specimen was tested while the strain gage reading was monitored.

Figure 3-49 Fashioning of the mold strain gage

Figure 3-50 Placement and finished look of strain mold gage

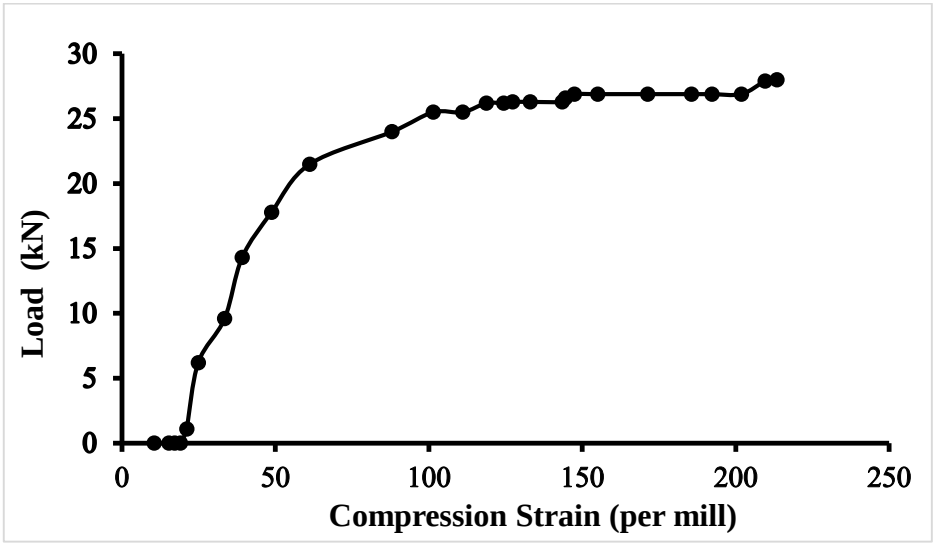

Figure 3-51 Load Vs strain of mica strain mold gage

Calculating the strain at failure and cross referencing it with the reading was used to verify the accuracy of the fashioned strain mold gage. The compressive strain measurement does not start from the origin of the graph because the specimen was experiencing strain caused by shrinkage prior to loading of the specimen. The location of the mold gage and the rationale behind it in the DCB series will be discussed in the instrumentation subtopic of this chapter.

Figure 3-52 Placing of the mold strain gage

Figure 3-53 Placement of the damaged bond section and casting of the second set of beams

3.4 Test set up

The beams were placed on two steel rollers and one-point monotonic loading was applied to the center of the beam until failure. A hydraulic jack, a displacement transducer and a surface measurement were all part of the test setup. A 1.5m shear span was used. To distribute the load and avoid local concrete crushing, a thick metal plate with a width of 13 cm was placed beneath the load cell.

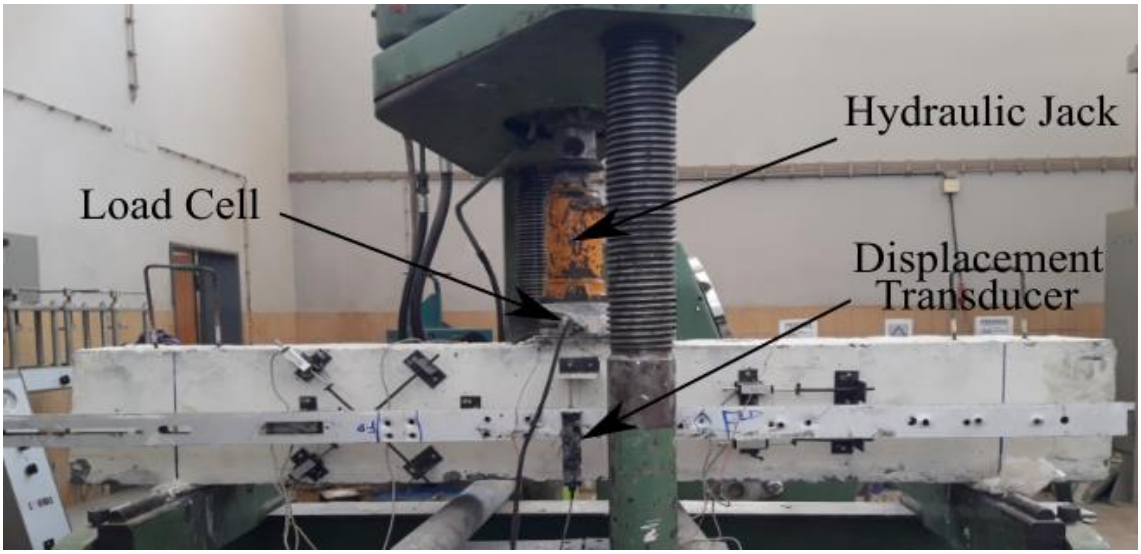

Figure 3-54 Test set up of the tests

Figure 3-55 Hydraulic jack and the load cell used for one point loading

3.5 Instrumentation

The instrumentation of the experimental program was designed to measure shear strain, shear transfers to the web and loading progression with deflection. This was accomplished by the use of load deflection monitoring, surface measurements, mold strain gage measurement and crack pattern monitoring.

The load-deflection progression was measured by the load cell and transducer connected to the data logger. The surface measurement included 5 DATA transducers connected to DATACOM system and setup at the locations shown in figures 3-56 and 3-57 to measure the shear strain. The strain mold gages were also placed in each beam of the second set at locations where the load application wouldn't disturb the reading as shown in figure 3-26

up to figure 3-29. To track the progress of cracking, a grid was drawn on the available parts of the beam specimens. For ease of interpretation, vertical lines on the beam at the beginning of the artificial bond cutting (gasket) and the deteriorated bond concrete section were drawn, and also the location of the mold gages in the second set is shown by a horizontal line on the surface of the beam.

Figure 3-56 Surface measurement instrumentation set up of the trial beam

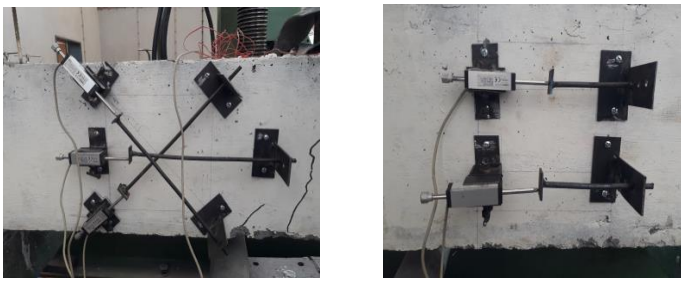

Figure 3-57 Close up of the trial beam surface measurement instrumentation

Following the trail beam testing, the following instrumentation (Figure 3-56 and 3-57) was applied to the remaining 7 beams. This includes measurements of the shear from surface instrumentation with two different gages (28 cm and 14cm) and a grid for monitoring crack patterns. The surface monitoring system was used to monitor the shear strain values at the front and back of the beam. The front surface monitoring system measurement was taken on a 20cm x 20cm area with a gage of 28 cm, while the back monitoring system monitoring system was taken on a 10cm x 10cm area with a gage of 14 cm.

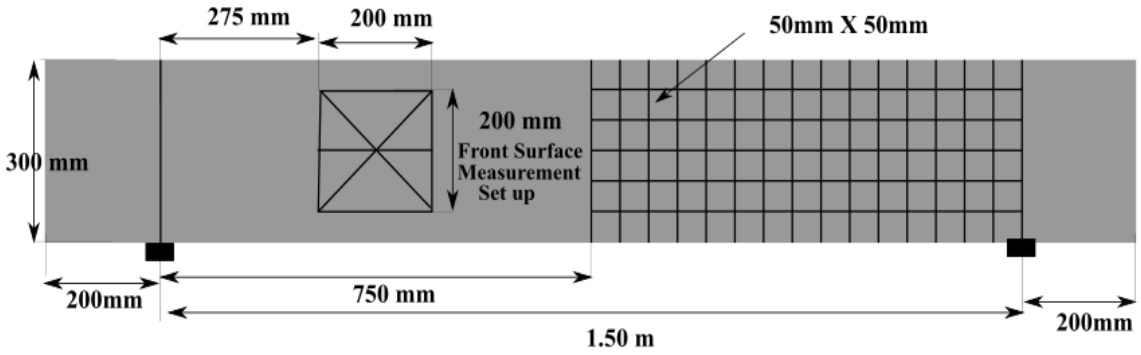

Figure 3-58 The front side surface measurement set up

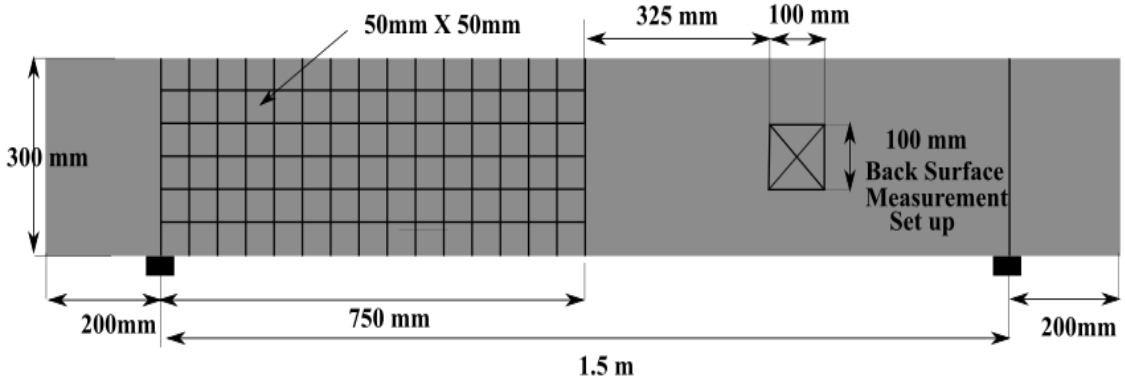

Figure 3-59 The back side surface measurement set up

Front side

Back side

Figure 3-60 A surface measurement set up on series BB and DCB

Figure 3-61 The DATA COM transducers

Figure 3-62 The data logger system

Figure 3-63 The DATA COM transducers monitoring system

CHAPTER 4 FEM ANALYSIS USING VECTOR 2D

4.1 About the software

VECTOR © is a collection of computer programs for nonlinear finite element analysis of reinforced concrete (NLFEARC). Over the last two decades, researchers at the University of Toronto have been studying reinforced concrete behavior and applications of the finite element method. These programs enable more accurate assessments of structural performance (strength, post-peak behavior, failure mode, deflections, and cracking) than linear-elastic methods by combining a variety of realistic nonlinear models for reinforced concrete with the powerful analytical capabilities of finite element analysis. Simultaneously, the finite element method facilitates analysts to address the composite nature of reinforced concrete material, changing material properties due to progressive cracking, challenging geometries and loadings – complexities that conventional analysis techniques may not be able to address.

VecTor2 is a two-dimensional reinforced concrete membrane structure analysis nonlinear finite element program. The program has been developed at the University of Toronto since 1990, when it was known as TRIX. This advancement coincided with experimental tests that confirmed VecTor2's ability to predict the load-deformation response of a variety of reinforced concrete structures with well-distributed cracking when subjected to short-term static monotonic, cyclic, and reverse cyclic loading. The Modified Compression Field Theory (Vecchio and Collins, 1986) and the Disturbed Stress Field Model (Vecchio, 2000) serve as the theoretical foundations for VecTor2 – analytical models for predicting the response of reinforced concrete elements subjected to in-plane normal and shear stresses. Cracked concrete is represented by VecTor2 as an orthotropic material with smeared, rotating cracks. To generate an efficient and robust nonlinear solution, the program employs an incremental total load, iterative secant stiffness algorithm.(Wong, Vecchio, & Trommels, 2013)

4.2 Specimens

From the all of the specimens that were experimented on only the beams in the BB series were modeled using the VECTOR 2 software. because of the complex nature of fabrication of the trial beam and the DCB series the 2D software was not equipped to handle the modeling of this beams

Table 4-1 Detail of modeled specimen

Specimen	Set	Dimension L/W/H	Reinforcement		% length of bond cut / concrete damage	Position of bond deterioration
			top	bottom		
Control	BB series	1.9m/25cm/30cm	2Φ14	3Φ20	0%	-
75BB1		1.9m/25cm/30cm	2Φ14	3Φ20	75%	at middle
75BB2		1.9m/25cm/30cm	2Φ14	3Φ20	75%	near supports

4.3 Material

In the input side of the software concerning concrete properties the cylindrical compressive and tensile strength values were inserted while other parameters are calculated by the software depending on the values inserted. In case of the reinforced bars the values of yield and ultimate strength including stiffness were inserted and other values were calculated using the default settings. All of this values used as an input were determined from AAIT material lab property testing and are mentioned in the chapter 3. The program calculates appropriate values using the following formulas.

Initial Tangent Modulus, E_c	$E_c = 5500\sqrt{f_c}\ MPa$
Cylinder Strain at peak strength, e_o	$\varepsilon_o = 1.8 + 0.0075\, f'c\ \ mill\ strain$
Thermal Expansion Coefficient	10×10^{-6} /°C
Density	2400 kg/m^3

4.4 Modeling

Before the modeling of the beams it was decided that, since the beams were symmetric it was better to model half of the beam for sake of a greater number of mesh resulting an accurate result. Two concrete materials were characterized for sections, one that has a web

reinforcement and another which does not. The stirrup was modeled as smeared reinforcement and the longitudinal reinforcements were placed at appropriate locations.

To characterize the bond loss in the BB series was characterized by choosing the unbounded bar or tendon option on the define bond properties part of the software. For portions of the bottom longitudinal reinforcement that are not covered by the gasket material a truss reinforcement with perfectly bonded over the entire length is chosen. For section where the gasket material used a link element is used as presented.

4.5 Loading and Support conditions

The beams were simply supported with 1.5 m distance between the supports. Since half of the beam was modeled with the left side of the beam was restrained in the y direction only. On the right of the beam the beam was restrained only in the x direction as shown in the figures below. Steel plates were placed at the support and at point of loading. a displacement controlled loading was preferred in the analysis.

4.6 Results of the FEM models

The result load deflection analysis of the beams modeled using VECTOR 2 are presented

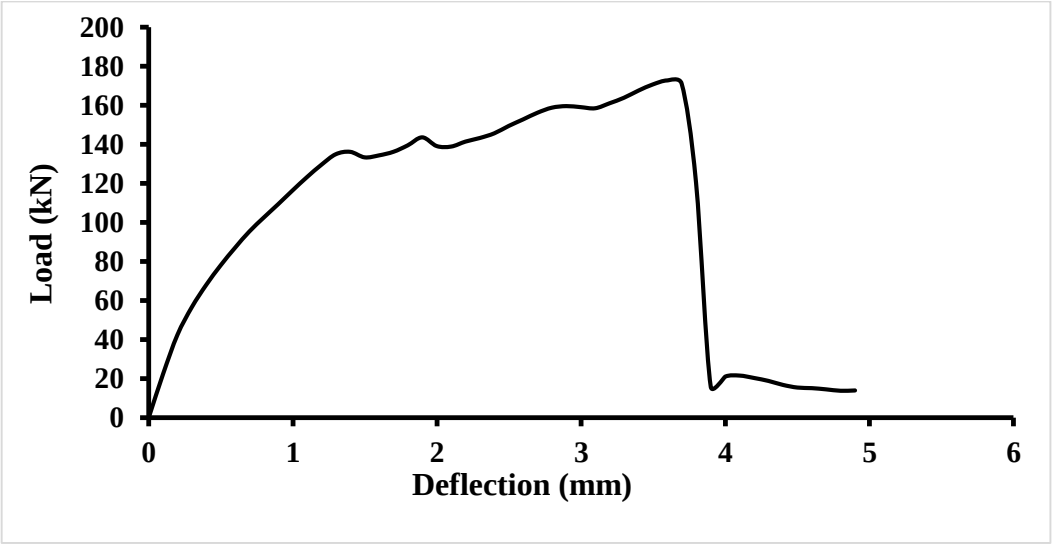

Figure 4-1 FEM control beam load vs deflection analysis

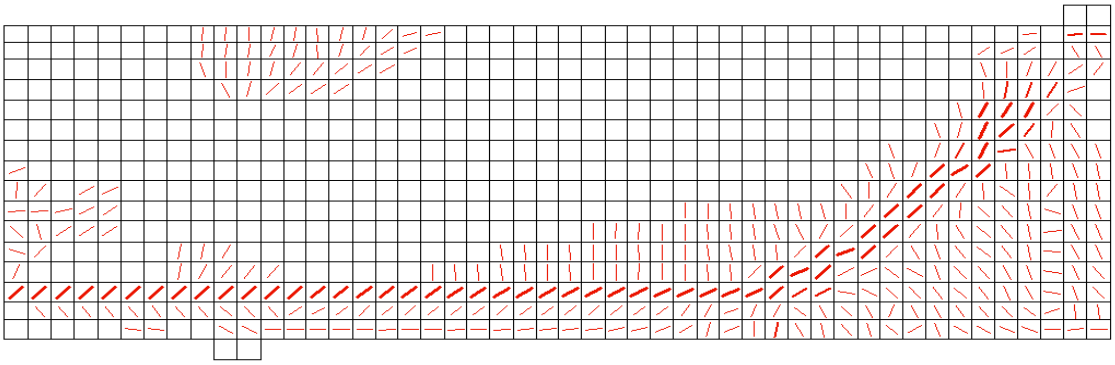

Figure 4-2 Cracking pattern of control beam according to VECTOR model

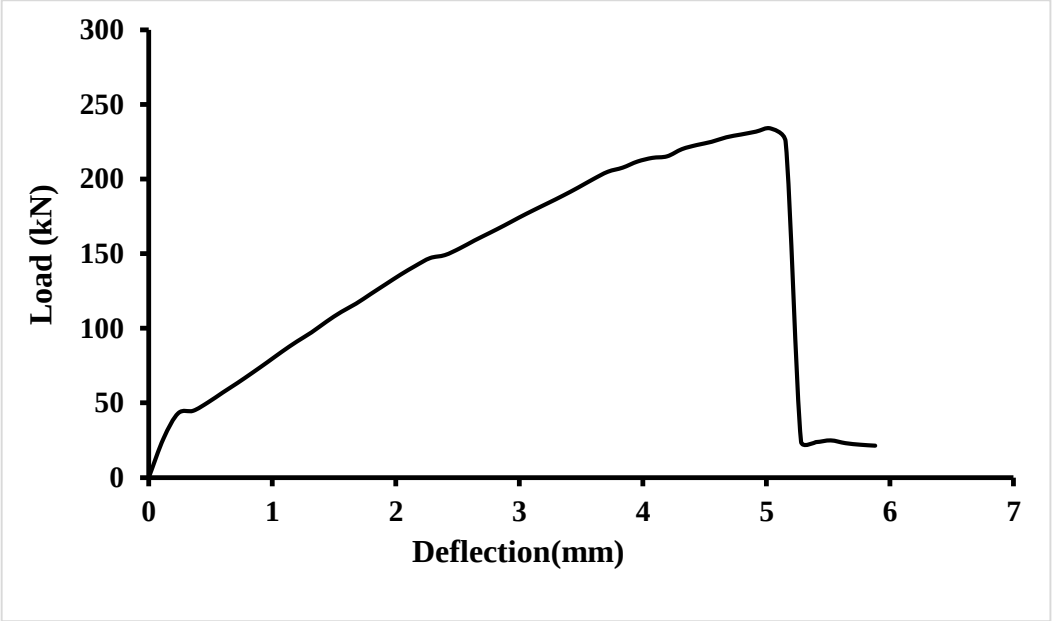

Figure 4-3 FEM beam 75BB1 load vs deflection analysis

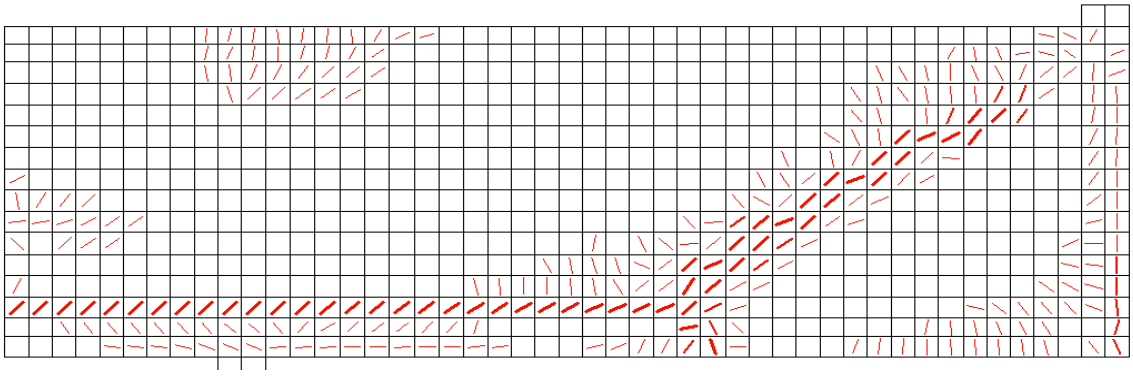

Figure 4-4 Cracking pattern of beam 75BB1 according to VECTOR model

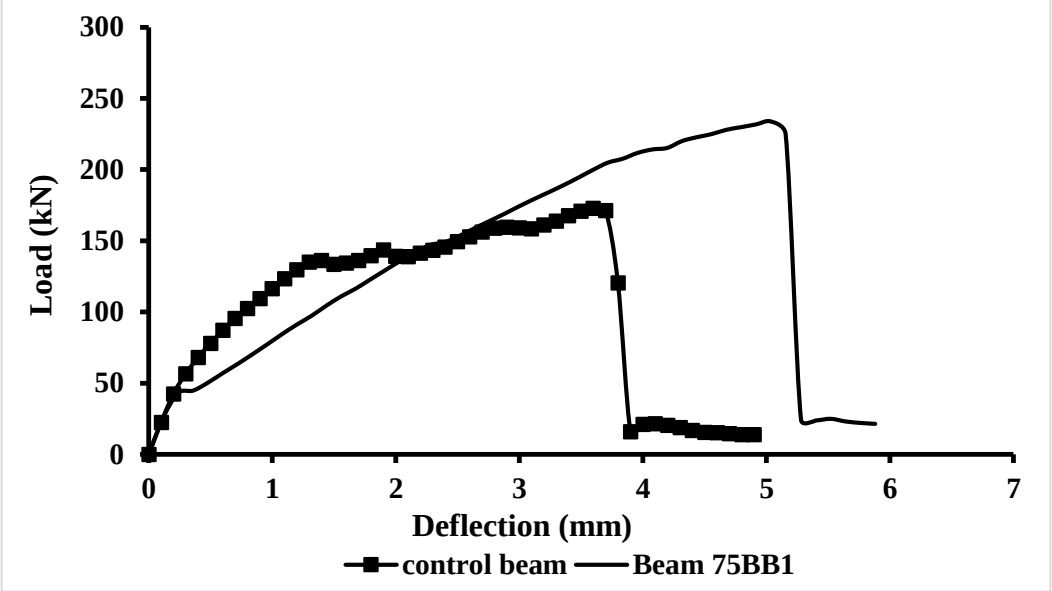

Figure 4-5 Comparison of the FEM beams result

The vector results show that control beam would fail at 172.7 kN. has a stiffer response than beam 75BB1 which failed at 233.8 kN. The resulted showed that 75% un-bonding of the shear span gave a higher shear capacity than the control beam.

CHAPTER 5 RESULT AND DISCUSSION

This chapter includes the results, observations and discussions of the results of the 8 beams in the experimental program. The following sections will explore each specimen, followed by the effect each experimental variable on the specimen result. Finally, the observations and results are addressed technically and in collaboration with chosen codes provision.

The other parameters calculated from the reading from the front gage readings are ε_x & ε_y (horizontal and vertical strain). The principal strain values were only able to be calculated only from the front surface measurement because the back side surface measurement lacks horizontal strain measurement. This and more detailed graphs of results are presented at Appendix C.

5.1 Result of the experimental program

5.1.1 The result of Trial beam

The beam showed very shallow flexural cracks until the beam failed in shear at a load of 159kN.This beam has attained 45.39% of its flexural capacity according to EURO code calculations. The instrumentation used in the trial beam was later modified to attain shear strain measurements on both sides of the beam rather than only on one.

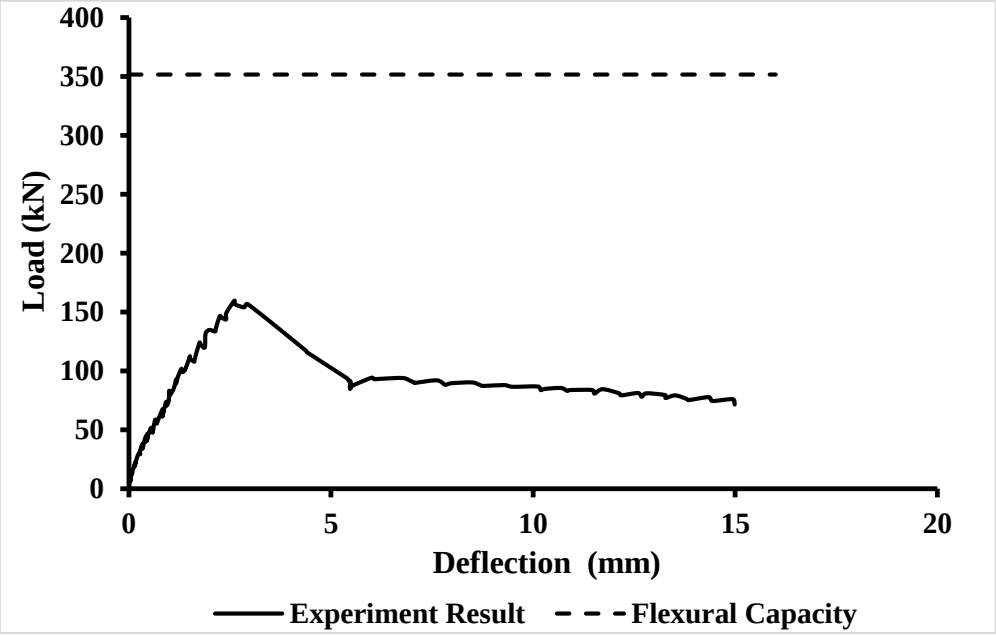

Figure 5-1 The load deflection progression of trial beam

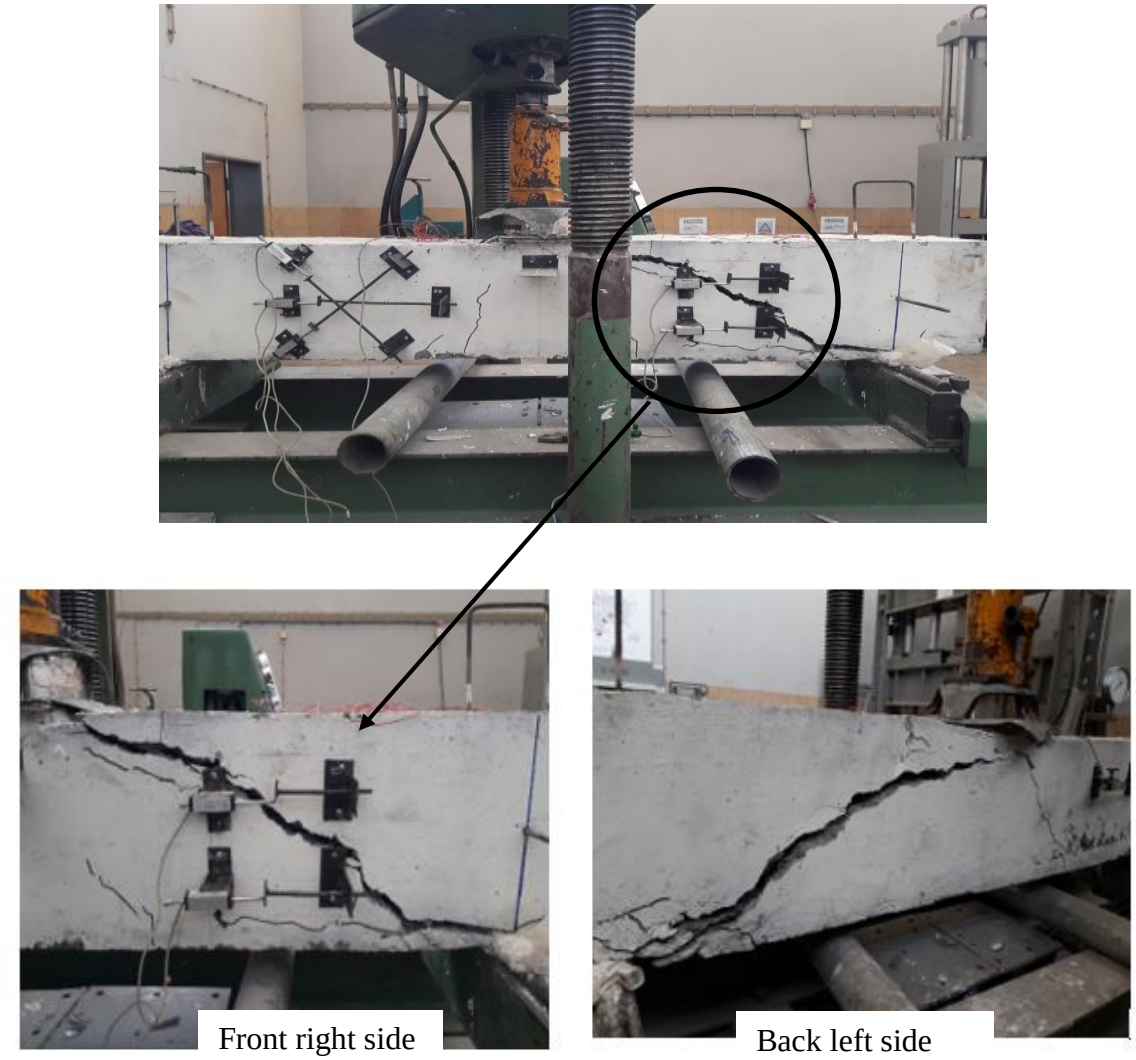

Figure 5-2 Close up crack patterns

5.1.2 The result of Control beam

The load deflection data and other results from surface measurement using two gages are included in the control beam test result. The beam experienced very thin cracks flexural cracks on both sides of the beam around 80 kN. which grew and increased in width. The critical shear crack was visible around 175kN, and the beam failed at 188kN. The figures below depict the test results. The control beam has reached 52.37% of its flexural capacity, according to Euro Code calculations. The 3 little cyclic loadings were unintentionally caused by attempts to measure crack width at different load stages.

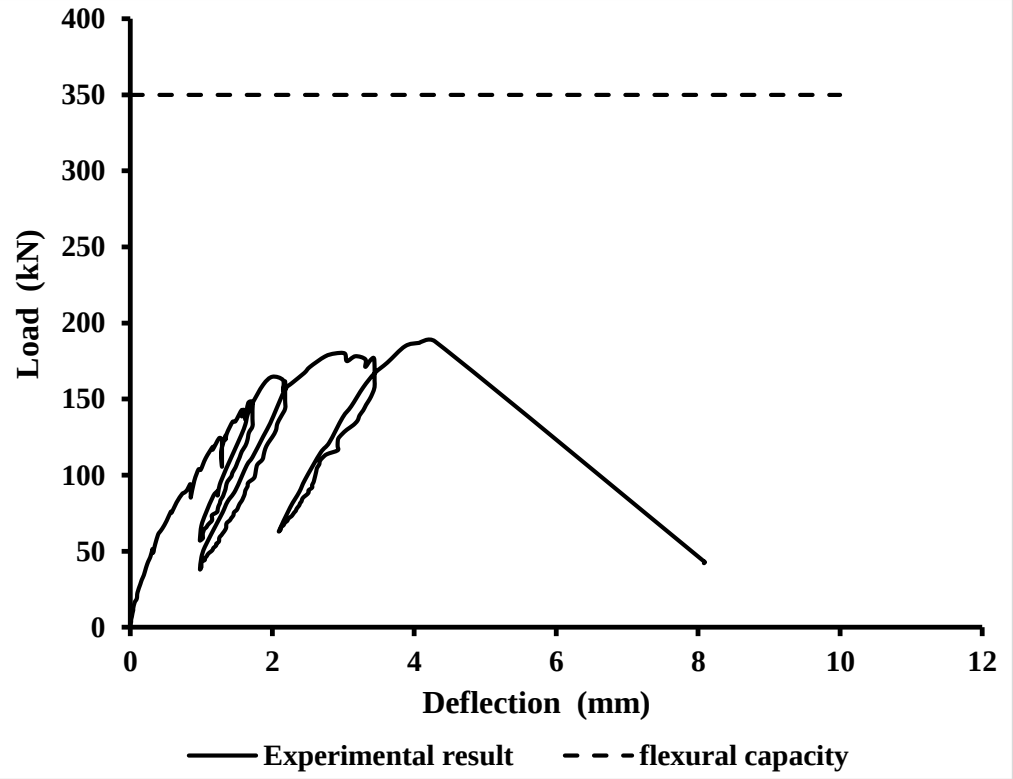

Figure 5-3 Load vs deflection of control beam

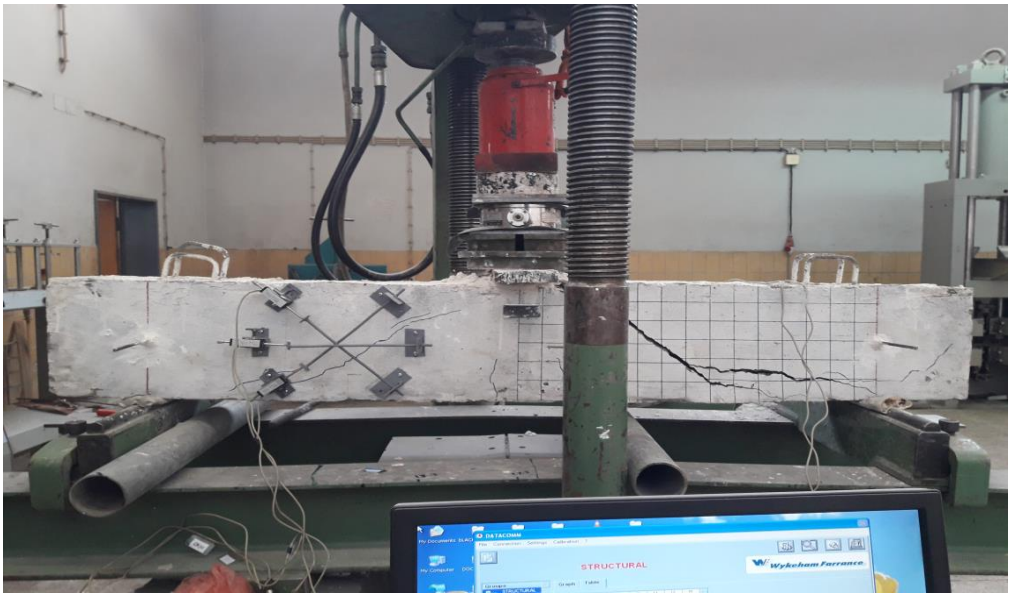

Figure 5-4 The control beam after failure

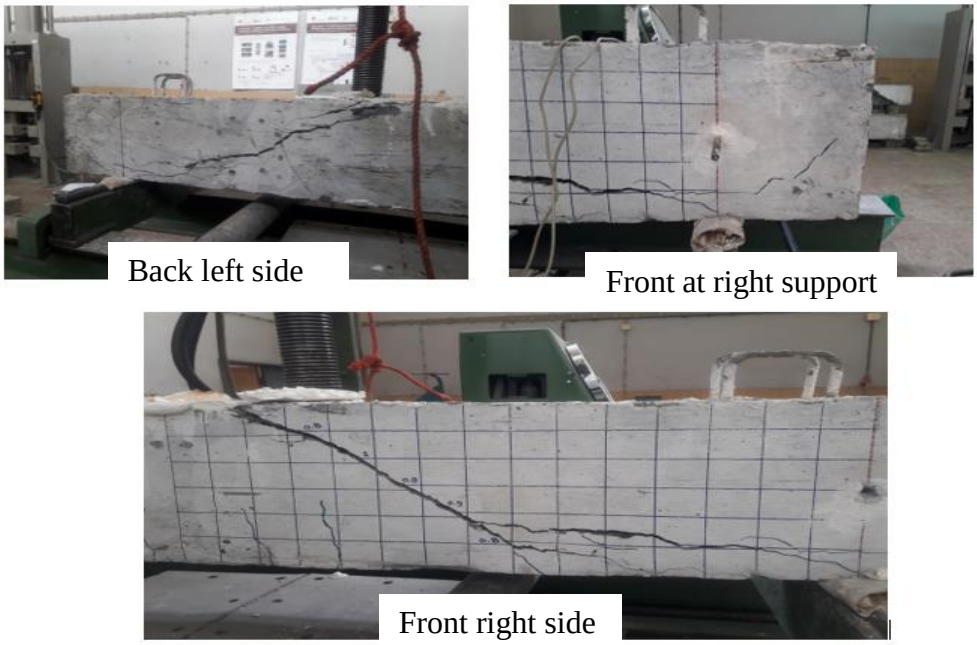

Figure 5-5 Close up on the cracks of control beam

5.1.3 The result of the beam 75BB1

The beam showed a clear flexural crack around load 100kN that extended to the web. This crack extended to the compression zone until the load reached 300kN, were a clear formation of crack starting from the start of bond cut to the point of loading was visible. At a load of 315 kN. the beam has failed suddenly. The beam has attained 87.77% of its flexural capacity according to the Euro Code calculations.

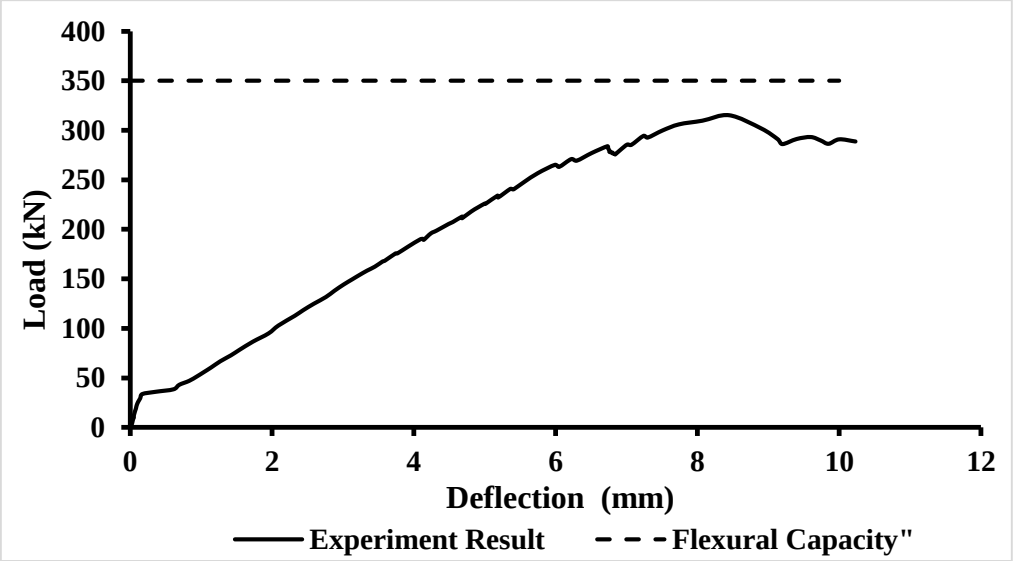

Figure 5-6 Load vs deflection of beam 75BB1

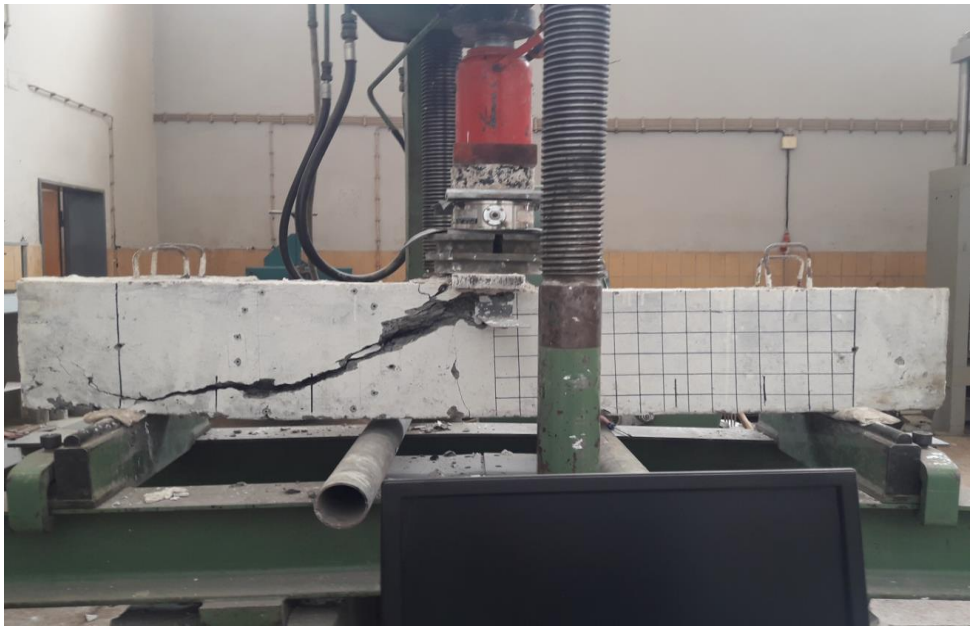

Figure 5-7 The beam 75BB1 after failure

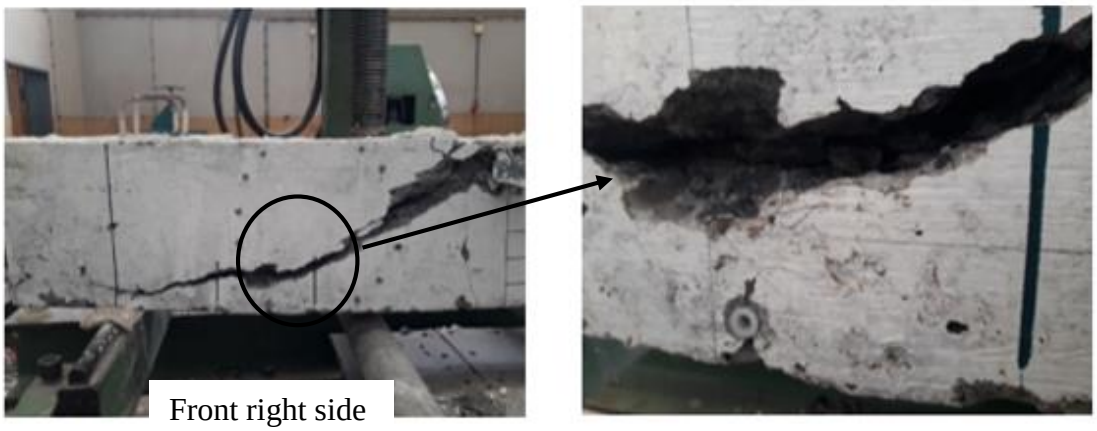

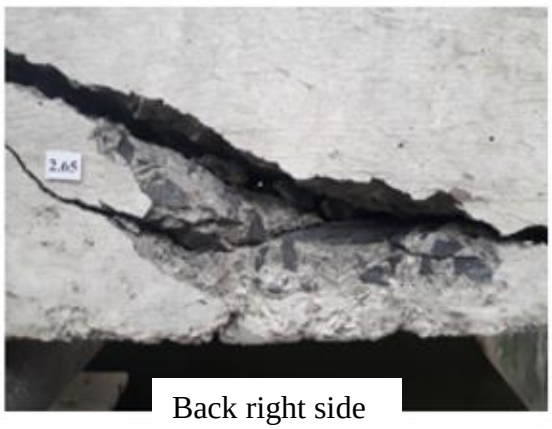

Figure 5-8 Close up on the cracks of beam 75BB1

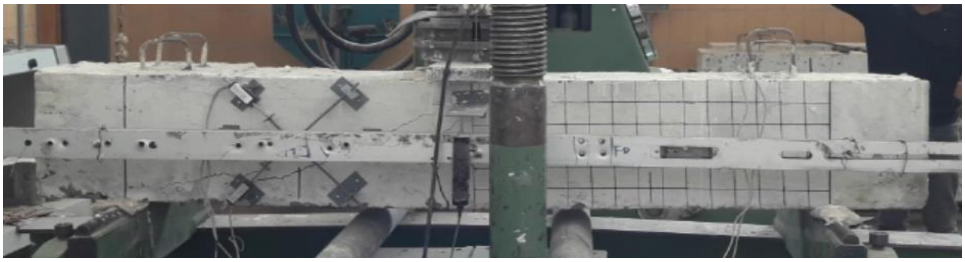

Figure 5-9 Cracks just before failure beam 75BB1

It can be seen from the figure 5-8 to 5-10 the diagonal shear crack is very deep and wide with a clear visibility of the top and the bottom longitudinal bars. The other visible cracks include a few flexural cracks and cracks that are around the diagonal shear crack. During the test it was observed that the critical diagonal crack started from the start of the point of bond change and further propagated to the compression zone and also following the line of the longitudinal reinforcement.

5.1.4 The result of the beam 75BB2

During loading cracks starting from both ends of the bond cut could be seen at load of 170kN. By the time the loading has progressed to 280kN the crack on the left side has progressed more in to the compression zone than the right one. Around a load of 315kN a crack that is initiated from the left crack has started to progress along the longitudinal reinforcement line. At a load of 350kN a cracking sound inside the beam was heard and this load was sustained until the beam failed explosively and the bottom cover at the left side of the beam has spalled. The beam has attained 99.72% of its flexural capacity according to Euro Code calculations.

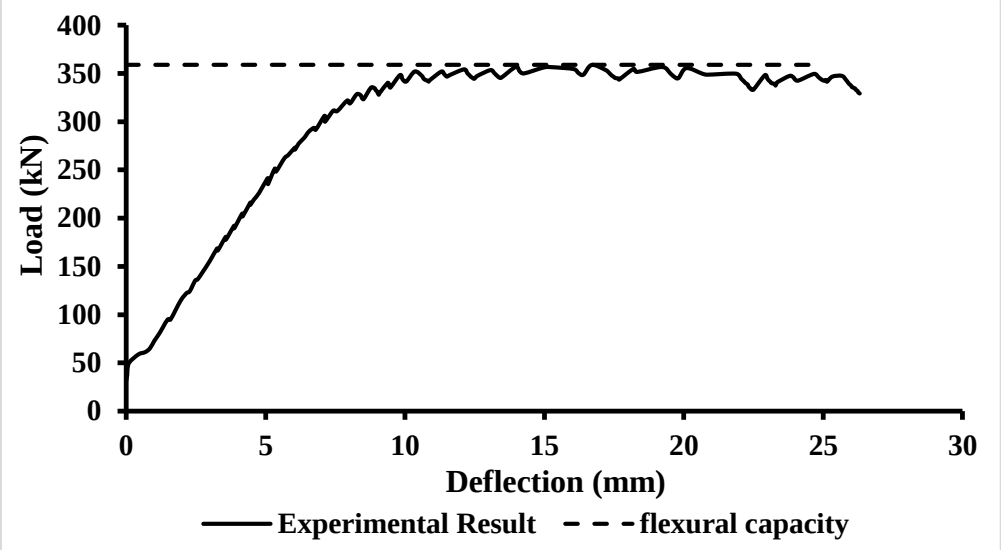

Figure 5-10 Load vs deflection of beam 75BB1

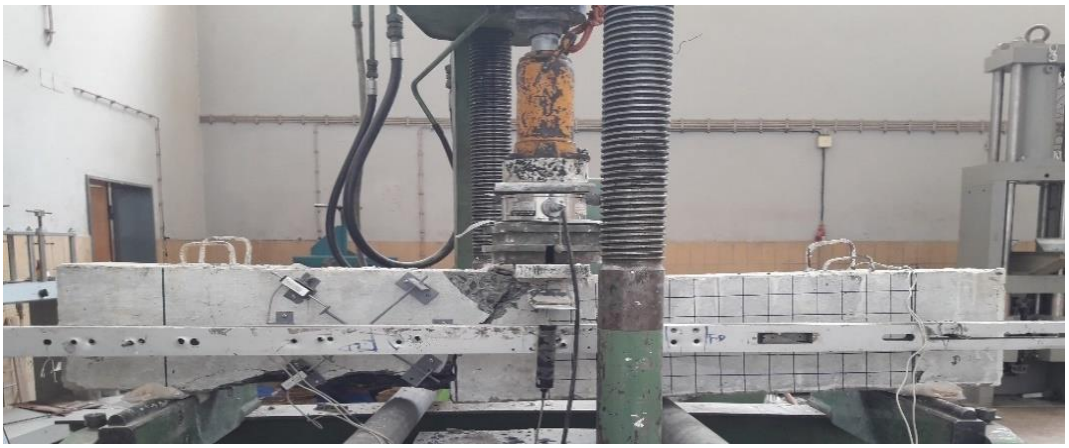

Figure 5-11 After failure beam 75BB2

Back right side

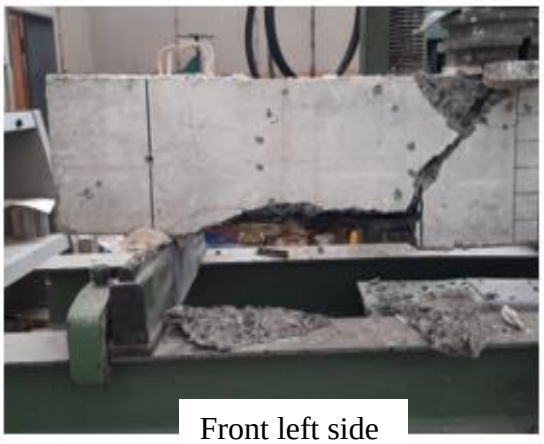

Front left side

The bottom of the beam

Figure 5-12 Close up on the cracks of beam 75BB2

5.1.5 The result of beam 50DCB1

This beam failed in a typical shear fashion. during the test at around 190kN diagonal cracks stating at points out side of the damage concrete region and propagating to the loading point were very visible. This cracks were present on both sides of the beam however the crack at the right side of the beam had a greater width and higher propagation to the compression zone. The beam finally failed at 218kN attaining 65% of its flexural capacity according to Euro Code. The load and deflection progression are shown on figure 5-12

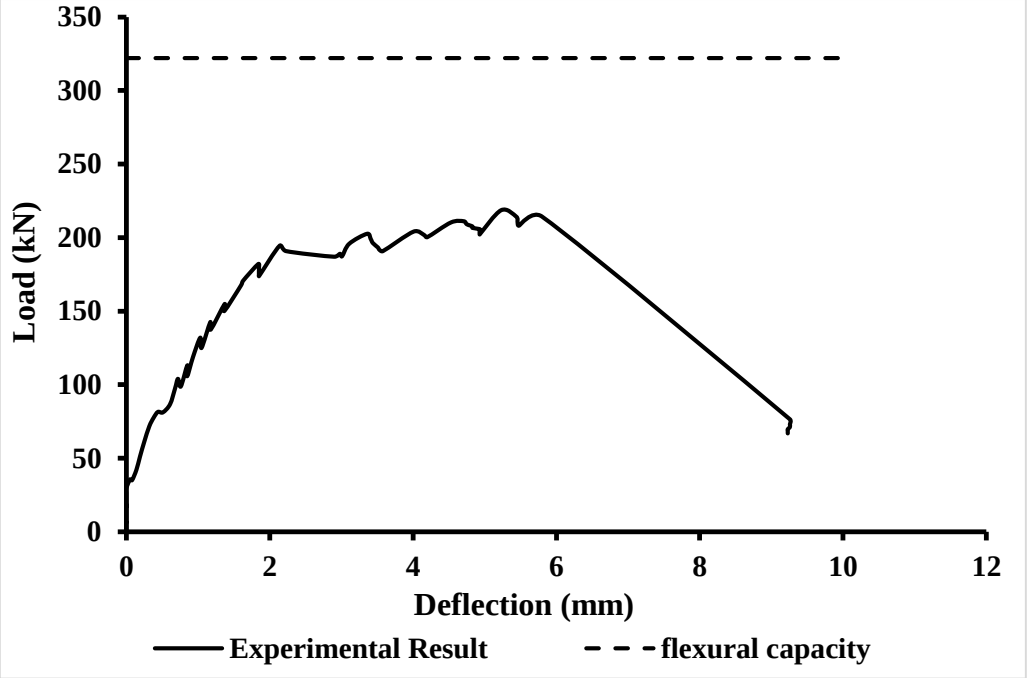

Figure 5-13 Load vs deflection of beam 50DCB1

Figure 5-14 The beam 50DCB1 after failure

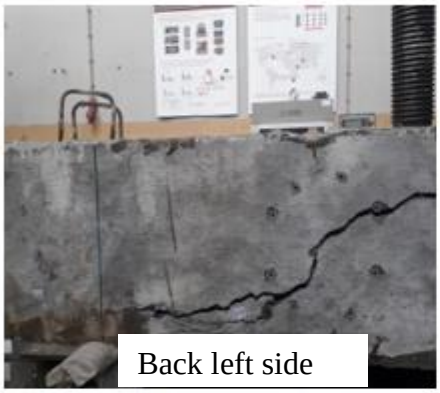

Figure 5-15 Close up on the cracks of beam 50DCB1

5.1.6 The result of beam 50DCB2

The beam showed a diagonal crack on the left side of the beam. This crack started with in the damaged concrete section and propagated to the compression zone. The beam finally failed at the load of 160.4 kN. The beam has attained 47.79% of its flexural capacity according to EC.

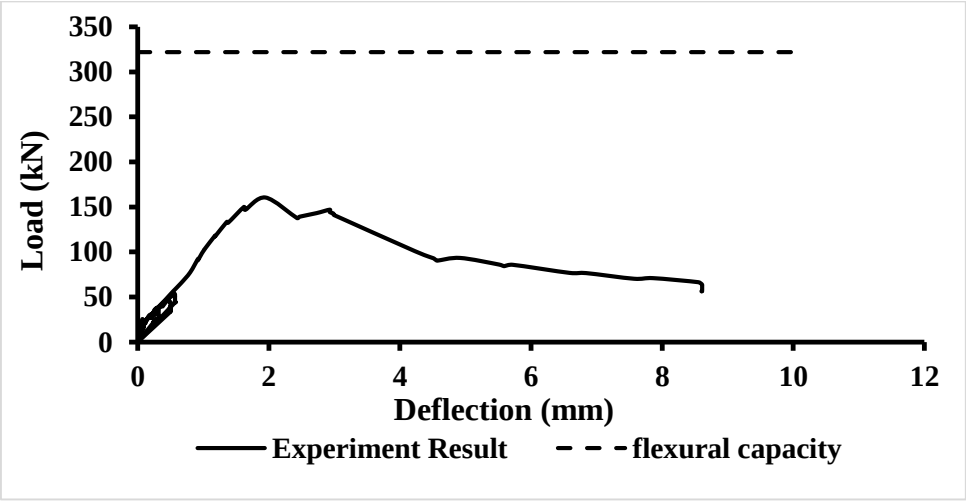

Figure 5-16 Load vs deflection of beam 50DCB2

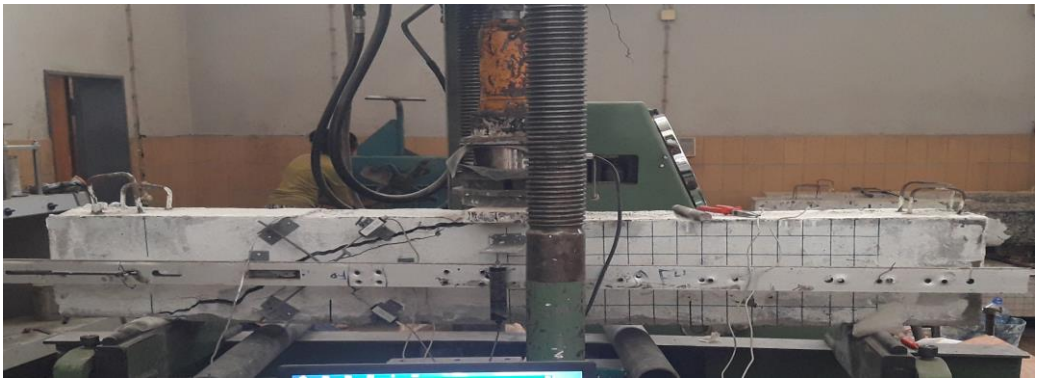

Figure 5-17 The beam 50DCB2 after failure

Figure 5-18 Cracks just before failure beam 50DCB2

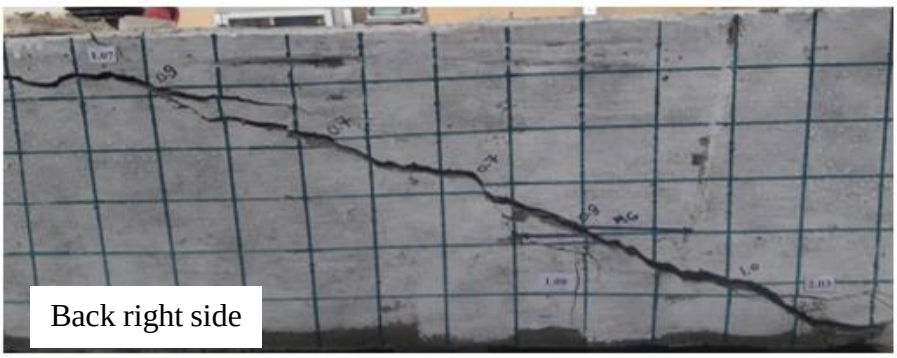

Figure 5-19 Close up on the cracks of beam 50DCB2

5.1.7 The result of beam 75DCB1

The beam showed visible diagonal cracks at around 190kN on both side of the beam but the cracks appear on the web of the beam. As the loading progressed the crack on the right side advanced to the beginning of the damaged concert section at the bottom of the beam. While the left side of the crack didn't advance to the bottom of the beam. The beam finally failed at a load of 287.6 kN. explosively with a spalling of bottom cover on the right side of the beam. The beam has attained 85.7% of its flexural capacity according to the Euro Code.

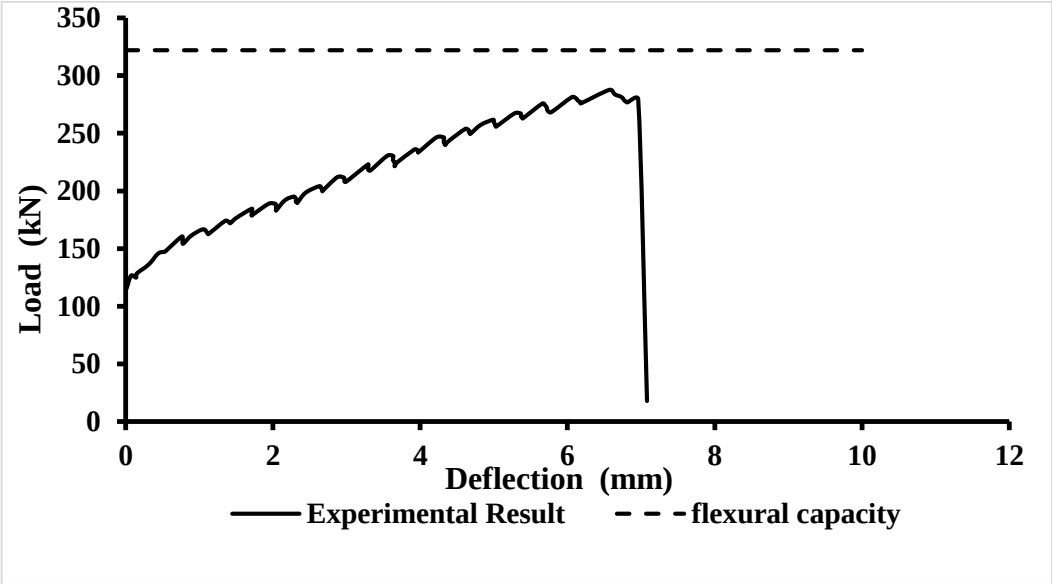

Figure 5-20 Load vs deflection of beam 75DCB1

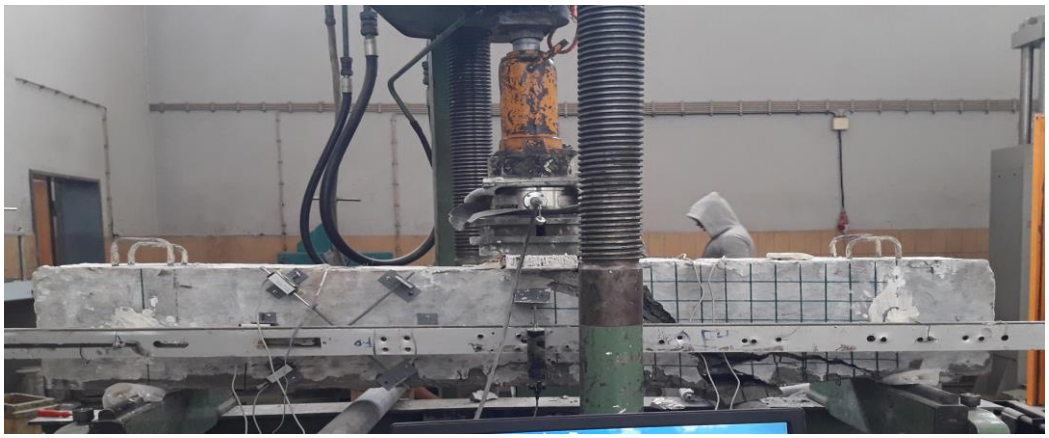

Figure 5-21 The beam 75DCB1 after failure

Figure 5-22 Cracks just before failure beam 75DCB1

Back right side

Bottom side of beam

Figure 5-23 Close up on the cracks and spalling of beam 75DCB1

5.1.8 The result of beam 75DCB2

The beam failed in shear at a load of 201.6 kN. achieving 60.7% of its flexural capacity. At around 177 kN. the critical diagonal crack on the right side was visible and the crack progressed to the compression region causing a shear failure.

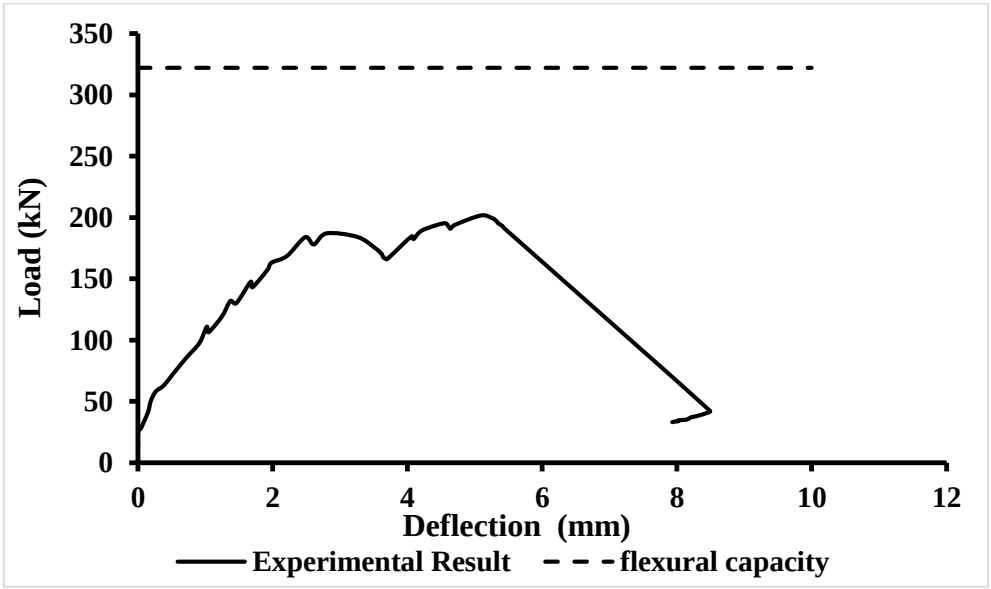

Figure 5-24 Load vs deflection of beam 75DCB2

Figure 5-25 The beam 75DCB2 after failure

Figure 5-26 Just before failure cracks beam 75DCB2

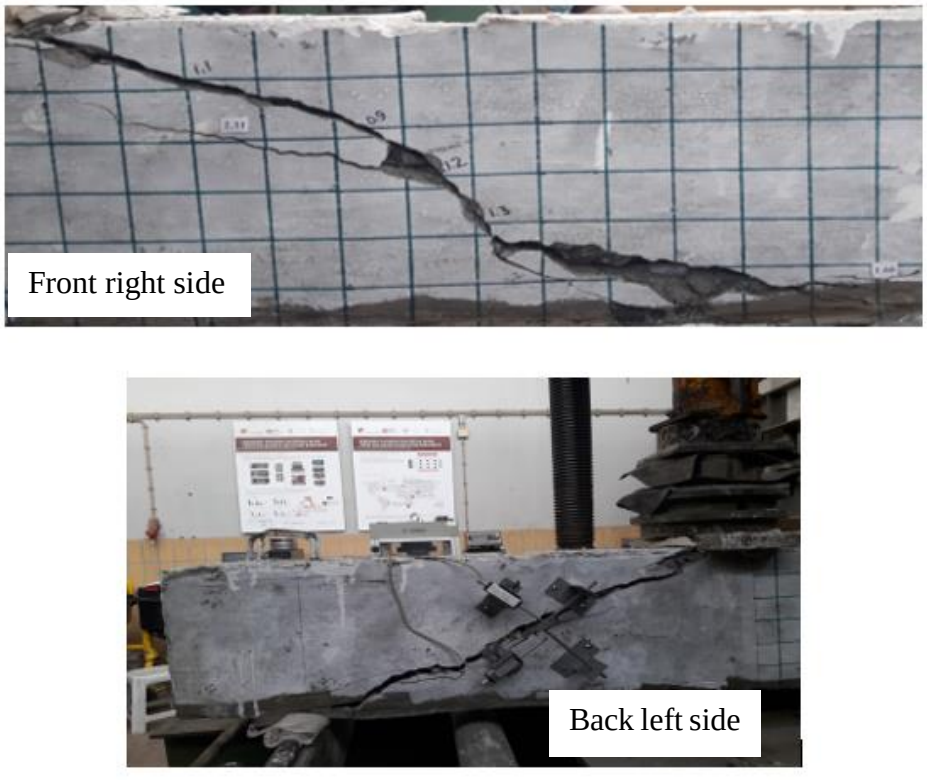

Figure 5-27 Close up on the cracks and spalling of beam 75DCB2

Table 5-1 The results of the experimental program

Specimen	Failure load (kN.)	Flexural capacity EU(kN.)	Flexural capacity ACI(kN.)	% of flexural capacity ACI	% of flexural capacity EU
trial beam	159.56	351.5	342.8	46.55	45.39
Control	188	359	351	53.56	52.37
75BB1	315.1	359	351	89.77	87.77
75BB2	358	359	351	100	99.72
75DCB1	287.6	335.6	322	89.32	85.7
75DCB2	201.6	335.6	322	62.61	60.07
50DCB1	218.6	335.6	322	67.89	65.14
50DCB2	160.4	335.6	322	49.81	47.79

5.2 Discussion

This section expands on the quantitative results that are measured and the observations witnessed during the testing of the two series and the trial beam. It also puts forward possible reasons for the results and the mechanism behind them. Additionally, it explains what the experimental variables' roles were in the results.

In analyzing the specimens as a whole, normalizing the difference in concrete strength between the two series was found to be necessary. It can be clearly seen from the graphs presented below that all of the beams in series 1 and 2 have better performances than that of the control beam. The graphs show beams 75BB1, 75BB2 and trial beam are less stiff than the control beam, while the beams of the DCB series are stiffer than the control beam. The beam 75DCB1 was found to have a higher shear capacity out of all of the specimens.

All of the specimens in the first (BB) series except beam 75BB2 have failed in shear. In the first (BB) series, the beams experiencing almost complete bond cut (75BB1 and 75BB2) were found to perform better than the control beam. It was also observed that the change in the location of the artificial bond cut around the support area rather than to the middle of the section resulted in better performance. In the damaged concrete series (DCB), the change in damaged concrete location change to the supports did not show a better performance as it was seen in the BB series.

By comparing the shear strain measurements of each specimen to that of the control beam, the shear strain of the beams 75BB1 and 75BB2 were much smaller than that of the control beam and negative in value. On the other hand, the beams of the DCB series showed much

larger shear strain values than that of the control beam. The same trend was observed in calculations of in-plane maximum shear strain and principal strain (tension ε_1).

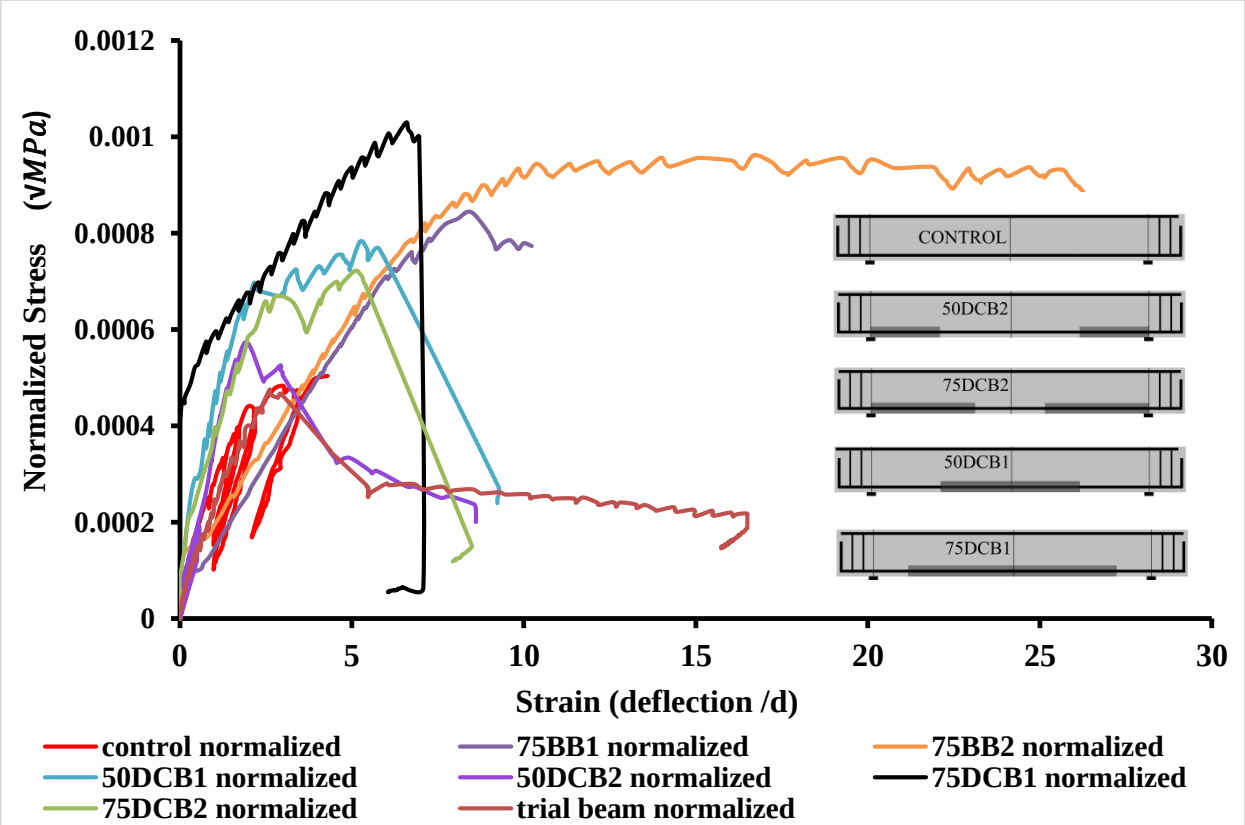

Figure 5-28 Normalized stress vs deflection of all specimens

Table 5-2 Normalized ultimate failure of specimen

No	Specimen	Series	Failure type	Cylindrical Compressive strength (MPa)	$\frac{load}{bd\sqrt{fc}}$ $(\sqrt{MPa})$
1	Trial beam	-	shear	27.36	4.75×10^{-4}
2	control beam	BB	shear	33.7	5.04×10^{-4}
3	beam 75BB1	BB	shear	33.7	8.45×10^{-4}
4	beam 75BB2	BB	flexure	33.7	9.62×10^{-4}
5	beam 75DCB1	DCB	shear	18.9	7.83×10^{-4}
6	beam 75DCB2	DCB	shear	18.9	5.74×10^{-4}
7	beam 50DCB1	DCB	shear	18.9	1.03×10^{-4}
8	beam 50DCB2	DCB	shear	18.9	7.22×10^{-4}

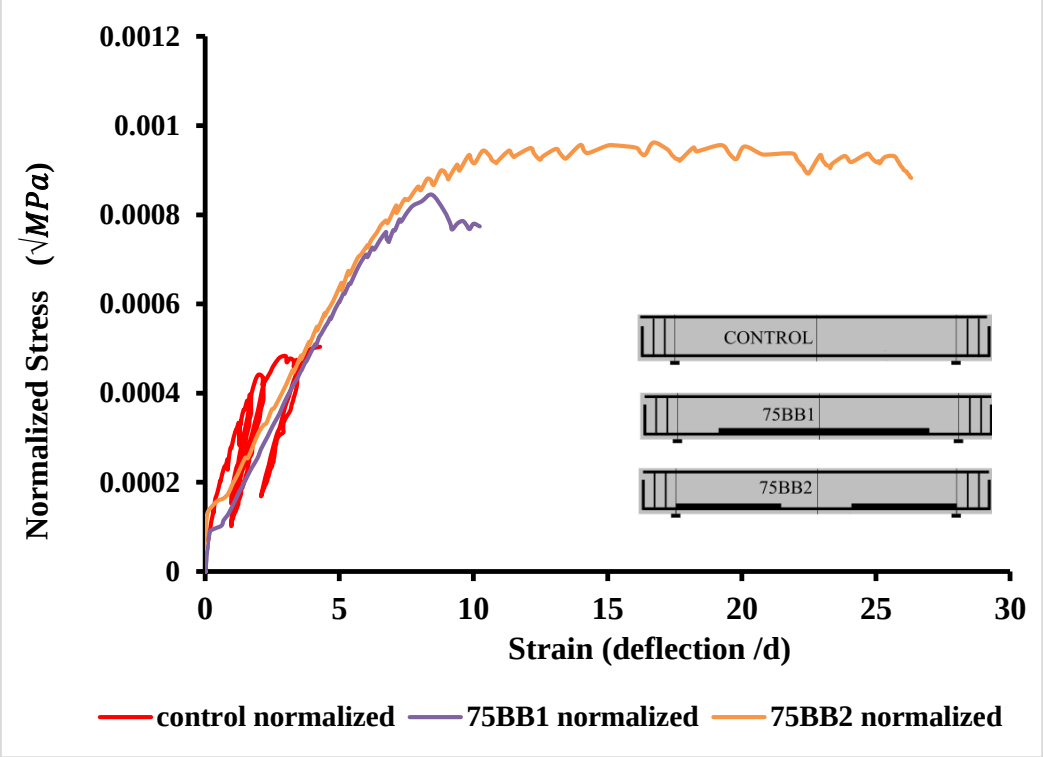

Figure 5-29 Normalized stress vs deflection of BB series specimens

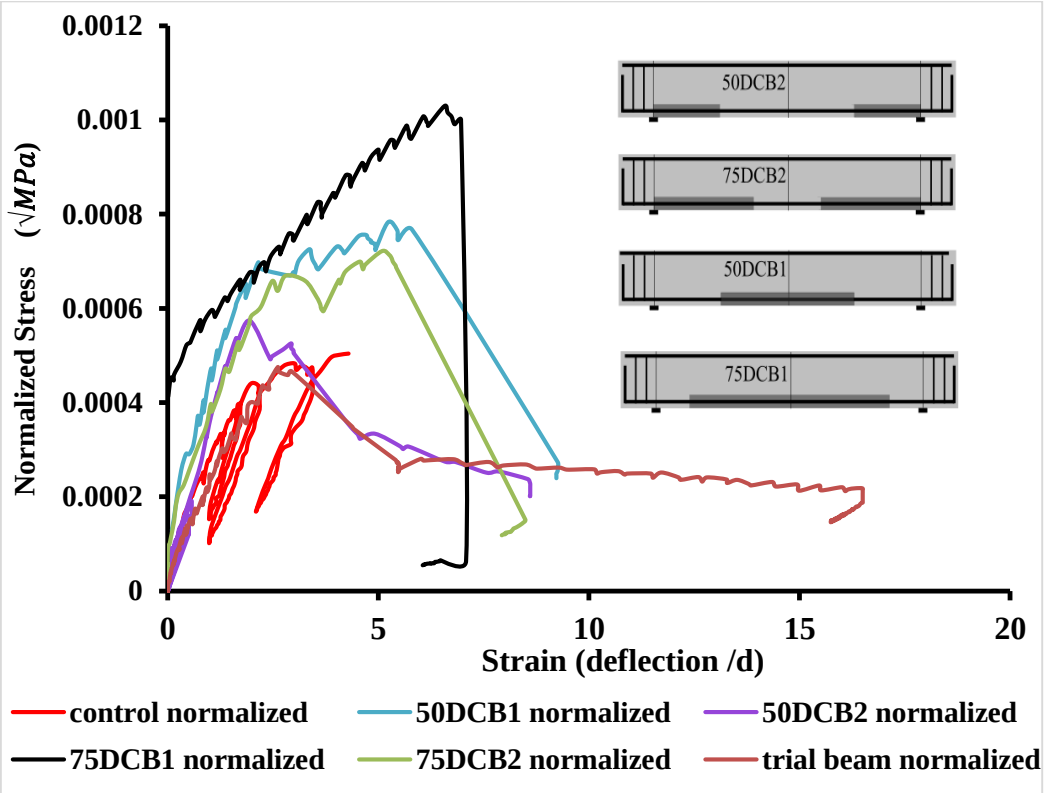

Figure 5-30 Normalized stress vs deflection of DCB series specimens

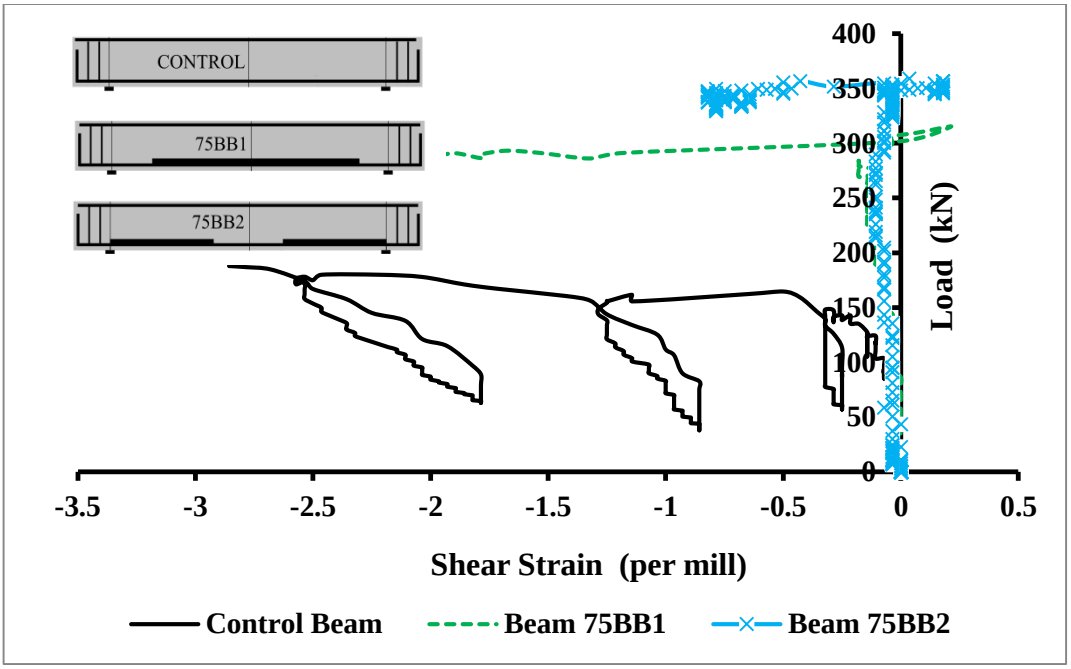

Figure 5-31 Load vs front side shear strain of BB series

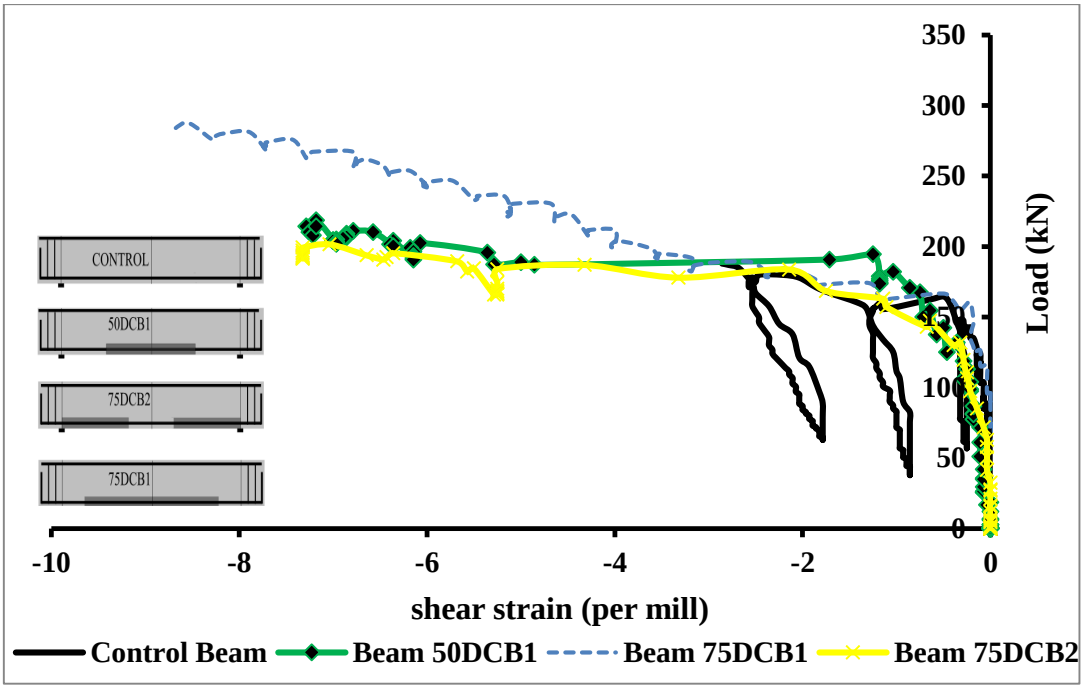

Figure 5-32 Load vs front side shear strain of DCB series

In Figure 3-57, it can be seen that the horizontal strain (ε_x) is measured at the center of the surface of beam from the front set up of the surface measurement while the strain mold gage (figure 3-26 up to 3-29) is placed just above the damaged bond concrete section at 12cm from the bottom of the beam. The strain mold gage also measures horizontal strain inside the beam at the middle of the section of the DCB series beams.

In comparing the horizontal strain measurements (ε_x) in the BB series (figure 5-33), it was observed that the control beam experienced only tension where beam 75BB1 experienced only compression and beam 75BB2 went through first tension and then compression. In the control beam, the critical diagonal crack formed on the right side of the beam, missing the front set up of surface measurement. In the case of the other two beams, the critical diagonal cracking formed on the left side of the beam crosses the surface measurement in beam 75BB1 but misses it in beam 75BB2 because of the steep angle of the crack and its point of initiation (see figure 5-34). It could be explained that the compression readings on beam 75BB1 were due to the compression strut formed in the surface measurement set up, while the latter compression horizontal measurements in beams 75BB2 could be caused by the formation of the diagonal crack nearby and finally the spalling observed under the set up. The control beam did not experience any compression measurement because the surface set up was far removed from its critical diagonal crack location.

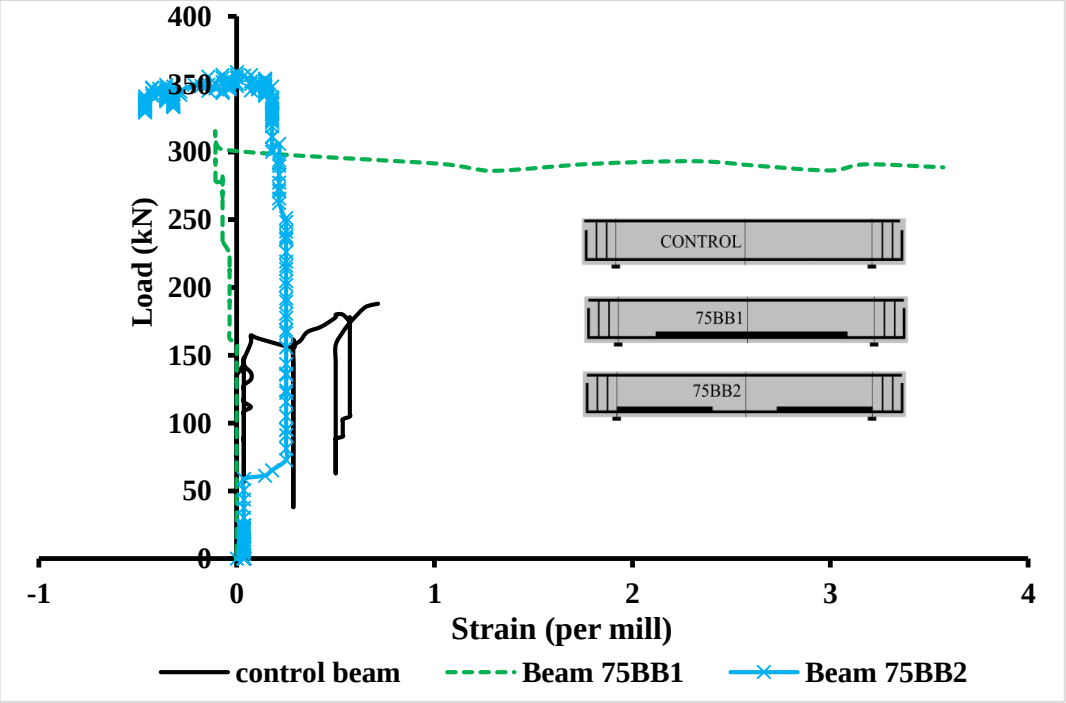

Figure 5-33 Front side horizontal strain Vs load of BB series

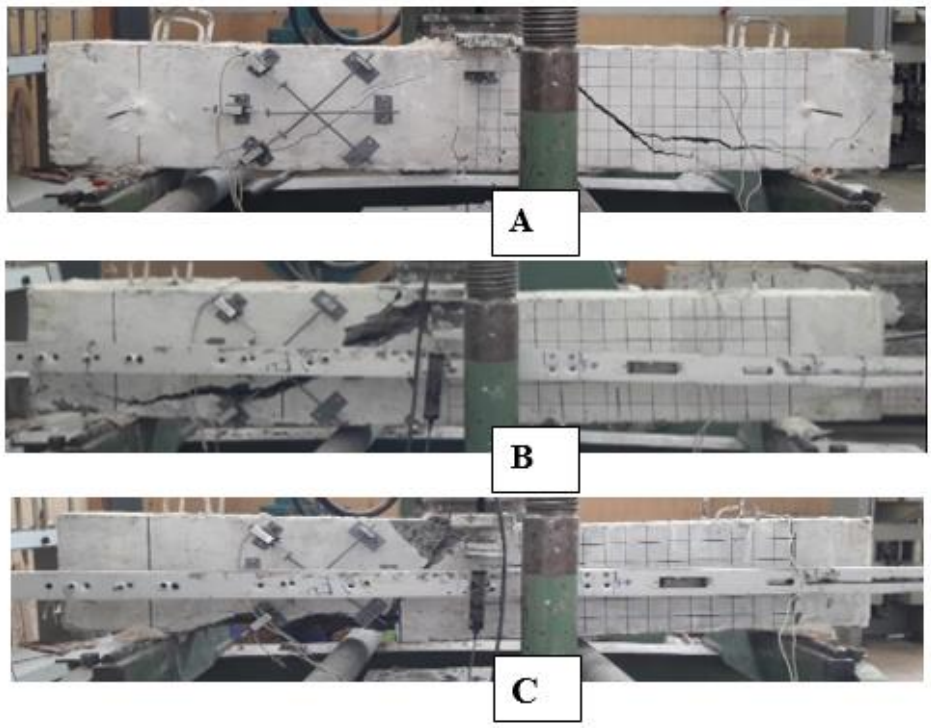

Figure 5-34 Comparison of crack formation of BB series A, control B,75BB1 C,75BB2

In the DCB series, both the horizontal strain (ε_x) measurement (figure 5-35) and the strain mold gage measurement (figure 5-36) were used to see the progression of stress transferred from the bars to the concrete in the web of the section. In beam 50DCB1 though the surface measurement and the strain mold gages were on different sides of the beam, both measurements recorded tension. The critical diagonal crack was far away from both measurements, and the measurements of the strain mold gage show that the existence of tension above the damaged concrete section (see figure 5-37). The readings from the strain mold gages can be seen in the figure below. Critical diagonal crack happened to be near the strain gage, hinting at the possibility that the formation of the compression strut could be the reason for the compression reading. In the case of the beam 75DCB1, both measurements recorded tension followed by compression. However, the switch from tension occurred at 188 kN in the horizontal strain measurement (ε_x) while the transition happened at 228.6 kN. In the strain mold gage measurements, possibly caused by the location of the two measurements in relation to the critical diagonal crack location. In the horizontal measurements (ε_x) of beam 75DCB2, the reading shows only tension measurements, while the strain mold gage showed a switch at 163kN from tension to compression.

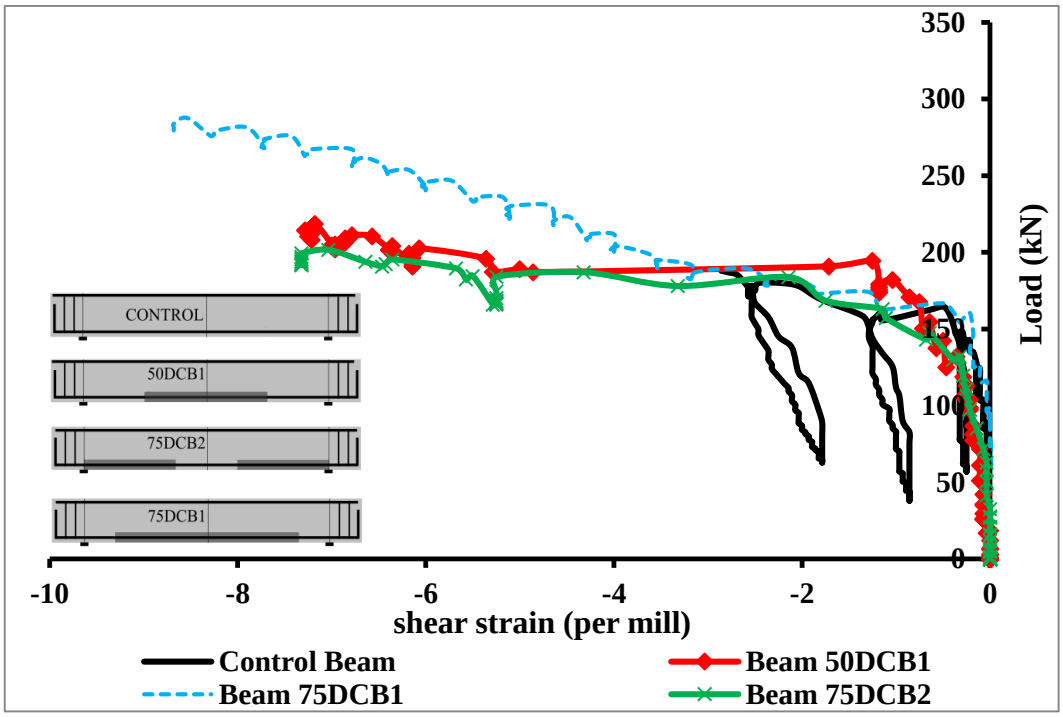

Figure 5-35 Front side horizontal strain Vs load of DCB series

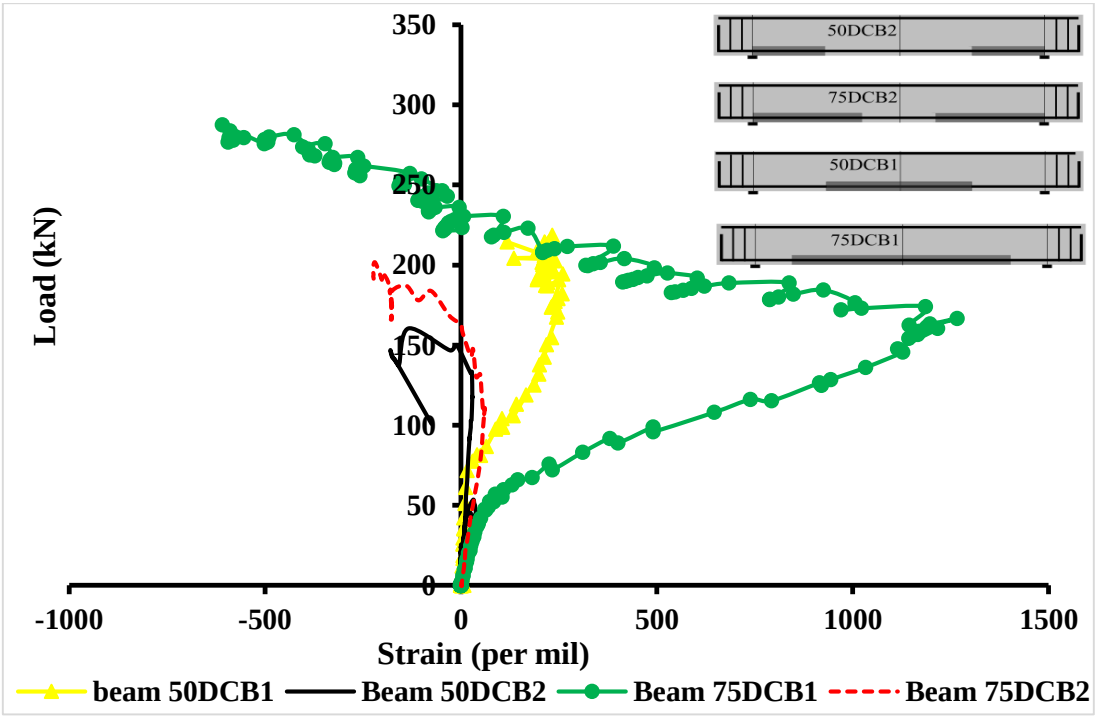

Figure 5-36 Strain mold gage results of the DCB series

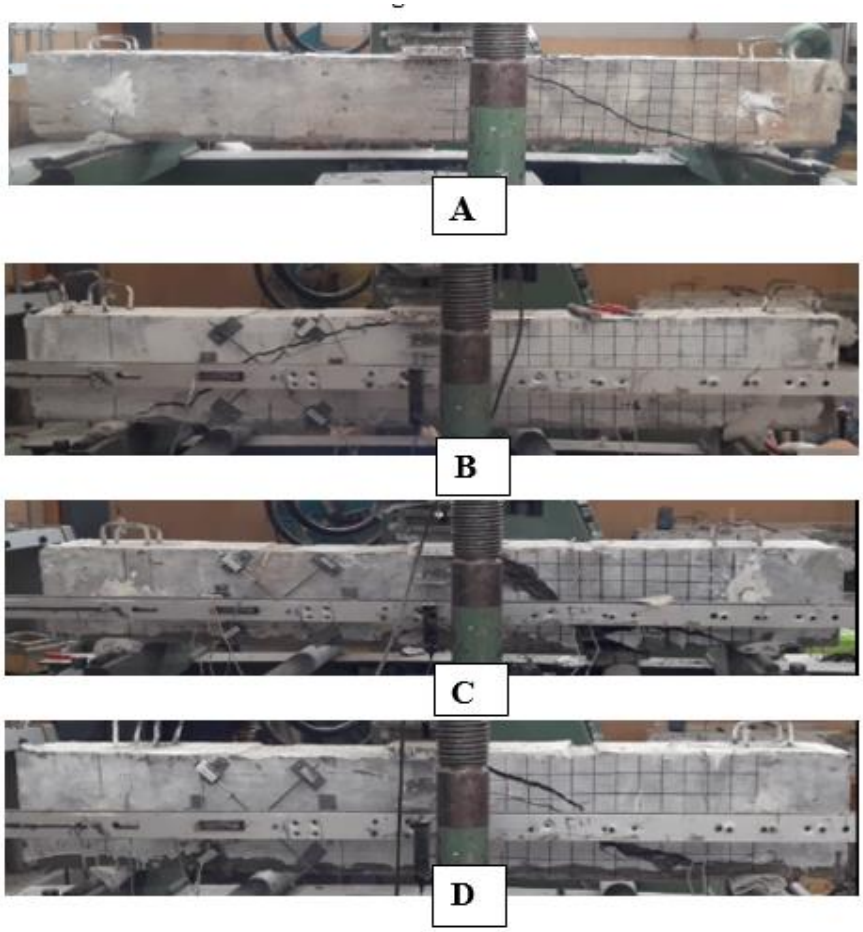

Figure 5-37 Comparison of crack formation of DCB series A, 50DCB1 B, 50DCB2 C, 75DCB1 D,75DCB2

5.2.1 The effect of location of bond cut or bond deterioration

5.2.1.1 The effect of location of bond cut in the BB series

Specimens 75BB1 and 75BB2 in the BB series were specifically designed to observe the effect of the location of the bond cut. Both specimens have a gasket covering 75 percent of their shear span. The results revealed that beam 75BB2 performs better (reaching its flexural capacity). It was observed that placing the artificial un-bonding material near supports produced better results. The figure 3-31 shows that beams 75BB1 and 75BB2 follow the same pattern in the early stages of loading but beam 75BB2 ultimate capacity was higher than 75BB1.

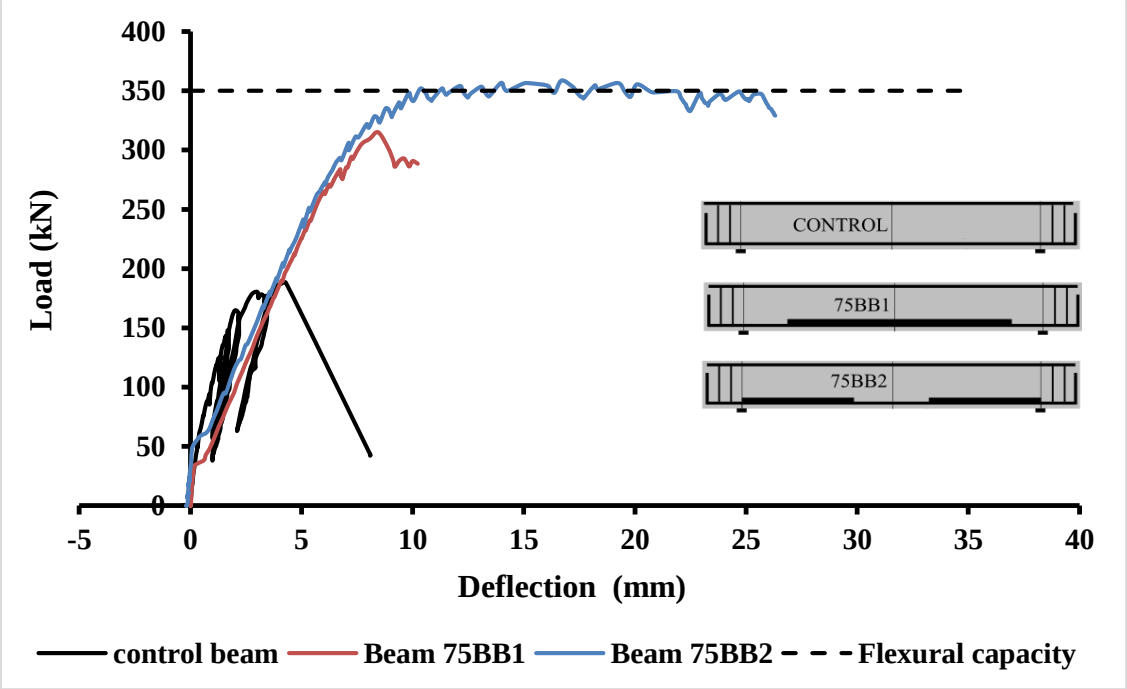

Figure 5-38 Load vs deflection of the BB series

Many researchers explained that the nature of local bond stress concentration immediately after flexural cracking is a major cause for the initiation of the flexural shear cracking in reinforced concrete beams. In their research Kim and white (Kim & White, 1991) reasoned that the enhancement in their bond cut series was caused by the absence of shear stress induced by bond. Which leads to the delay of shear crack resulting in avoidance of the shear failure. This could explain the enhancement of both beams 75BB1 and 75BB2 from the control beam.

Just from analyzing the formation of the critical diagonal crack on beam 75BB1 and 75BB2. It can be seen that the critical diagonal crack formed on beam 75BB2 was much steeper than 75BB1, implying that the compression strut formed on beam 75BB2 is much stronger. It is evident that a steeper compression strut is able to support a much greater compression force, which could be the reason why, even though the two beams have the same percentage of bond cut, they show an almost 40kN difference in ultimate capacity.

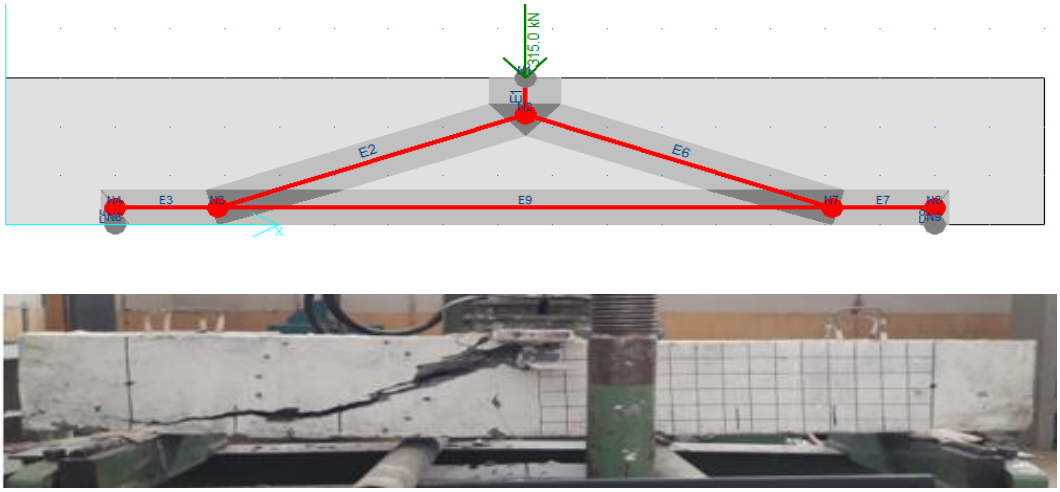

Figure 5-39 The diagonal critical crack of beam 75BB1

Figure 5-40 The diagonal critical crack of beam 75BB2

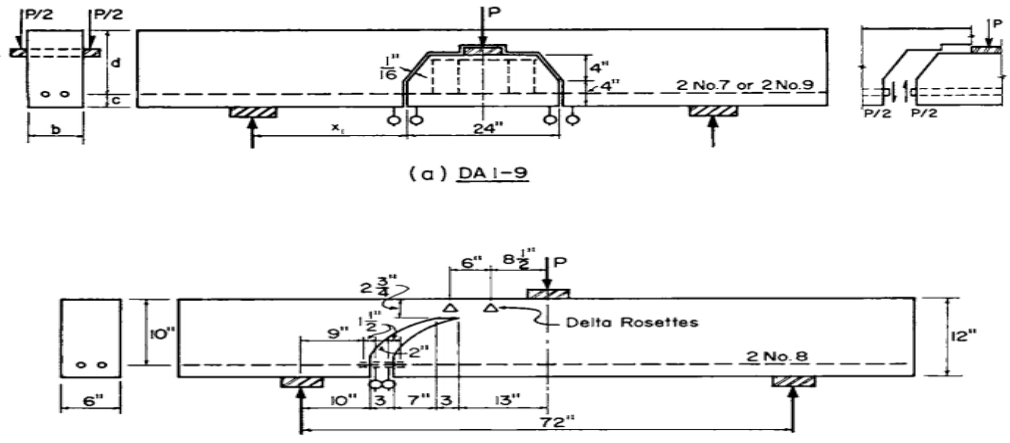

Figure 5-41 Specimen for the dowel test(Krefeld & Thurston, 1966)

The tests and analyses presented in their paper William J. Krefeld and Charles W. Thurston (Krefeld & Thurston, 1966) showed that the total transverse shear at the cracked sections of beams without stirrups is resisted by both the concrete remaining intact above the inclined crack and the longitudinal reinforcement. The magnitude of the shear resisted by the reinforcement (and the concrete below) can be appreciable. Regardless of this magnitude, however, the critical extension of the diagonal crack at its upper end occurs when the dowel force transmitted by the reinforcement produces horizontal cracking of the concrete along the bars. Then further redistribution of internal forces results, with continued local bending of the bars, rotational deformations of the concrete, and increasing propagation of the crack in the compression zone. This explains the 40kN capacity difference between the beam 75BB1 and the beam 75BB2. The position of the artificial un-bonding material in beam 75BB2 is directly in the path of the horizontal(dowel) crack progression. The horizontal(dowel) cracks in both beams (control beam and beam 75BB1) progressed immediately after the formation of the critical diagonal crack. However, in beam 75BB2, the horizontal crack couldn't progress in the artificially un-bonded zone (figure 5-45), which changed the trajectory of the crack downward (see figure 5-44). Finally, spalling of the bottom cover in the artificially un-bonded region and rapid progression of the critical diagonal crack to the point of loading happened simultaneously, causing failure.

The same paper concluded that the action "triggering" the propagation of the crack in the compression zone, leading ultimately to disintegration and separation, is the cracking or splitting above the bars at the bottom of a critical diagonal crack. At the time this splitting occurs, the diagonal crack has generally extended just above the neutral axis into the compression zone. The tensile stress that causes the horizontal cracking (dowel cracking) is a combination of bond, horizontal shear and vertical shear (dowel) resisted by the bars and concrete below the bar.

Based on the progression of the critical diagonal crack explained by William J. Krefeld and Charles W. Thurston, if the progression of the dowel cracking is prevented, the advancement of the critical diagonal crack into the compression zone will be inhibited, causing a redistribution of internal forces leading to the change in trajectory of dowel cracking in beam 75BB2 and possibly its delayed failure.

Figure 5-42 Control beam critical diagonal crack

Figure 5-43 Beam 75BB1 critical diagonal crack

Figure 5-44 Beam 75BB2 critical diagonal crack

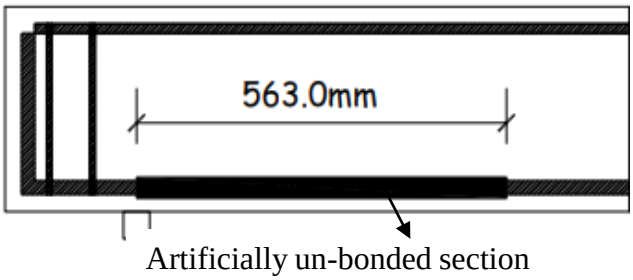

Figure 5-45 The effect of location of bond deterioration zone in the DCB series

5.2.1.2 The effect of location of bond cut in the BB series

Un like the BB series the specimens in this series didn't achieved better performance with change of location of the damaged concrete sections. The specimens 50DCB1 and 75DCB1 had a 50kN and 87kN capacity difference respectively from their corresponding beams 50DCB2 and 75DCB2.The changes in the critical diagonal crack formation seen in the BB series were not observed in this series. Most of the diagonal cracks followed the theoretical trajectory from point of loading to the support.

In beams 75DCB1,75DCB2 and 50DCB2(figure 5-47 to 5-49) it was observed that the change in crack propagation to avoid the deteriorated concrete section (indicated by the red rectangle in the following figures). In beam 50DCB2 and 75DCB2 shown below the critical crack becomes a horizontal crack (shown with the black ovals) following the vertical height of the bond deterioration section until a point of access is obtained near the support. The vertical line on the right side of the crack shows the start of the deteriorated concrete section. As from the figure below similar formation of crack could also be seen in beam 75DCB1 where the critical crack avoids venturing in to the damage concrete section until passing this zone.

The unusual stiffness of the 75DCB1 series were investigated and the possible explanation is the instrumentation, particularly the displacement transducer not being in contact with the fixed plate. The video taken during the testing was examined but no conclusive evidence was found for this possibility.

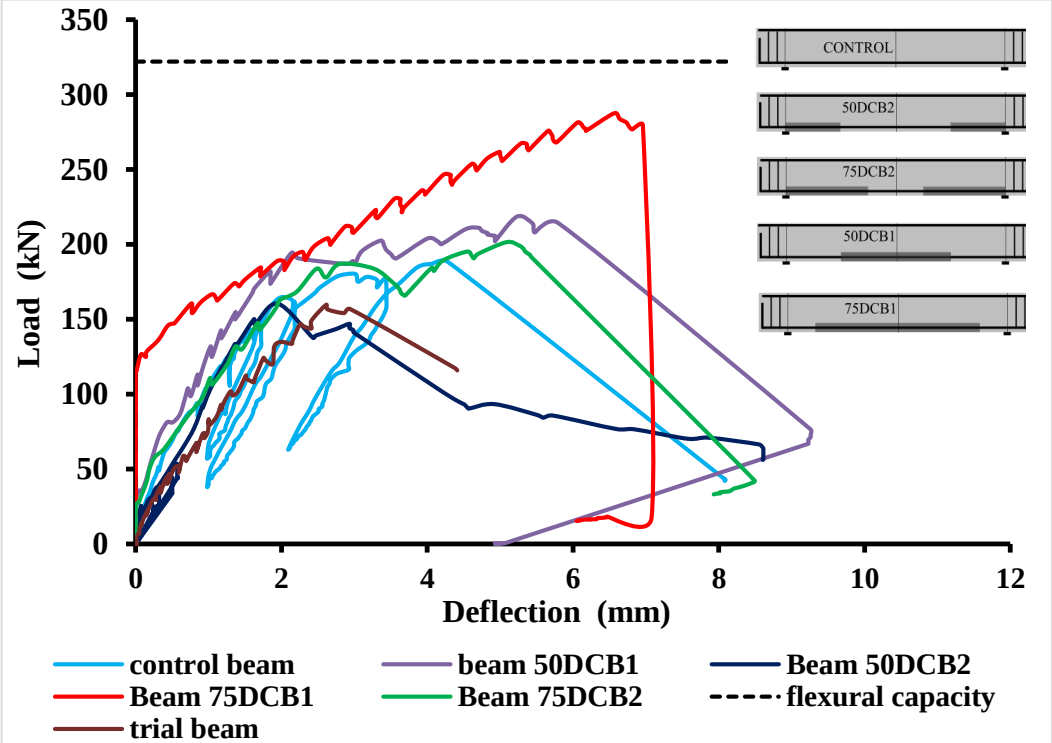

Figure 5-46 Load vs deflection of the DCB series

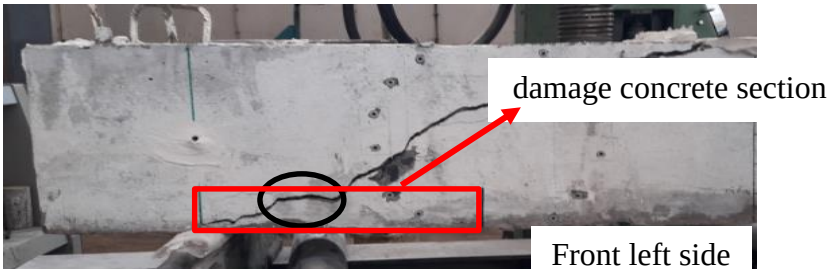

Figure 5-47 Beam 50DCB2 critical diagonal crack

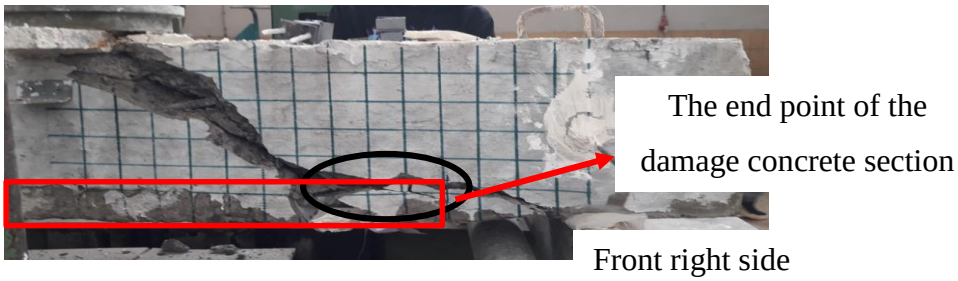

Figure 5-48 Beam 75DCB1 critical diagonal crack

Figure 5-49 Beam 75DCB2 critical diagonal crack

Although the length and fabrication of the damaged concrete section differ from the DCB series, avoidance of the damaged concrete section is also seen in the trial beam too. The delay of cracking of the concrete along the longitudinal reinforcement (dowel or horizontal cracking) was not observed in the trial beam nor on the DCB series beam specimens. In the case of the DCB, the reason for the better results of beams 75DCB1 and 50DCB1 from beams 75DCB2 and 50DCB1 is unclear. The progression of the critical diagonal formation nor the readings did not hint at a reason for their better performance.

Table 5-3 change in ultimate capacity from the control beam

Specimen	Increase/decrease from control ultimate capacity
trial beam	-6%
beam 50DCB1	55%
beam 50DCB2	14%
beam 75DCB1	104%
beam 75DCB2	43%

5.2.2 The effect of percentage of length affected by bond cut or bond deterioration

5.2.2.1 The effect of percentage of length affected bond cut the BB series

This series experimented with a bond cut of 0% and 75%. Though the percentages in between should also be studied, an increase in the percentage of length of shear span affected by bonds cut showed a better performance in this series. Previous experiments mentioned in figure 5-40 involving bond cutting using PVC pipe indicate that the maximum enhancement in performance was achieved at around 50%. Some researchers reported maximum performance at 100% of the bond cut.

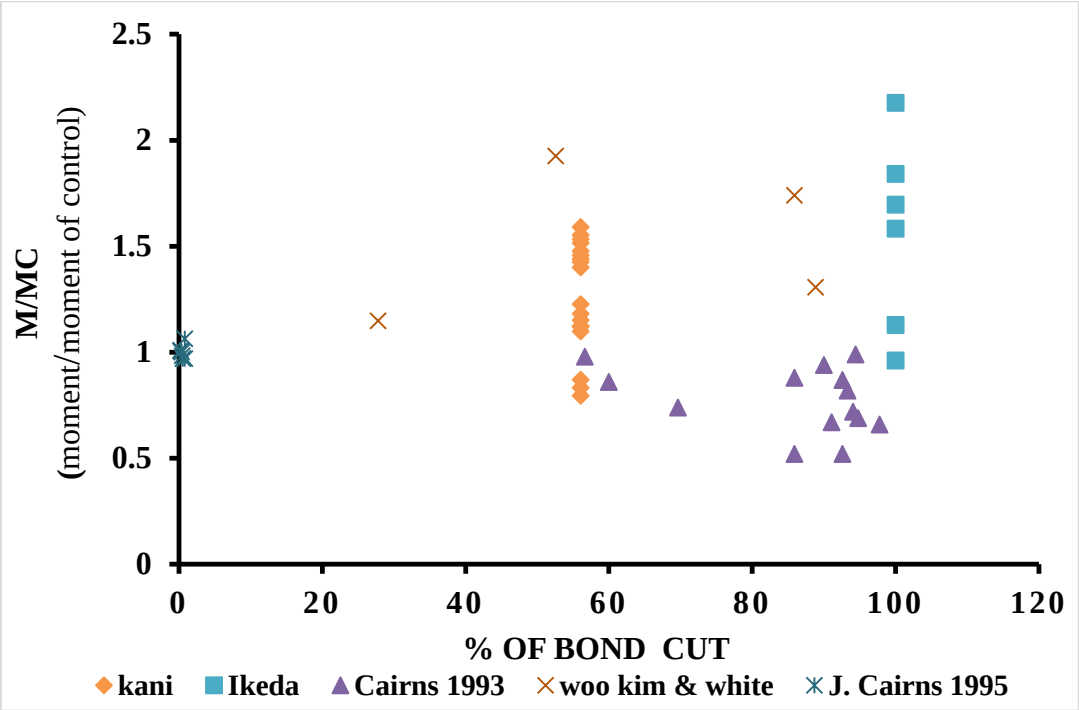

Figure 5-50 Relation between shear capacity enhancement and % of bond cut from other researchers work

Many researchers believe that the nature of local bond stress concentration immediately after flexural cracking is a major cause for the initiation of the flexural shear cracking in reinforced concrete beams, as shown in Figure 2-3. In their research, Kim and White reasoned that the enhancement in bond cut series was caused by the absence of shear stress induced by the bond, which led to the delay of shear crack and resulting in avoidance or delay of the shear failure. This could explain the enhancement of both beams 75BB1 and 75BB2 from their control beam.

It is clear that most slender beams resist action in a combination of two mechanisms, the first being composite beam action, which arises from the transmission of a tensile force into the steel by means of bond stresses. For a beam to fully resist using this mechanism requires a full bond, which is not possible with the bond slip and cracking the section experiences as loading progresses. It becomes necessary for the second mechanism to be activated, which expresses shear resistance by inclined internal compression and represents what is known as "arch action," since it arises from an arch-like variation in the height of the location of the compressive resultant.

When bond loss is introduced from the beginning of the loading, the prominence of composite beam action in shear resistance is undermined and arch action is expected to prevail. In the case of the BB series, this is indicated by the change in critical diagonal cracking of beams 75BB1 and 75BB2 from the control beam. This shows the position of the compression strut has been modified in the two beams to account for the internal stress redistribution caused by the bond loss.

The vertical cracks in the compression zone of the beam around the support, reported by the researchers mentioned in chapter 2, were not observed in the BB Series. These cracks were also used as an indication of prominent arch action in beams.

5.2.2.2 The effect of percentage of length affected bond deterioration DCB series

In this series, increasing the quotient of the shear span affected by bond deterioration by transversal cracking was found to be better for the performance of the beam despite the positioning of the deteriorated concrete section. In this series, beams with damaged bond deterioration in the middle (75DCB1 and 50DCB1) have a higher ultimate capacity than beams 75DCB2 and 50DCB2.

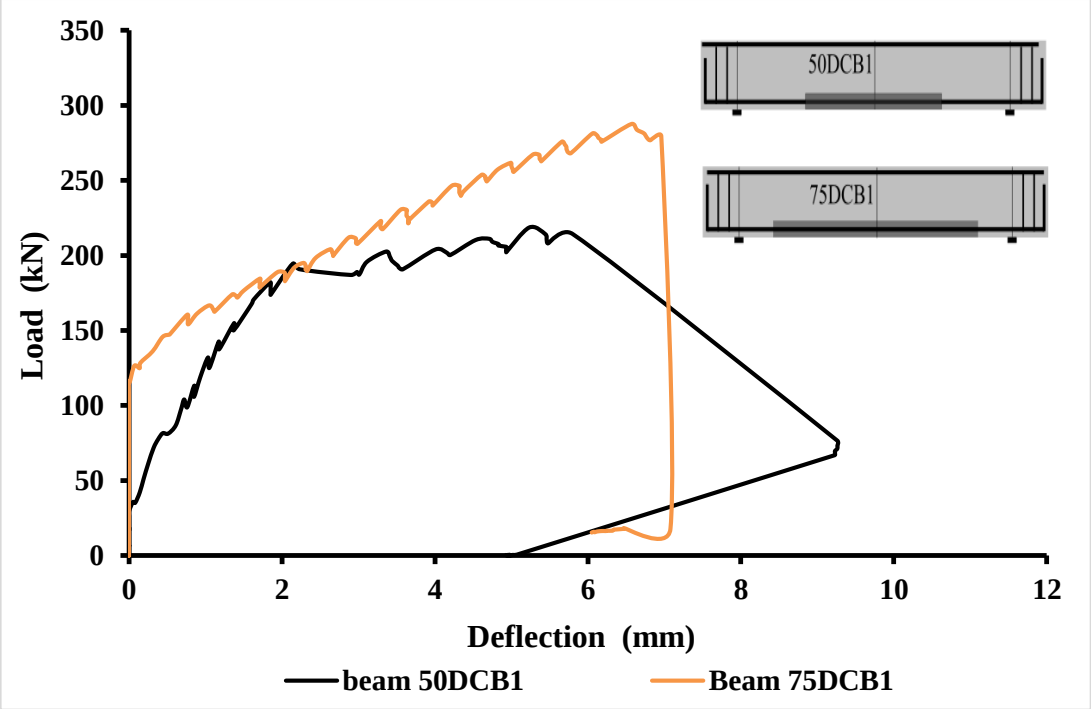

Figure 5-51 The load vs deflection of beams 50DCB1 and 75DCB1

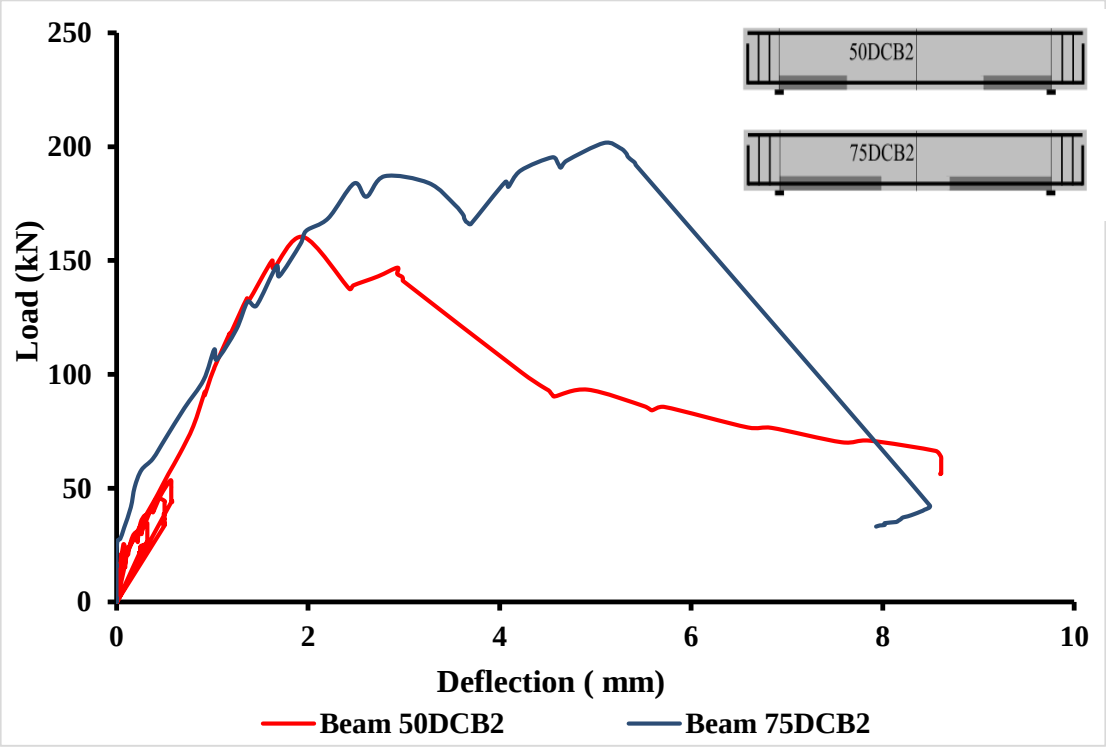

Figure 5-52 The load vs deflection of beams 50DCB2 and 75DCB2

Overall, the two series showed that at the specified percentage of bond cut and bond damage by cracking, the 75% was found to have higher performance, agreeing with most researchers that an increase in percentage will yield better results.

5.2.3 The effect of bond cutting and bond damage by cracking

While the BB series was so effective in bond cutting, the propagation of the critical diagonal crack was immensely affected and shear failure was avoided or delayed in the specimens. But in the case of the DCB series, the deteriorated bond concrete section was not as effective as the gasket in changing the trajectory of diagonal crack formation.

Of the phenomena observed, the most intriguing was the initiation of the critical diagonal crack in the BB series. It was clearly observed in beams 75BB1 and 75BB2. The diagonal crack started at the points of change in bond condition (the interface between the artificial un-bonding and normal bond condition). This affected the angle of the compression strut position, affecting the resistance of the beams. In the DCB series, though some deviations in the formation of the horizontal (dowel) cracking were observed, a severe change in the positioning of the critical diagonal crack was not observed.

In both series, the progression of the horizontal crack was affected by the delay of the crack formation and change in projected crack path due to spalling of the bottom cover. It is clearly proven by other researchers that the delay of the horizontal cracking affects the propagation of the top end of the diagonal critical crack in the compression zone.

The formation of the compression strut was also affected by the method of bond cutting and deterioration caused by transversal cracking. In the BB series, its position was dependent on the change in bond condition of the longitudinal bar. This was not the case in the DCB series where the specimens followed mostly theoretical compression strut from the point of loading to the support.

The other significant change shown between the two series is the sign of the shear strain (Υ_{xy}),Which indicates the type of average deformation the area within the surface measurement was experiencing. A positive shear strain physically means the increase of the angle θ (figure 5-53), while a negative value indicating a decrease the angle θ. The most probable combined stress state to cause a positive shear strain is a compression stress at the corners of the rectangular section. Most likely a negative one is caused by a combined tensile stress state that is applied at the corner of the rectangular section.

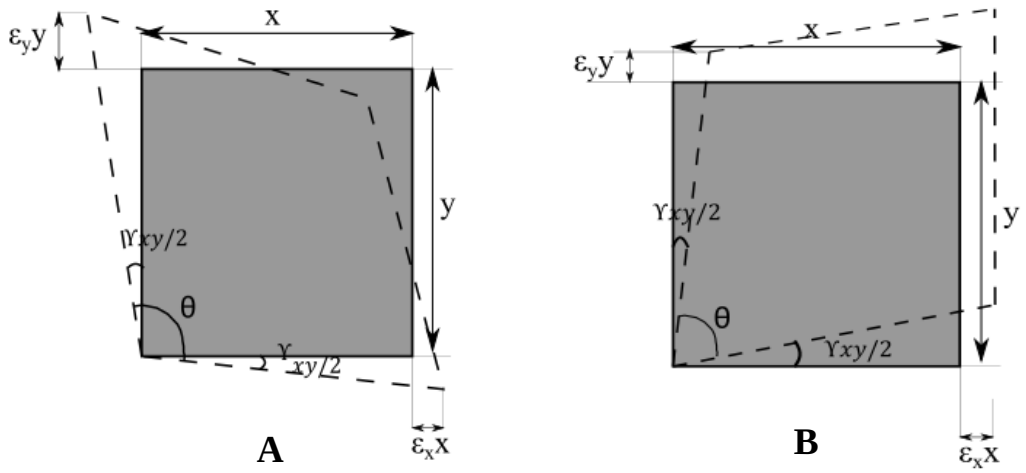

Figure 5-53 A, positive shear strain deformation B, negative shear deformation

By taking account the horizontal, vertical and shear strain measurement the progress of the angle θ was monitored for the beam specimens to physically understand the deformations they went through. The result showed that only specimens that showed an increase and then decreases starting from a specific load point in the angle θ are specimen 75BB1 and 75BB2, where a gasket was used to cut bond. The other specimens including the control specimen showed a constant increase in the angle θ. This implies that beams 75BB1 and 75BB2 experienced compression force followed by a decrease in compression force while the other specimen experienced constant increase in compression force. Probably indicating the shift or failure of the compression strut in beams 75BB1 and 75BB2.

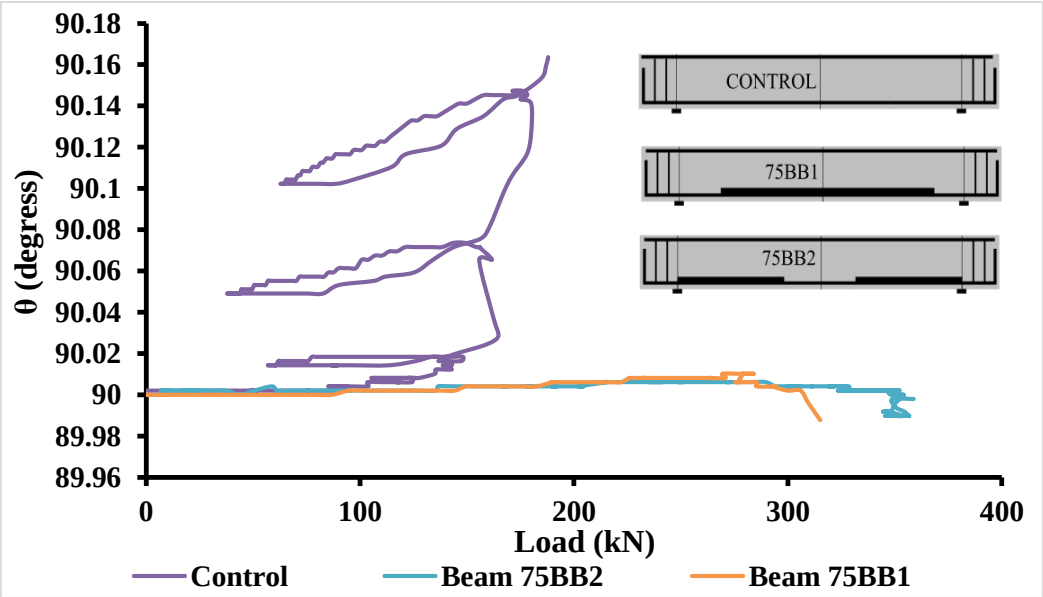

Figure 5-54 Angle θ for the BB series

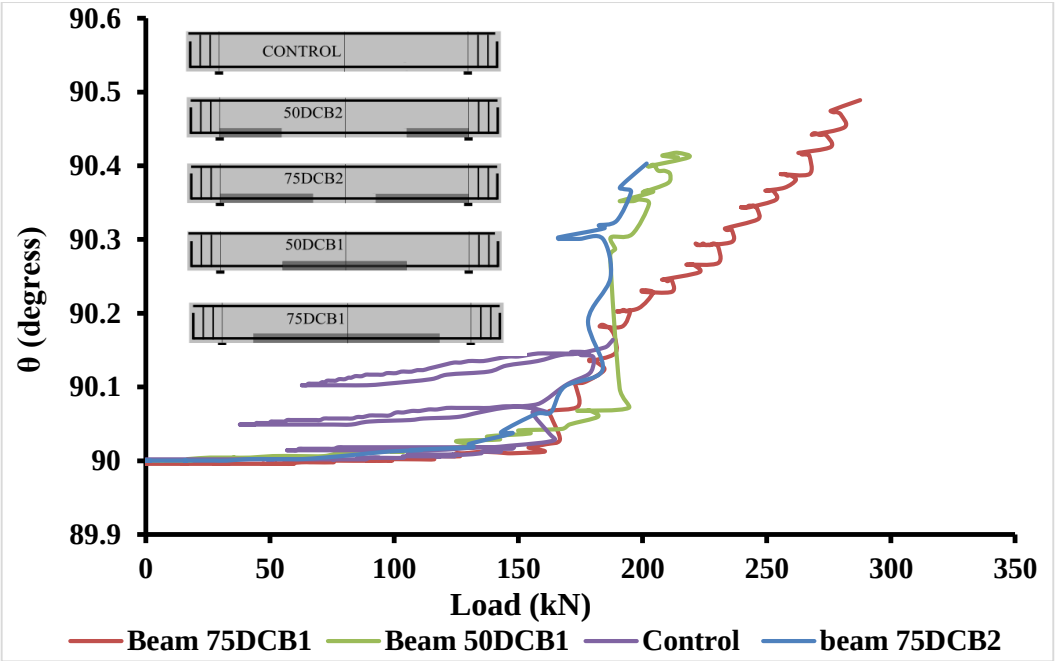

Figure 5-55 Angle θ for the DCB series

Taking account of the principal strains and shear strain, Mohr's circles for every specimen every 50kN intervals were drawn as shown in Appendix E. The other observation is noticed by comparing the strain states of the specimen were at point of failure, as it could be observed on from figure 5-56 and 5-57 the strain levels of the BB series are more than 10times smaller than what the DCB series is experiencing.

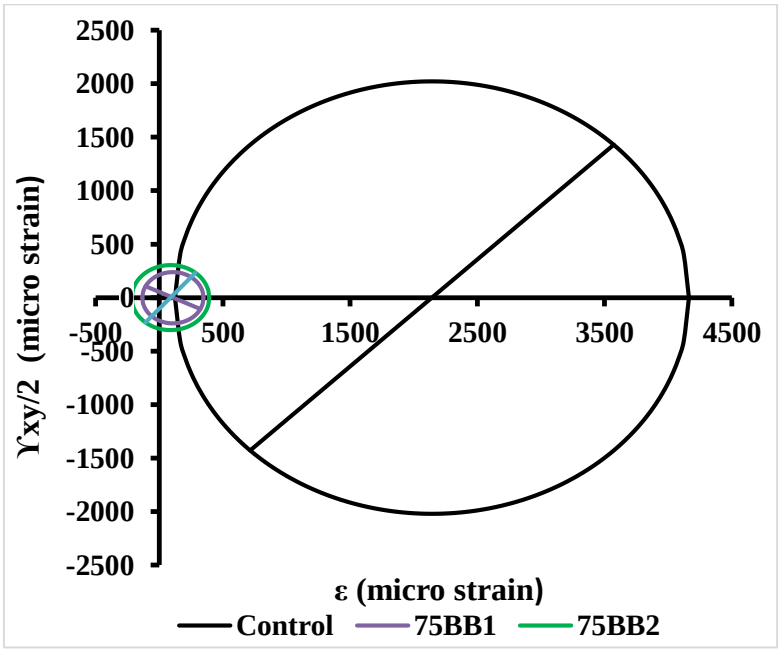

Figure 5-56 Mohr's circle at point of failure for the BB series

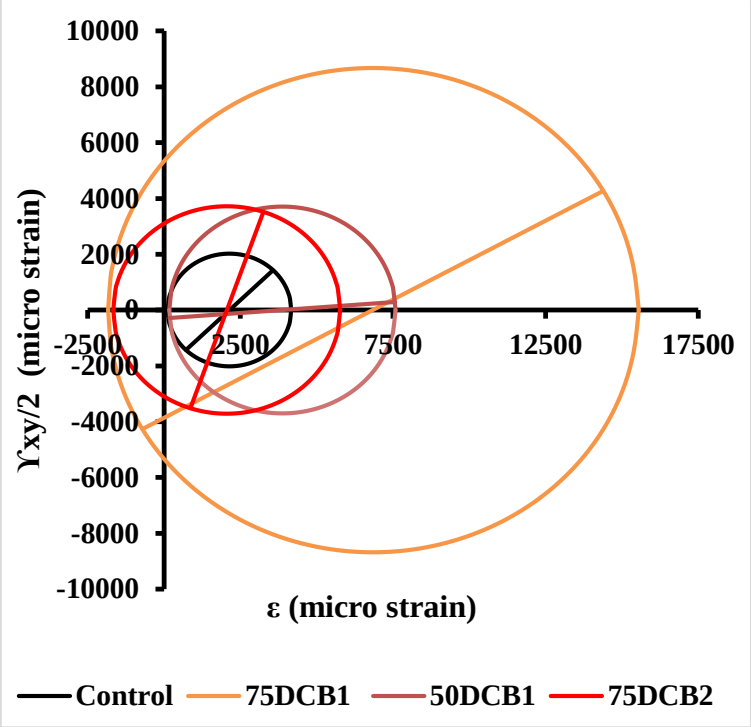

Figure 5-57 Mohr's circle at point of failure for the DCB series

5.2.4 Comparison of FEM analysis results with experimental results

In analyzing the FEM results in tandem with the experimental results, it could be seen that the FEM captured the stiffness of the control beam, though it did not accurately determine the ultimate capacity determined by the experiment. The FEM's ultimate capacity prediction showed a 16% decrease from the experimental value. In the 75BB1 beam, the FEM prediction of ultimate capacity showed a 35% decrease from the value determined by the experiment. In the FEM of the beam 75BB2, the ultimate capacity of the beam was not captured.

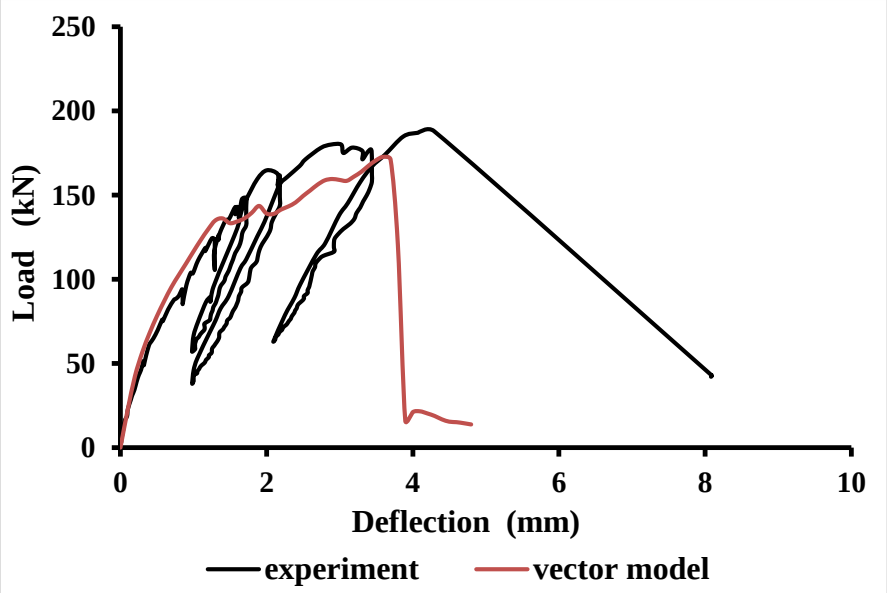

Figure 5-58 Comparing the FEM and experimental result of control beam

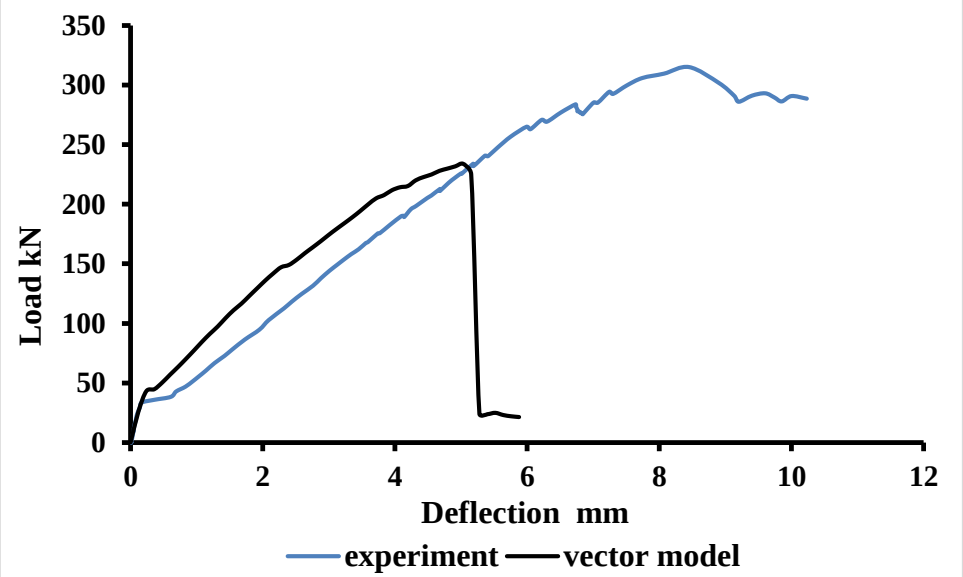

Figure 5-59 Comparing the FEM and experimental result of beam 75BB1

5.2.5 Comparison with available design codes

5.2.5.1 On shear capacity calculations

The results obtained from the experiment were compared to available codes. The objective was to monitor if the codes implement parameters that consider the bond between the concrete and the longitudinal rebar. Most shear capacity codes did not include a parameter to quantify this effect, but some did include a parameter to account for shear resistance of cracked concrete, which depends on longitudinal strain and factored shear force or an

equivalent crack spacing parameter. This parameter was present; the effect the quality of the bond has on the shear resistance of concrete was found to be lacking.

Table 5-4 Concrete shear capacity according to codes

No	Codes	Concrete contribution to shear	remark on variables involved
1	ACI 318-02	$V_c = 2\sqrt{f_c}b_w$d	No variables to account for the bond loss between concrete and longitudinal bar
2	ACI 318-08	$V_c = 0.17\sqrt{f_c}b_w$d	No variables to account for the bond loss between concrete and longitudinal bar
3	CSAA23.3-94 SIMPLIFIED METHOD	$V_c = 0.2\sqrt{f_c}b_w$d when $A_V \geq \frac{0.06b_w s\sqrt{f_c}}{f_y}$ or d≤ 300mm	No variables to account for the bond loss between concrete and longitudinal bar
4	CSAA23.3-94 GENERAL METHOD	$V_{cg} = \beta\sqrt{f_c}b_w d_v$ (mm ,MPa)	β = factor accounting for shear resistance of cracked concrete which depends on longitudinal strain and factored shear force or crack spacing parameter. A variable is present but difficult to determine.
5	AASHTO LRFD Bridge Design Specifications (2001)	$V_c = 0.0316\ \beta\sqrt{f_c}b_w d_v$ (in,ksi)	β = factor accounting for shear resistance of cracked concrete which depends on longitudinal strain and factored shear force or equivalent crack spacing parameter. A variable is present but difficult to determine.
6	CSA A23.3 2004 edition (M.P. Collins, 2002)	$V_{cg} = \beta\sqrt{f_c}b_w d_v$ (in,psi)	β = factor accounting for shear resistance of cracked concrete which depends on longitudinal strain and factored shear force or equivalent crack spacing parameter. A variable is present but difficult to determine.

7	Euro code EC2 Part 1 (1991) Standard Method	$V_{RD1} = \beta\tau_{rd}\, k(1.2 + 40\rho_l)b_w$d (mm, MPa)	β is an enhancement factor that can be applied if the member is loaded by a concentrated load situated at a distance, x ≤ 2.5d, from the face of the support. Otherwise, β = 1. τ_{rd} = basic design shear strength (= 0.25 f_{ctk} 0.05).variable present but usually taken as 1.
8	Euro code EN 1992-1-1 (2002)	$V_{Rd,c} = \left[C_{Rd,c}k(100\rho_1 f_{ck})^{1/3} + k_1 6_{cp}\right] b_w$d (mm, MPa)	No variables to account for the bond between concrete and longitudinal bar
9	Euro code EN 1992-1-1 (2003)	$V_{Rd,c} = \left[0.12k(100\rho_1 f_{ck})^{1/3} - 0.156_{cp}\right] b_w$d (mm, MPa)	For members not requiring web reinforcement no variables to account for the bond loss between concrete and longitudinal bar
10	German Code DIN 1045-1 (2001)	$V_{Rd,c} = \left[0.1\eta_1 k(100\rho_1 f_{ck})^{1/3} - 0.126_{cp}\right] b_w$d (mm, MPa)	For members not requiring web reinforcement no variables to account for the bond loss between concrete and longitudinal bar
11	Japanese Code (JSCE Standards, 1986)	$V_{cd} = f_{ycd} b_w/\Upsilon_b \;\; f_{ycd} = 0.9\beta_d\beta_p\beta_n(f_c)^{1/3}$ (kgf/cm2)	No variables to account for the bond loss between concrete and longitudinal bar

From the above tabulated codes, a few were chosen to compare how the shear capacity of each beam in the experimental program was represented. The results are shown below.

Table 5-5 Different codes coefficient of variation in relation with experimental result

	Shear capacity difference from experiment					
Beam	ACI 318-08	CSA A23.3-94 Simplified Method	Euro code EC2 (1991) Standard Method	Euro code EN 1992-1-1 (2002)	German Code DIN 1045-1 (2001)	Japanese Code (JSCE Standards, 1986)
Trial beam	22.648	12.566	6.286	5.254	38.377	8.483
Control	30.593	19.404	9.551	14.113	49.618	17.574
75BB1	94.143	82.954	73.101	77.663	113.168	81.124
75BB2	115.593	104.404	94.551	99.113	134.618	102.574
75DCB1	96.315	87.936	86.369	77.920	107.200	80.774
75DCB2	53.315	44.936	43.369	34.920	64.200	37.774
50DCB1	61.815	53.436	51.869	43.420	72.700	46.274
50DCB2	32.715	24.336	22.769	14.320	43.600	17.174
Mean	63.392	53.746	48.483	45.840	77.935	48.969
S.D	34.919	34.654	34.140	35.157	36.001	35.228
C.V	**0.551**	**0.645**	**0.704**	**0.767**	**0.462**	**0.719**

Table 5-6 Different codes coefficient of variation in relation with each series experimental result

Beams	statically values	ACI 318-08	CSA A23.3-94 Simplified Method	Euro code EC2 Part 1 (1991) Standard Method	Euro code EN 1992-1-1 (2002)	German Code DIN 1045-1 (2001)	Japanese Code (JSCE Standards, 1986)
Series BB	Mean	80.110	68.920	59.068	63.629	99.135	67.090
	S.D	44.204	44.204	44.204	44.204	44.204	44.204
	C.V	**0.552**	**0.641**	**0.748**	**0.695**	**0.446**	**0.659**
Series DCB	mean	61.040	52.661	51.094	42.645	71.925	45.499
	S.D	26.501	26.501	26.501	26.501	26.501	26.501
	C.V	**0.434**	**0.503**	**0.519**	**0.621**	**0.368**	**0.582**

It can clearly be seen from the tables codes like the Euro Code (2002) and Euro Code (1991) (standard method) gave better predictions in the BB series, and codes like the Japanese Code and Euro Code EN 1992-1-1 (2002) were found to give better predictions in the DCB series. As a whole, the Japanese Code and Euro code EN 1992-1-1 (2002) gave better predictions.

CHAPTER 6 CONCLUSIONS AND RECCOMENDATIONS

6.1 Conclusion

The following are the conclusions reached about the study based on the measurements, observations and analysis described in the previous chapters.

Considering the ultimate capacity of both methods of bond cutting or deterioration, it was found that all the specimens except in the case of trial beam had better performance than that of the control beam. The DCB series beams had a stiffer response than the BB series and are more likely to satisfy the serviceability limit of Euro or ACI codes.

On both series the higher percentage of bond cut or deterioration (75%) gave a better result in ultimate capacity. The location of the bond cut or bond deterioration was found to have a profound effect on the results observed. In the BB series, locating the artificial un-bonding material(gasket) near the supports was a better option than center placement. This is possibly caused by the delay of the dowel cracking as it is shown in (Krefeld & Thurston, 1966) and the shift of the compression strut location in the BB series. Though no dramatic shift from the theoretical compression strut was observed in the DCB series, a bond loss is known to facilitate the dominance of arch action over beam action.

Beams 75BB1and 75BB2 experienced negative shear strain hinting at a possible shift of the compression strut and a much lesser principal strains compared to the control and the DCB series. The FEM

The major finding of the research was that the location of the bond cut or bond deterioration has a major effect on the enhancement of beam shear capacity. In the BB series positioning the bond cut location near the supports was found to be better for the beams shear capacity, while positioning the damaged concrete section at the middle of the length of the beam in DCB series showed a better shear capacity. The cutting of the bond affected and dictated the location and initiation of the critical diagonal cracking and also its propagation to the point of loading in the BB series.

6.2 Recommendation

The following are the recommendations that are made based on the results and analysis conducted.

1. A further study in the BB series with percentages of bonds cut other than those tested in this research should be investigated.
2. The effect of the experimental variables on beams with stirrup and with cyclic loading should be investigated.
3. Since bond between concrete and rebar is affected by many factors other variables like cover should be experimental variables in other studies
4. Concerning fabrication of the DCB series, a better slit forming method other than laminated paper should be considered in further studies.
5. A better instrumentation that would also monitor the horizontal cracking like a pie gage should be utilized. A number of mold gages should also be utilized at different levels of the cross section and locations to monitor shear transferred to the web in both series of the experiment.
6. The results in the DCB series caused by change in location of the bond deterioration zone and the large values of the principal strain could not be explained. Other further studies should look in to this results.
7. A 3D FEM should also be used to analyze all of the specimens.

REFERENCES

Bilcik, J., & Holly, I. (2013). Effect of reinforcement corrosion on bond behaviour. *Procedia Engineering*, *65*(June), 248–253. https://doi.org/10.1016/j.proeng.2013.09.038

Cairns, J., & Zhao, Z. (1994). Behaviour of concrete beams with exposed reinforcement. *Proceedings of the Institution of Civil Engineers: Structures and Buildings*, *104*(3), 351–355. https://doi.org/10.1680/istbu.1994.26785

Committee, T. H. E. A., & Tension, D. (1964). The Riddle of Shear Failure and its Solution. *ACI Journal Proceedings*, *61*(4), 441–468. https://doi.org/10.14359/7791

de Normalisation, C., & NORMUNG, E. (2003). European Standard Norme Européenne Europäische Norm. *Recherches*, *14689*(November), 1.

Feldman, L. R., & Bartlett, F. M. (2008). Bond in flexural members with plain steel reinforcement. *ACI Structural Journal*, *105*(5), 552–560. https://doi.org/10.14359/19938

Kim, W., & White, R. N. (1991). Initiation of shear cracking in reinforced concrete beams with no web reinforcement. *ACI Structural Journal*, *88*(3), 301–308. https://doi.org/10.14359/9447

Kim, W., & White, R. N. (1999). Shear-critical cracking in slender reinforced concrete beams. *ACI Structural Journal*, *96*(5), 757–765. https://doi.org/10.14359/729

Krefeld, W., & Thurston, C. W. (1966). Contribution of Longitudinal Steel to Shear Resistance of Reinforced Concrete Beams. *ACI Journal Proceedings*, *63*(3), 325–344. https://doi.org/10.14359/7626

Masukawa, J. (2012). *Degradation of Shear Performance of Beams due to Bond Deterioration and Longitudinal Bar Cutoffs*. 353. Retrieved from http://www.iitk.ac.in/nicee/wcee/article/11_1208.PDF

Muttoni, A., & Ruiz, M. F. (2008). Shear strength of members without transverse reinforcement as function of critical shear crack width. *ACI Structural Journal*, *105*(2), 163–172. https://doi.org/10.14359/19731

Ouglova, A., Berthaud, Y., Foct, F., François, M., Ragueneau, F., & Petre-Lazar, I. (2008). The influence of corrosion on bond properties between concrete and reinforcement in concrete structures. *Materials and Structures/Materiaux et Constructions*, *41*(5), 969–980. https://doi.org/10.1617/s11527-007-9298-x

Wong, P. S., Vecchio, F. J., & Trommels, H. (2013). VecTor2 & FormWorks User's Manual (2nd edn). *University of Toronto: Toronto, ON, Canada*, Available from: http://www.civ.utoronto.ca/vector/.

Y.Yang, Veen, C. van der, Hordijk, D., & Boer, A. de. (2016). The shear capacity of reinforced concrete members with plain bars. *Structural Faults + Repair*.

APPENDIX A, PULL OUT SPECIMEN DESIGNING BOND STRENGTH EQUATIONS FROM CODES AND RESEARCHER'S

Codes and researcher's equations for bond strength used to decide the pull out specimen details

Parameters

Parameters	Values	Remark
f_{ck}	25	Characteristic strength
f_c	16.666	Compressive Strength
d_b	20	Bar Diameter
c	65	Cover
C	75	Radius Of Cylinder
f_{ct}	2.245	Tensile Strength Of Concrete
A_b	314.159	Slip
c_x	65	The Side Cover
cy	65	The Bottom Cover
c_s	65	Spacing B/N Bars
l_d	80	Embedment Length
C_{max}	65	Max(Min(C_x,C_s/2),C_y)
C_{min}	65	Min(C_x,C_y,C_{si})
A_b	314.159	Area of re-bar
C_{min}	32.5	Min(C_x,C_y,C_s/2)

The Equations Considered

No	Code and researchers	proposed equation
1	CBE-FIP(good bond condition)	$\tau u = 2.5\sqrt{f_c'}$ at pull-out failure
		$\tau u = 2.5\sqrt{f_c'}$ at pull-out failure
	CBE-FIP(other bond condition)	$\tau u = 1.25\sqrt{f_c'}$ at pull-out failure
		$\tau_u = 5 \times \left(\frac{\sqrt{fc}}{20}\right)^{0.25}$ at splitting failure
2	Australian Standard 3600	$\tau_u = 5 \times \left(\frac{\sqrt{fc}}{20}\right)^{0.25}$ at splitting failure
3	Orangun et al.	$\tau u = 0.083045 \times \sqrt{fc} \times \left(1.2 + 3\left(\frac{c}{db}\right) + 50\left(\frac{db}{ld}\right)\right)$
		$\frac{u}{\sqrt{fc}} = \left(1.2 + 3\left(\frac{cmin}{db}\right) + 50\left(\frac{db}{ld}\right)\right)$
4	Darwin et al	$\tau u = 0.083045 \times \sqrt{fc}\left(2.12\left(\frac{c}{db}\right) + 0.5\right) \times \left(0.92 + 0.08\left(\frac{cmax}{cmin}\right) + 75\left(\frac{db}{ld}\right)\right)$

		$[63 \times ld \times (cmin + 0.5 \times db) + 2130 \times Ab] \times \left(\frac{0.1 \times cmax}{cmin} + 0.9\right)$
5	Esfahani & Rangan	$\tau u = 8.6 \times \left(\frac{\frac{c}{d}+0.5}{\frac{c}{d}+5.5}\right) \times fct$
6	ACI 44.1R-06	$\frac{u}{\sqrt{fc}} = 0.33 + 0.025 \times \frac{c}{db} + 8.3 \times \frac{db}{ld}$
7	Hadi	$\tau u = 0.083045 \times \sqrt{fc}\left[22.8 - 0.208 \times \left(\frac{c}{db}\right) - 38.212 \times \left(\frac{db}{ld}\right)\right]$
8	fib, Model Code 2010 - Vol. 1, 2010	$= \eta 2 \times 6.54 \times (fck)^{0.25} \times \left(\frac{20}{\Phi}\right)^{0.2} \times \left[\left(\frac{cmax}{\Phi}\right)^{0.33} \times \left(\frac{cmin}{cmax}\right)^{0.1} + 8ktr\right]$
9	ACI code	$u = 20.23 \times \frac{(fck)^{1/2}}{db}$
11	Shima	$u = 20.23 \times \frac{(fck)^{1/2}}{db}$
10	Shahriar Quayyum & AhmedRteil	$\frac{Uc}{\sqrt{f_c'}} = 0.03 + 0.14 * \frac{c}{d_b} + 9 * \frac{d_b}{l_d}$
11	Wambeke & Shield	$\frac{\tau b}{\sqrt{f_c'}} = 4 + 0.3 * \frac{c}{d_b} + 100 * \frac{d_b}{l_d}$

APPENDEX B, DCB SERIES SLIT AND BOND DETERIORATION PLACEMENT DETAILS

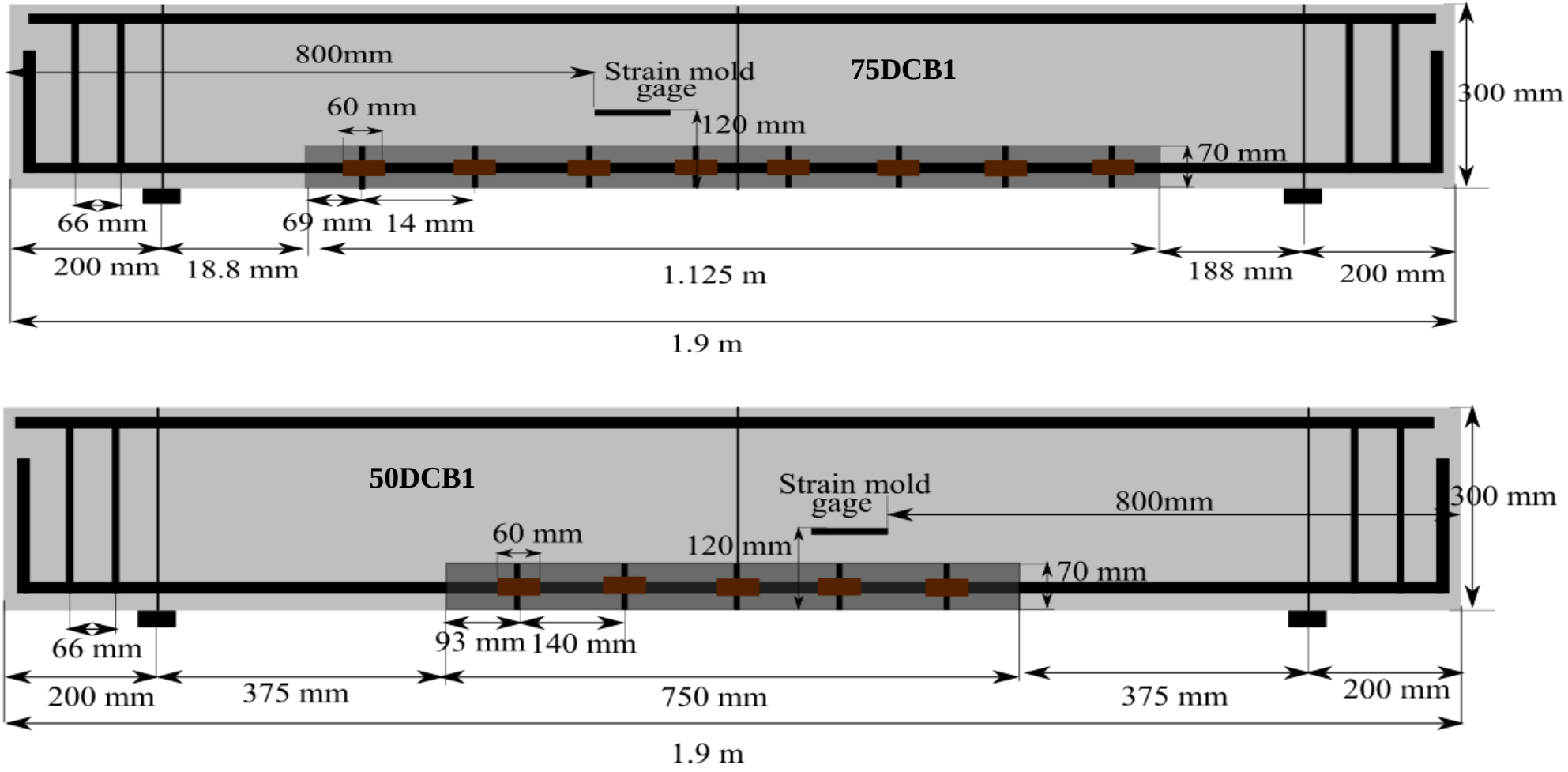

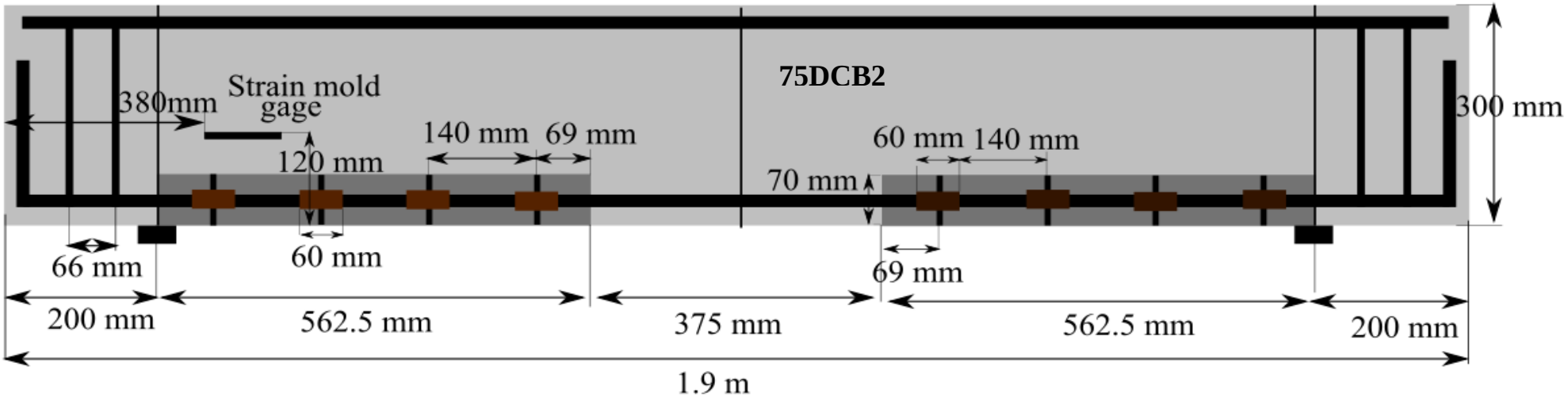
75DCB2
380mm
Strain mold gage
120 mm
140 mm
69 mm
60 mm
140 mm
70 mm
300 mm
66 mm
60 mm
69 mm
200 mm
562.5 mm
375 mm
562.5 mm
200 mm
1.9 m

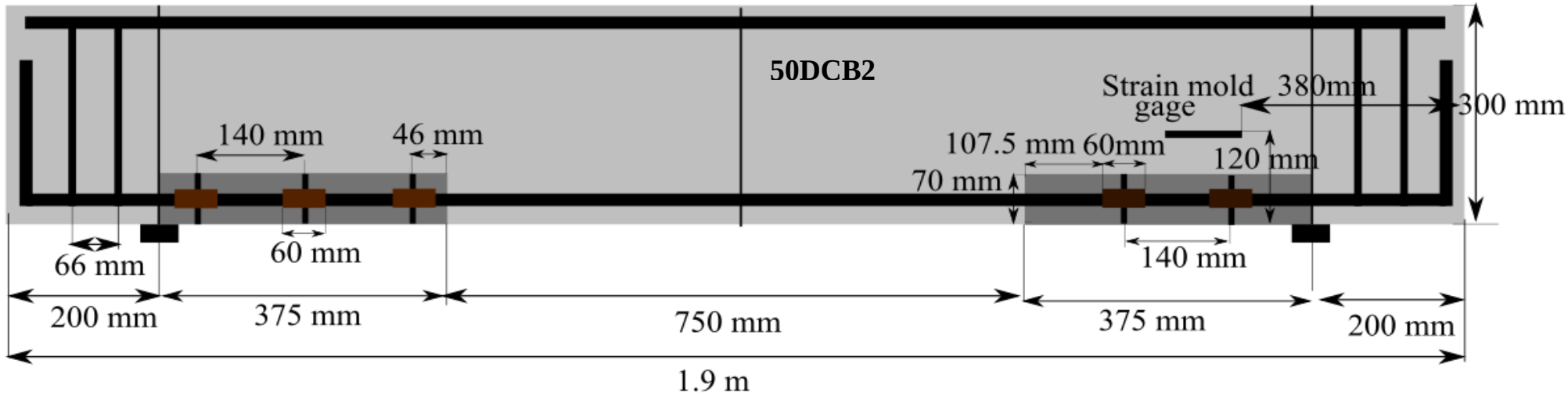
50DCB2
Strain mold gage
380mm
300 mm
140 mm
46 mm
107.5 mm
60mm
120 mm
70 mm
66 mm
60 mm
140 mm
200 mm
375 mm
750 mm
375 mm
200 mm
1.9 m

APPENDEX C, DETAILED GRAPHS OF RESULTS FROM THE EXPERIMENTAL PROGRAM

1, Control beam

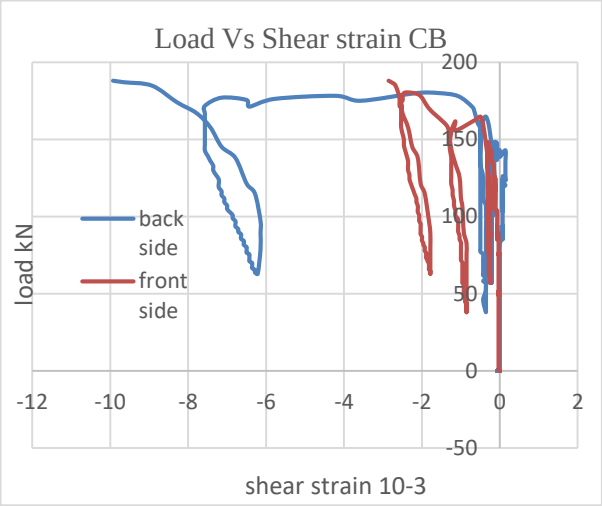

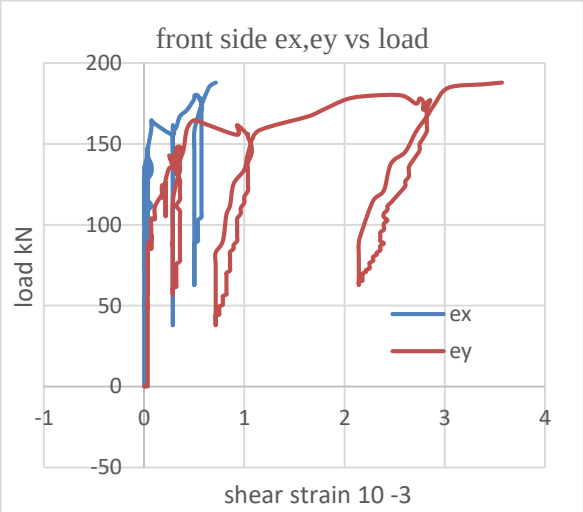

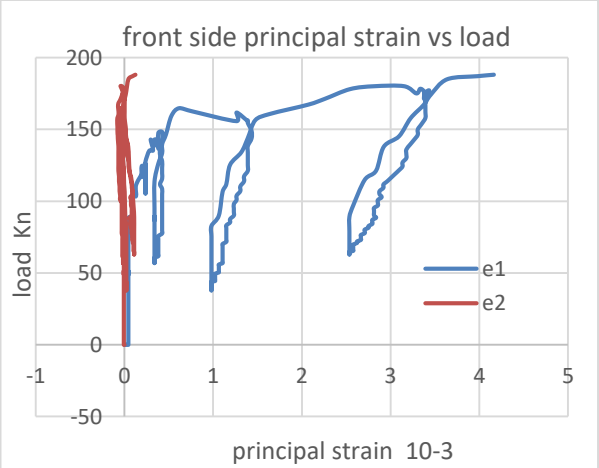

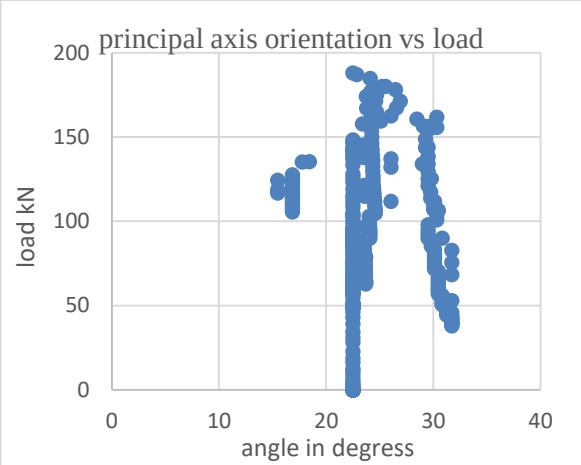

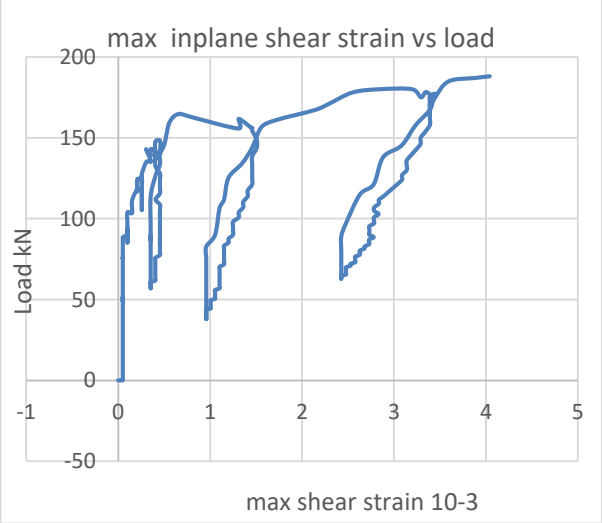

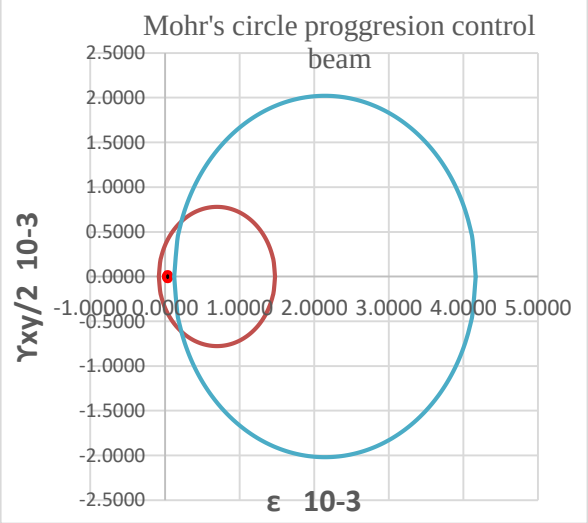

2,75BB1

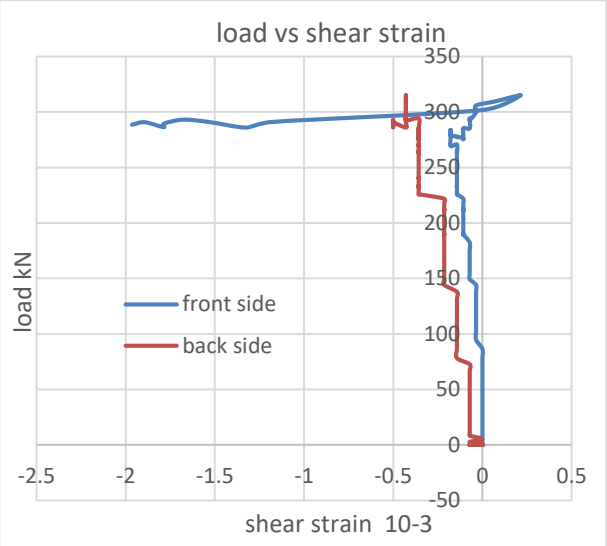
load vs shear strain
load kN
front side
back side
shear strain 10-3

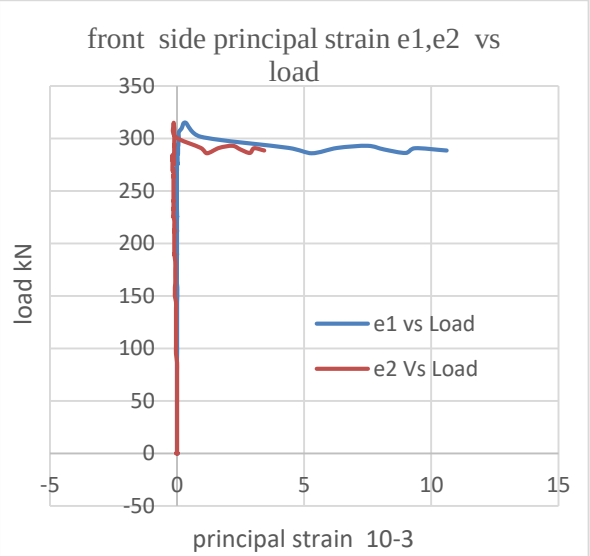
front side principal strain e1,e2 vs load
load kN
e1 vs Load
e2 Vs Load
principal strain 10-3

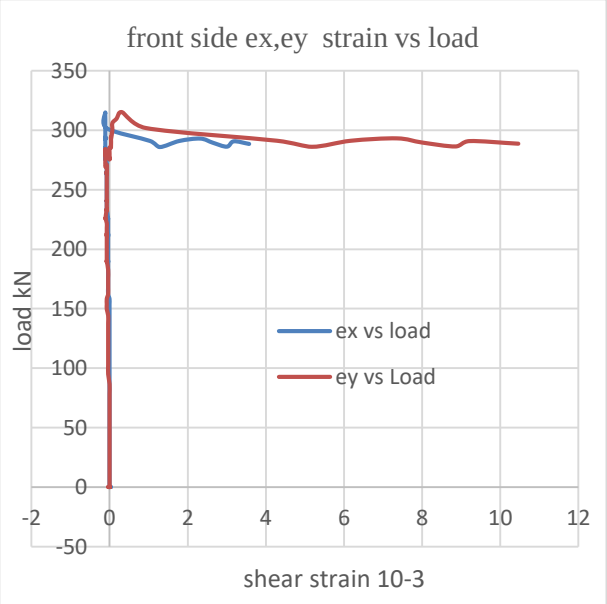
front side ex,ey strain vs load
load kN
ex vs load
ey vs Load
shear strain 10-3

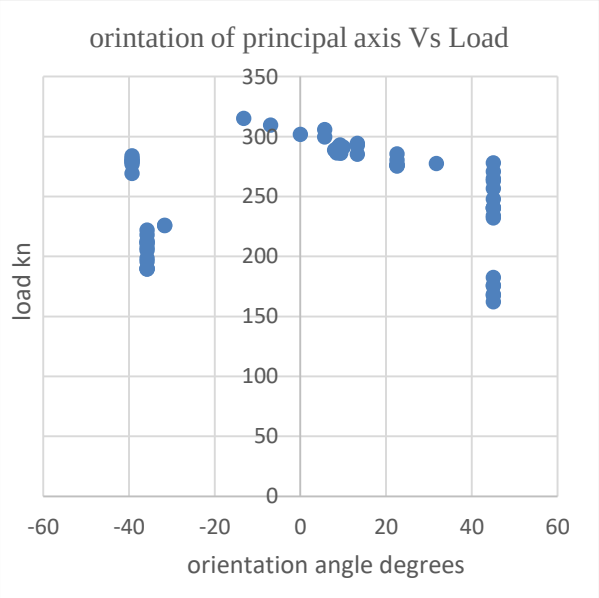
orintation of principal axis Vs Load
load kn
orientation angle degrees

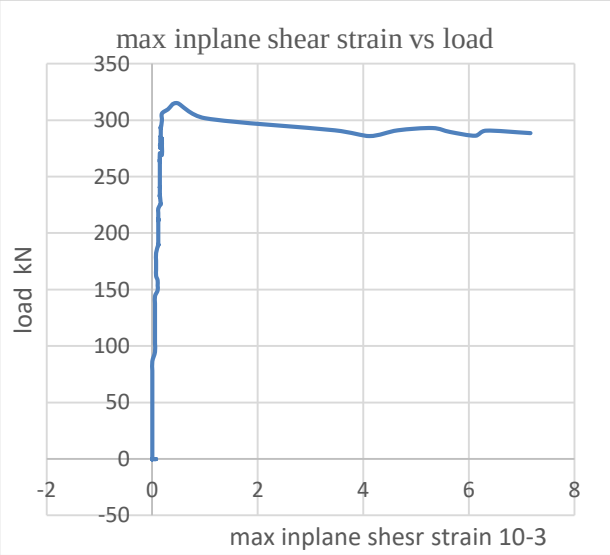
max inplane shear strain vs load
load kN
max inplane shesr strain 10-3

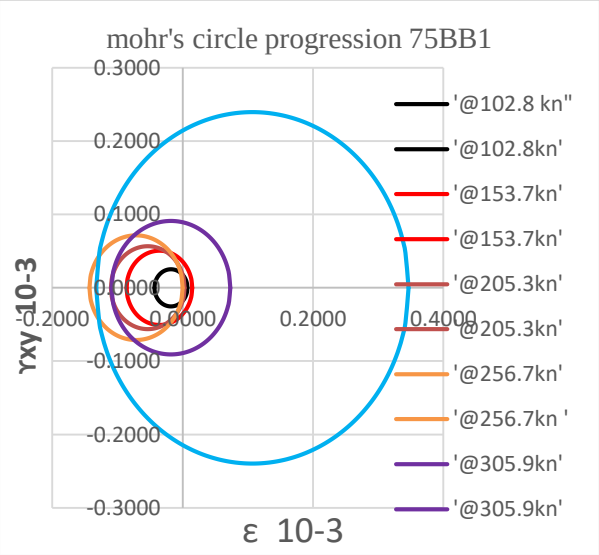
mohr's circle progression 75BB1
γxy 10-3
ε 10-3
'@102.8 kn"
'@102.8kn'
'@153.7kn'
'@153.7kn'
'@205.3kn'
'@205.3kn'
'@256.7kn'
'@256.7kn '
'@305.9kn'
'@305.9kn'

3,75BB2

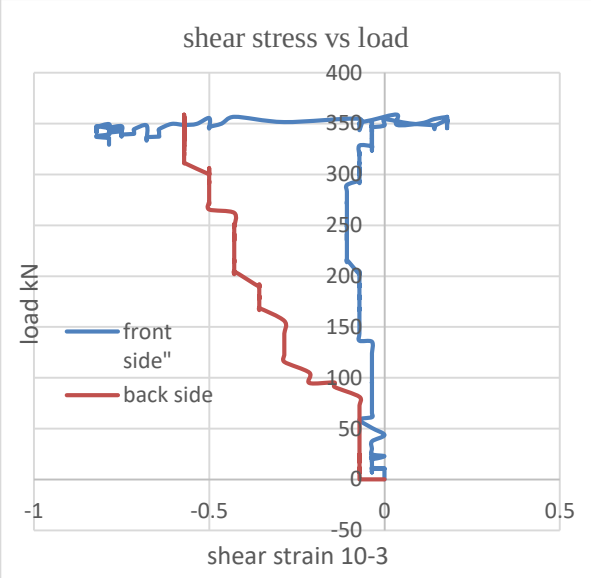
shear stress vs load
load kN
front side"
back side
shear strain 10-3

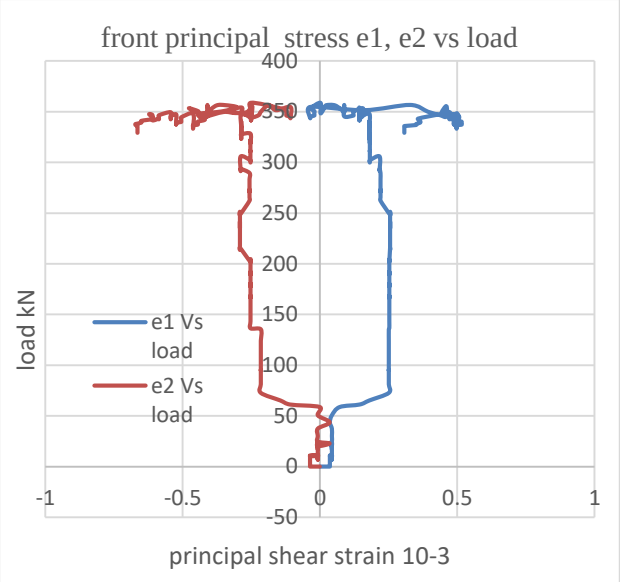
front principal stress e1, e2 vs load
load kN
e1 Vs load
e2 Vs load
principal shear strain 10-3

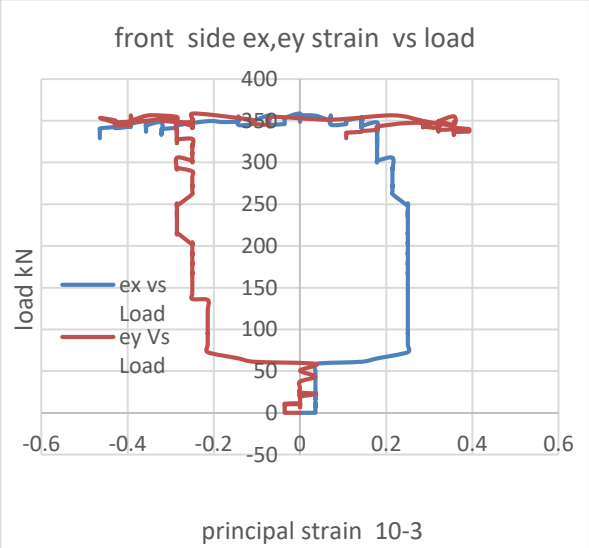
front side ex,ey strain vs load
load kN
ex vs Load
ey Vs Load
principal strain 10-3

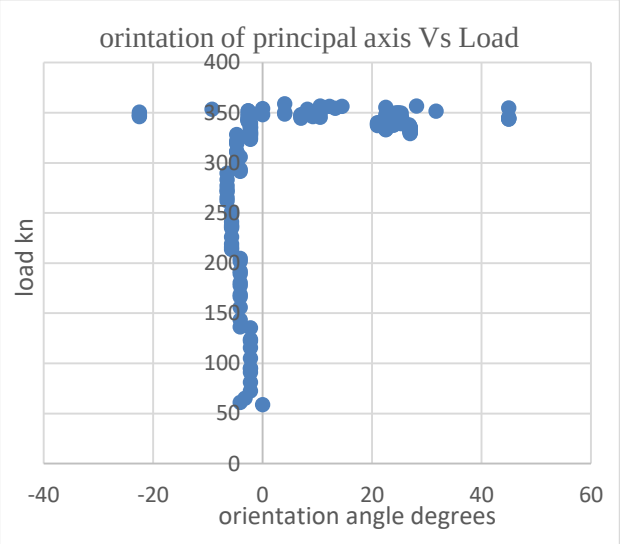
orintation of principal axis Vs Load
load kn
orientation angle degrees

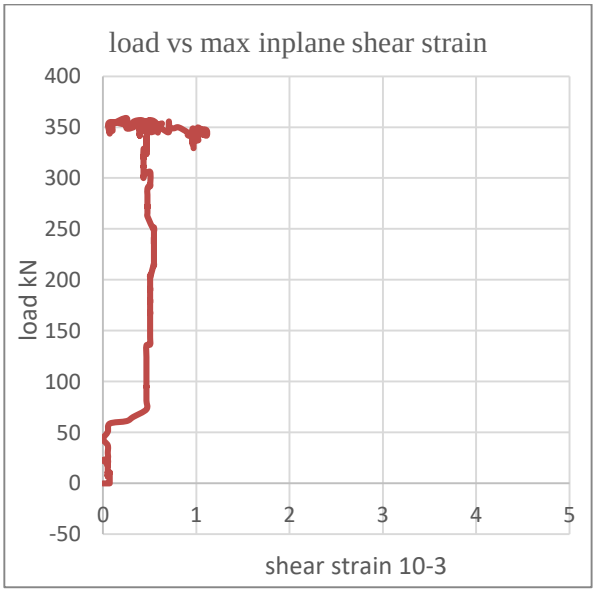
load vs max inplane shear strain
load kN
shear strain 10-3

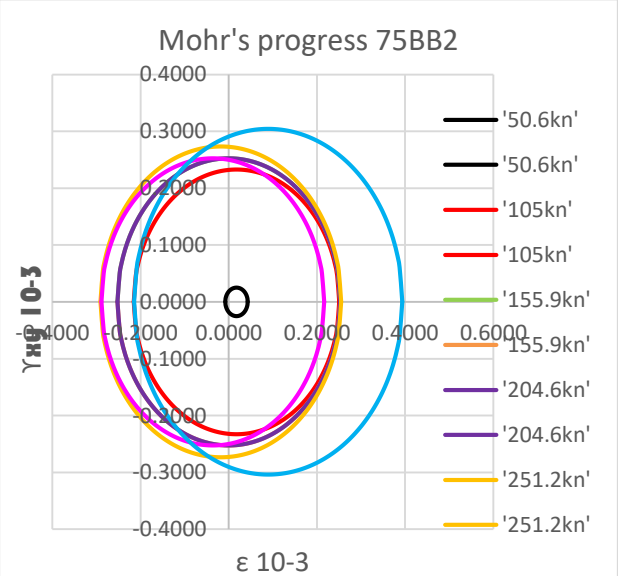
Mohr's progress 75BB2
'50.6kn'
'50.6kn'
'105kn'
'105kn'
'155.9kn'
'155.9kn'
'204.6kn'
'204.6kn'
'251.2kn'
'251.2kn'
ε 10-3

4,50DCB1

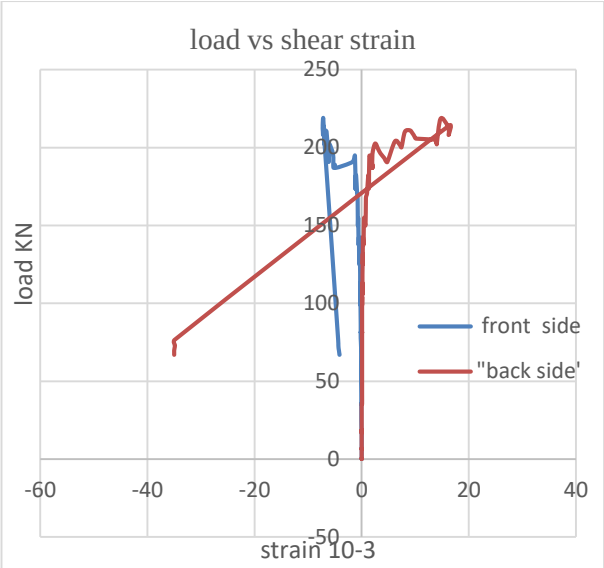
load vs shear strain
load KN
strain 10-3
front side
"back side'

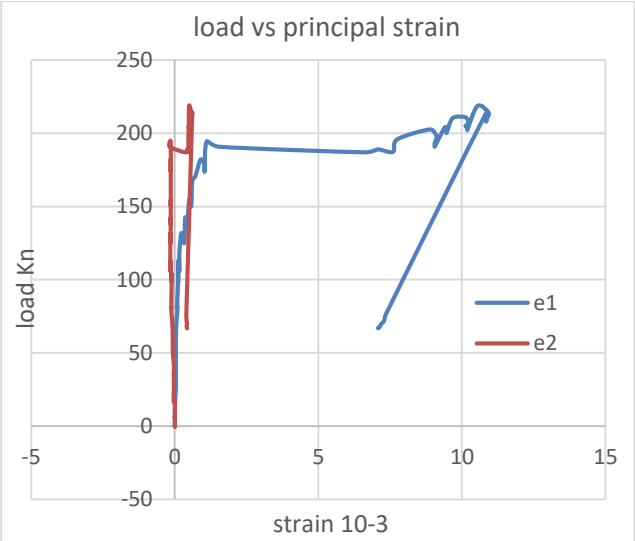
load vs principal strain
load Kn
strain 10-3
e1
e2

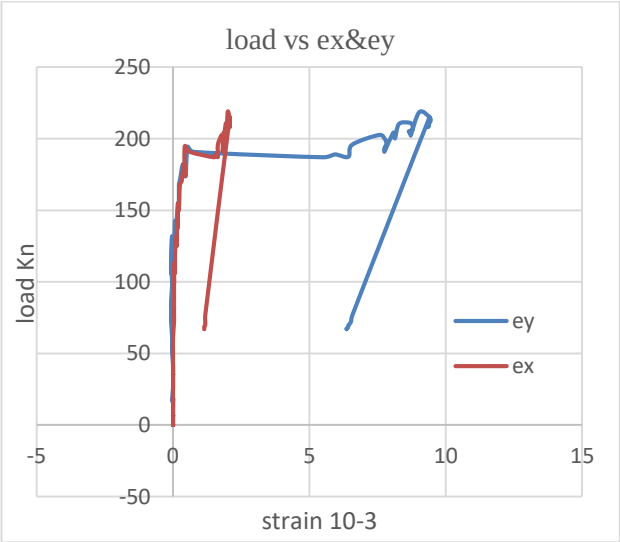
load vs ex&ey
load Kn
strain 10-3
ey
ex

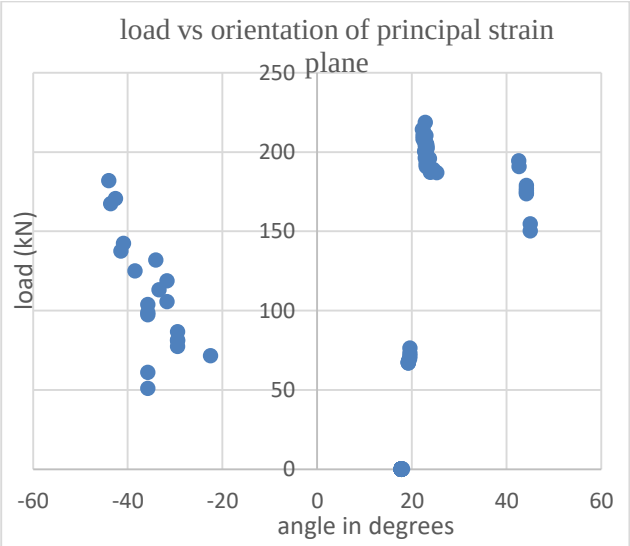
load vs orientation of principal strain plane
load (kN)
angle in degrees

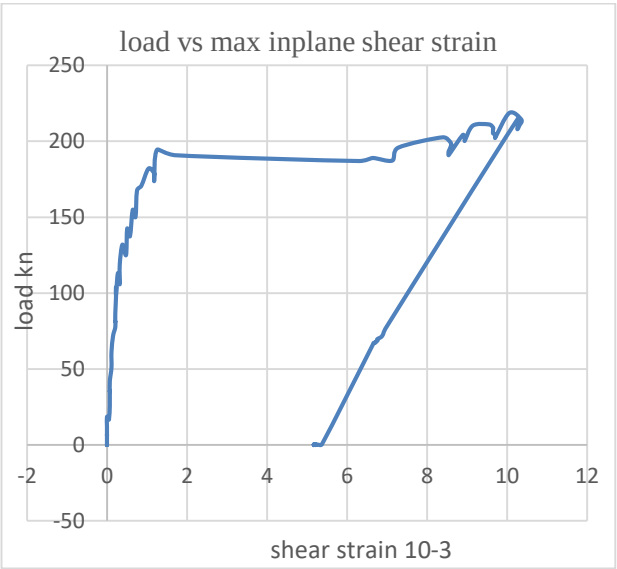
load vs max inplane shear strain
load kn
shear strain 10-3

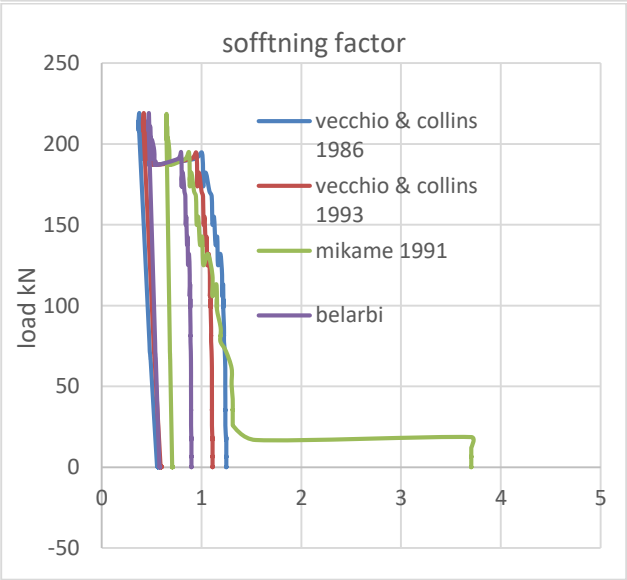
sofftning factor
load kN
vecchio & collins 1986
vecchio & collins 1993
mikame 1991
belarbi

5,75DCB1

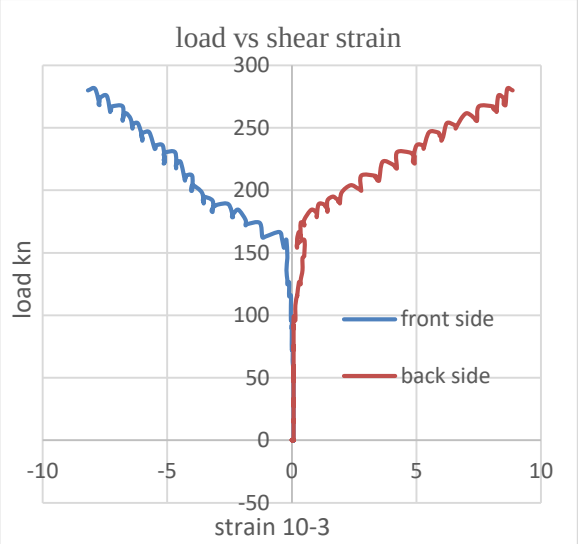
load vs shear strain
load kn
300
250
200
150
100
50
0
-50
-10
-5
0
5
10
front side
back side
strain 10-3

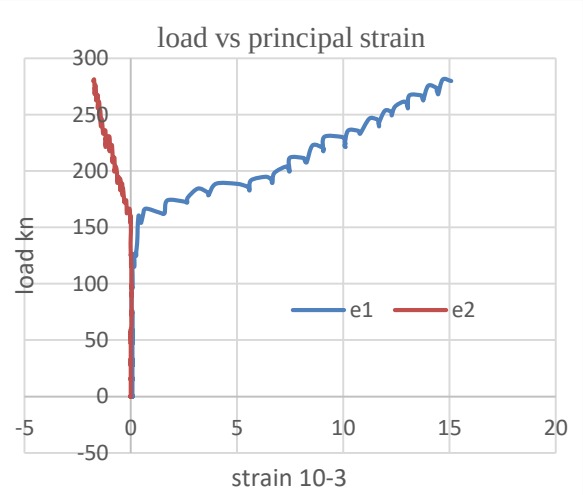
load vs principal strain
load kn
300
250
200
150
100
50
0
-50
-5
0
5
10
15
20
e1
e2
strain 10-3

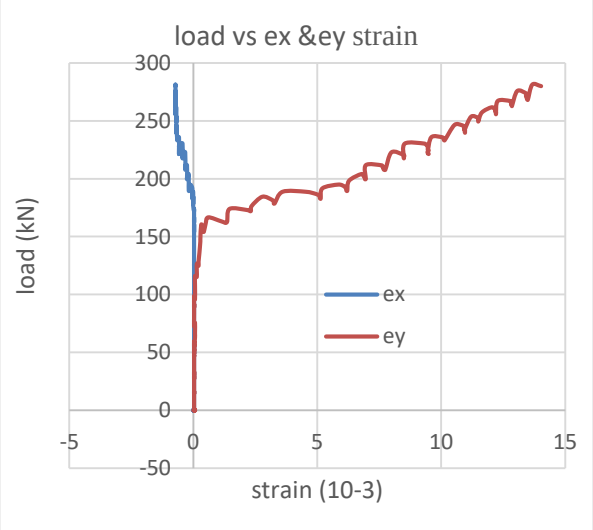
load vs ex &ey strain
load (kN)
300
250
200
150
100
50
0
-50
-5
0
5
10
15
ex
ey
strain (10-3)

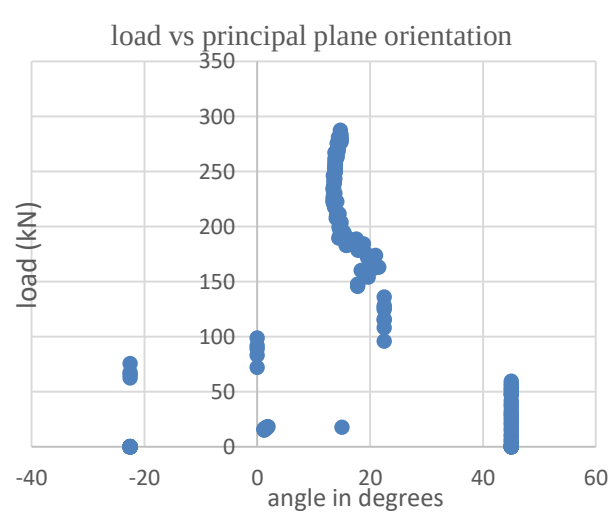
load vs principal plane orientation
load (kN)
350
300
250
200
150
100
50
0
-40
-20
0
20
40
60
angle in degrees

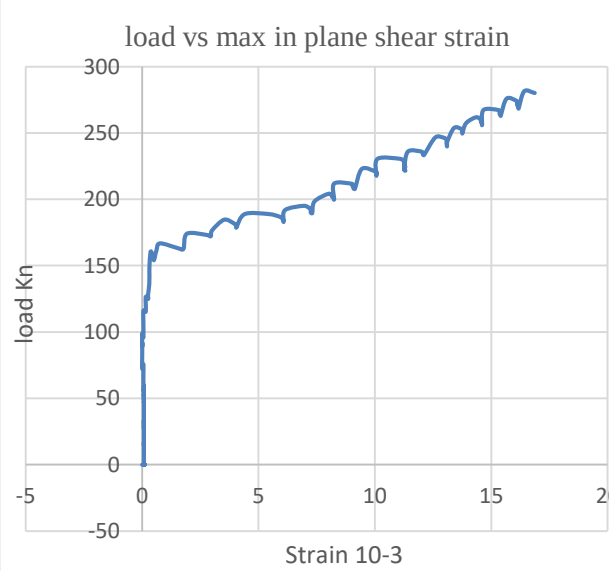
load vs max in plane shear strain
load Kn
300
250
200
150
100
50
0
-50
-5
0
5
10
15
Strain 10-3

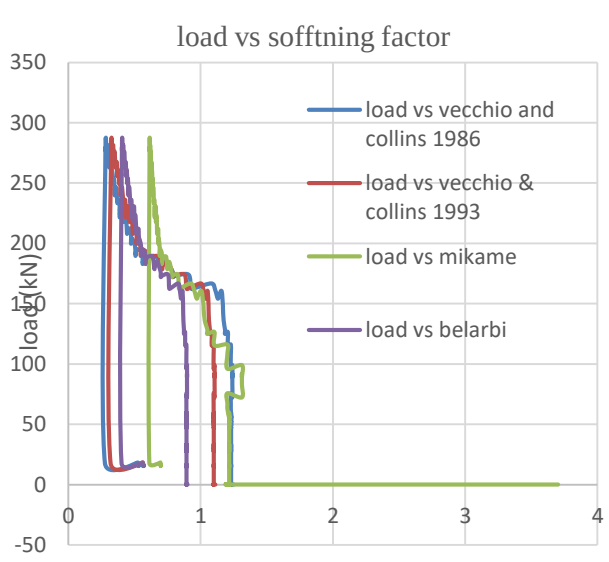
load vs softtning factor
load (kN)
350
300
250
200
150
100
50
0
-50
0
1
2
3
4
load vs vecchio and collins 1986
load vs vecchio & collins 1993
load vs mikame
load vs belarbi

6, 75DCB2

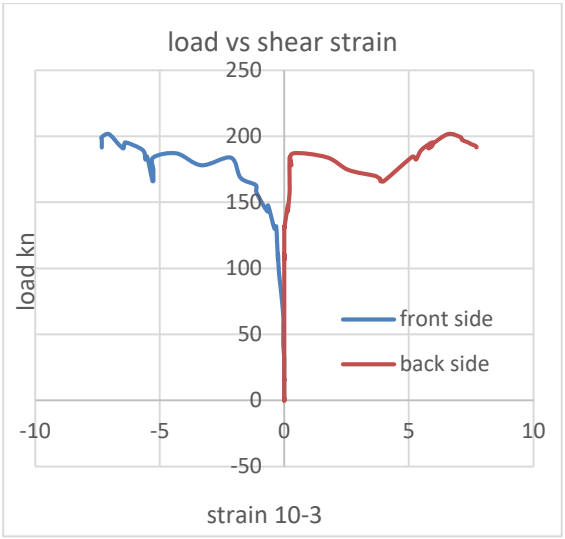
load vs shear strain
load kn
strain 10-3
front side
back side

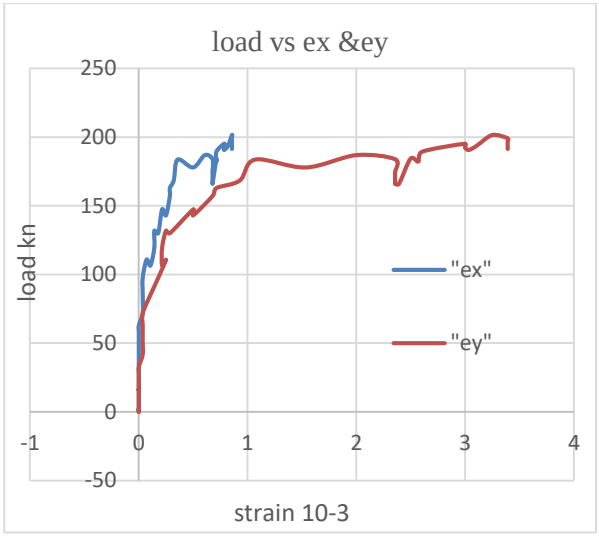
load vs ex &ey
load kn
strain 10-3
"ex"
"ey"

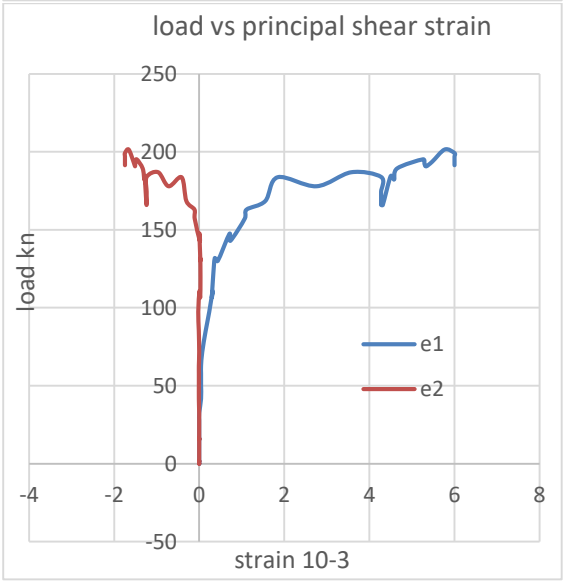
load vs principal shear strain
load kn
strain 10-3
e1
e2

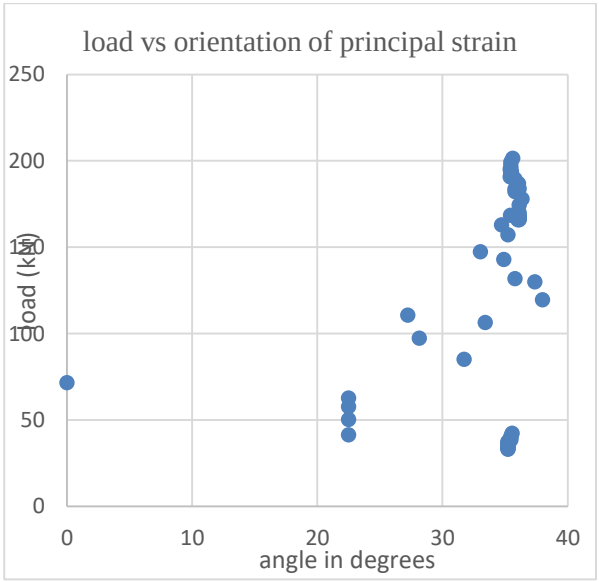
load vs orientation of principal strain
load (kN)
angle in degrees

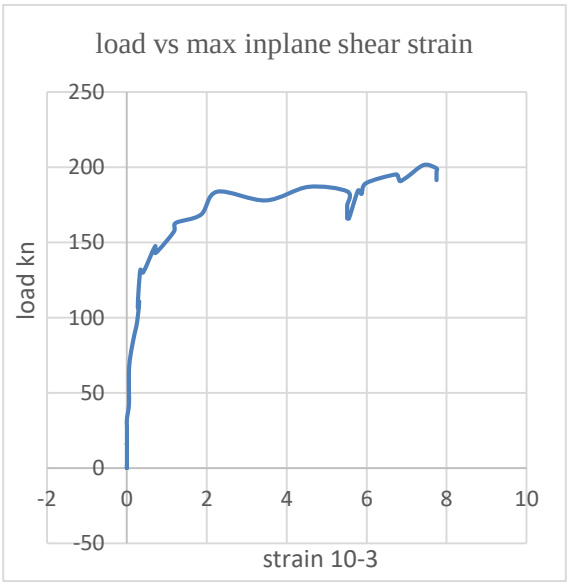
load vs max inplane shear strain
load kn
strain 10-3

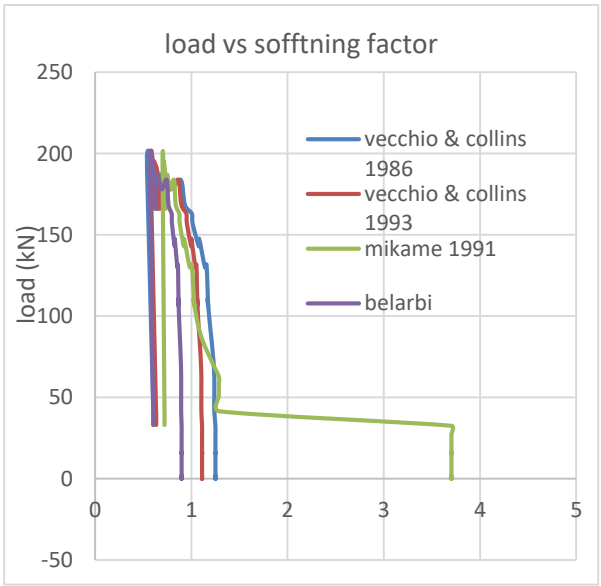
load vs sofftning factor
load (kN)
vecchio & collins 1986
vecchio & collins 1993
mikame 1991
belarbi

APPENDIX D, PICTORIAL REPRESENTATION OF DEFORMATION AT 50kN INTERVAL OF SPECIMEN

CONTROL BEAM

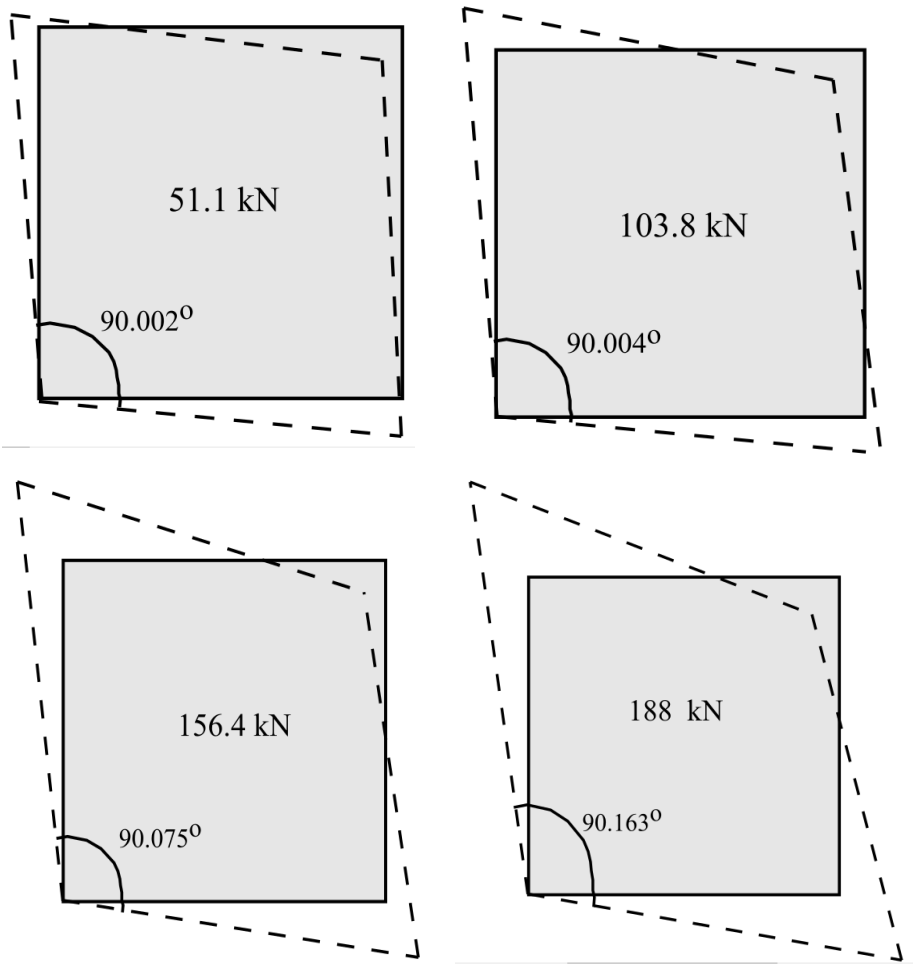

BEAM 75BB1

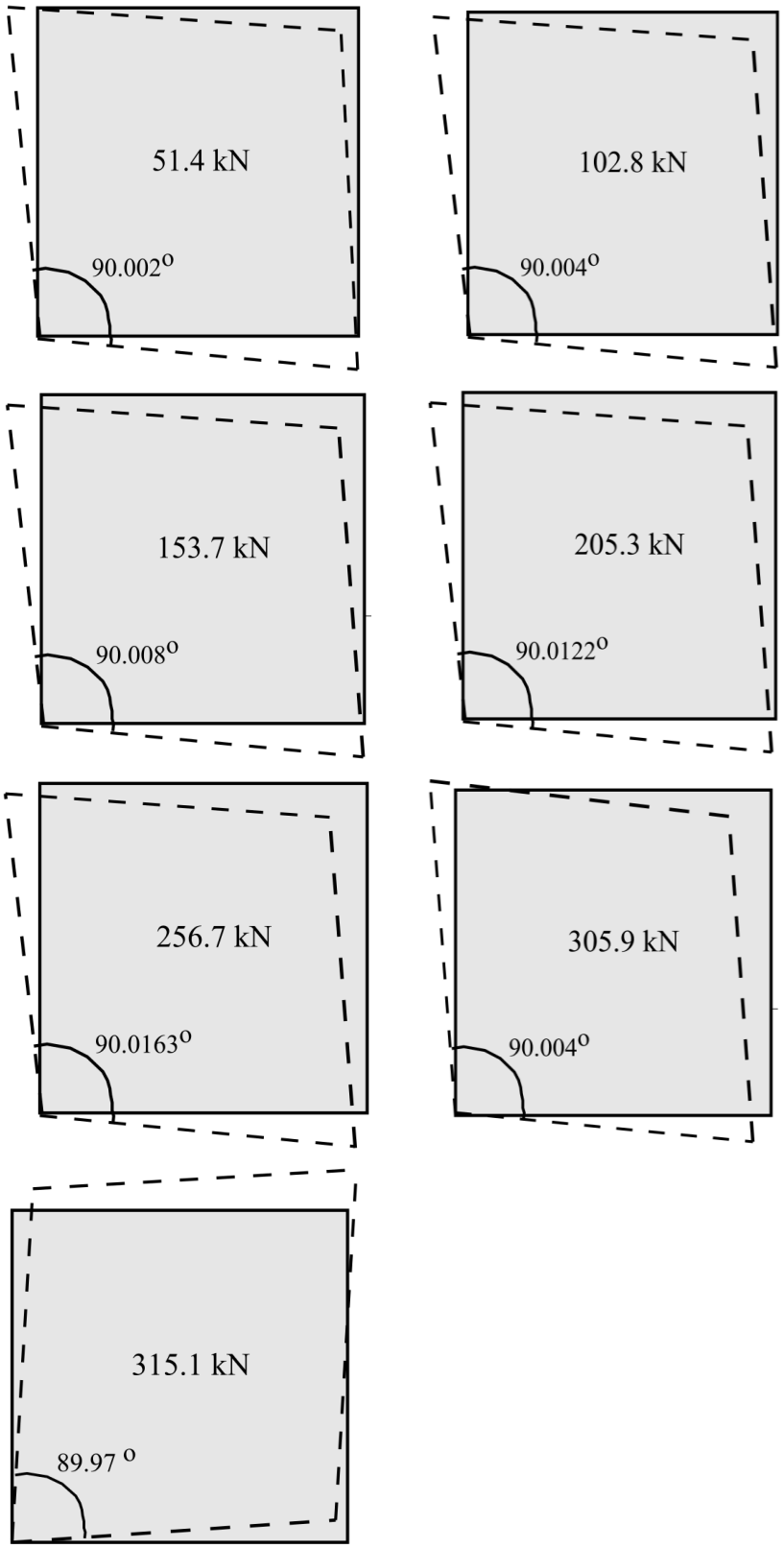
51.4 kN
90.002°
102.8 kN
90.004°
153.7 kN
90.008°
205.3 kN
90.0122°
256.7 kN
90.0163°
305.9 kN
90.004°
315.1 kN
89.97 °

BEAM 75BB2

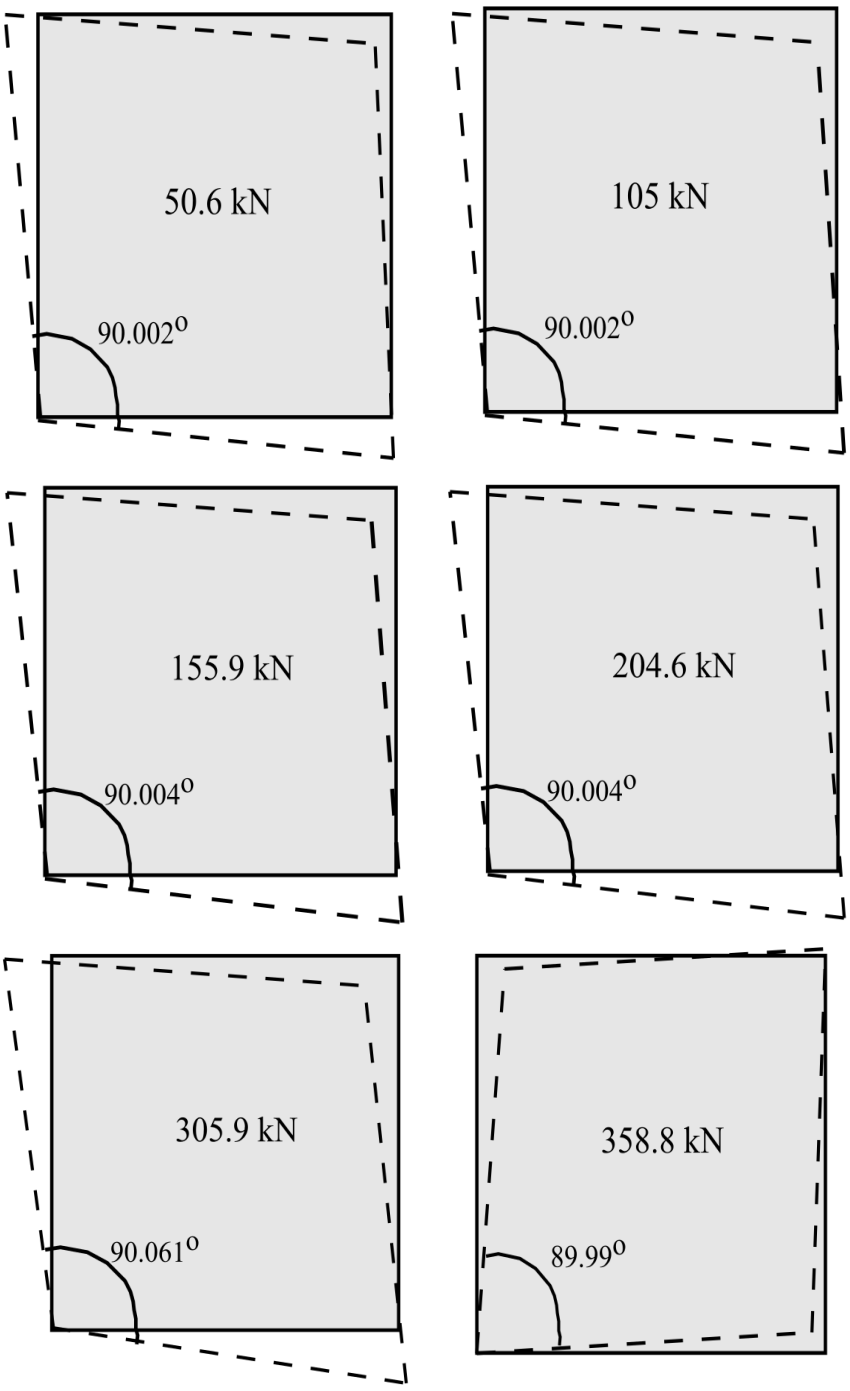
50.6 kN
90.002°
105 kN
90.002°
155.9 kN
90.004°
204.6 kN
90.004°
305.9 kN
90.061°
358.8 kN
89.99°

BEAM 50DCB1

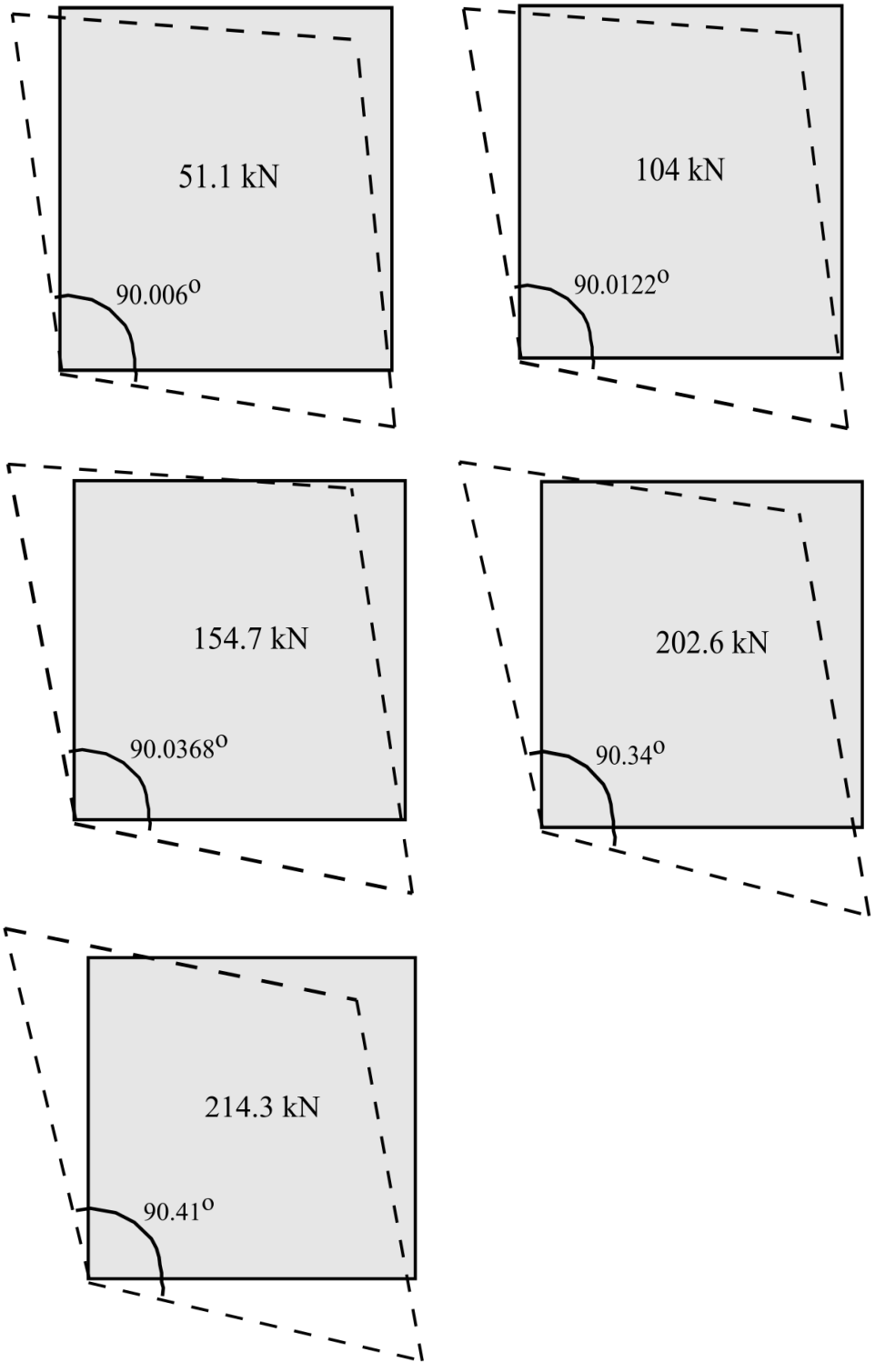
51.1 kN
90.006°
104 kN
90.0122°
154.7 kN
90.0368°
202.6 kN
90.34°
214.3 kN
90.41°

BEAM 75DCB1

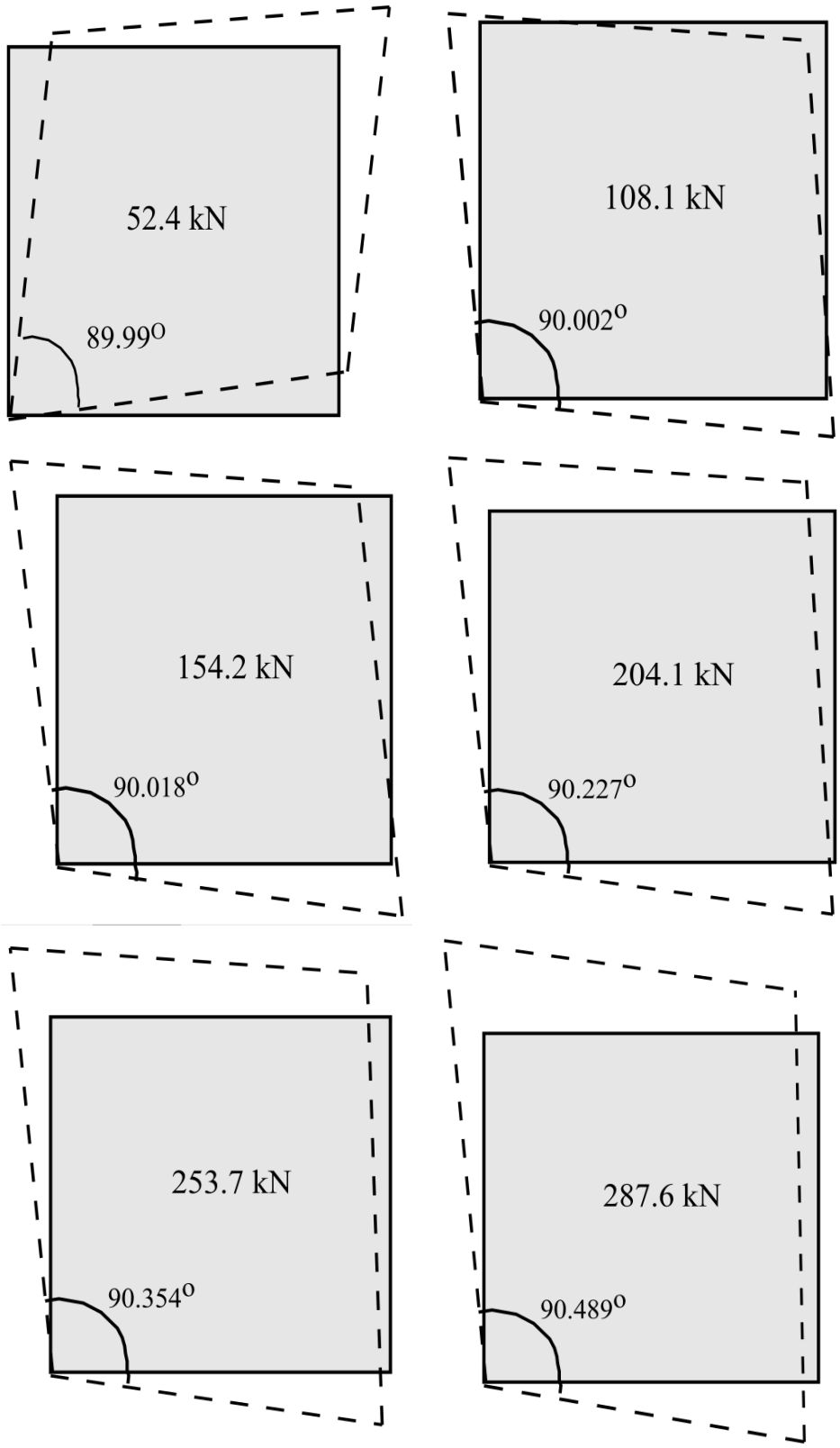
52.4 kN
89.99O
108.1 kN
90.002O
154.2 kN
90.018O
204.1 kN
90.227O
253.7 kN
90.354O
287.6 kN
90.489O

BEAM 75DCB2